TEMPERATURE MEASUREMENT IN ORTHOGONAL MACHINING OF SAE 1015 STEEL USING AN INFRARED CAMERA

By

AMOL AVINASH BHOME

Bachelor of Engineering,

Vishwakarma Institute of Technology,

University of Pune, India

1999

Submitted to the Faculty of the
Graduate College of the
Oklahoma State University
In partial fulfillment of
The requirements for
The Degree of
MASTER OF SCIENCE
December, 2004

TEMPERATURE MEASUREMENT IN

ORTHOGONAL MACHINING OF SAE 1015 STEEL

USING AN INFRARED CAMERA

Thesis Approved:

Dr. R. Komanduri

Dr. C. E. Price

Dr. R. D. Delahoussaye

Dr. G. Emslie

Dean of the Graduate College

ACKNOWLEDGEMENTS

I am highly indebted to my father Mr. Avinash B. Bhome, mother Mrs. Ujjwal A. Bhome, brother Mr. Unmesh A. Bhome and fiancée Vrushali, who are always encouraging and inspiring; and without whose ever-present support and countless sacrifices I would not have come this far. Special thanks are due to my roommates in Nandanvan for their continued support during my studies.

I would like to thank my advisor, Dr. Ranga Komanduri, for his guidance, input, and advice and for allowing me to conduct research in the field of metal cutting.

I would also like to thank Dr. C.E. Price and Dr. R. Delahoussaye for agreeing to serve on my committee and for always being encouraging.

This project is funded by a grant (DMI-0000079) from the Division of Design, Manufacture and Industrial Innovation (DMII) of the National Science Foundation (NSF). The author thanks Drs. W. DeVries, G. Hazlerigg, Delci Durham, J. Cao, J. Larsen-Basse and B.M. Kramer for their interest and support of this work.

I would also like to express my special appreciation for Dr. Z.B. Hou for his continued support and guidance throughout this work. Special thanks are due to Dr.

Robert Ivester of NIST for extending help as regards calibration of the infrared camera and valuable guidance throughout this work.

Thanks are due to Mr. Robert Gerlick and Ms. Catherine Higgins for their valuable help in experimentation part of this work.

Thanks are also due to Mr. Sony Varghese, Mr. Rutuparna Narulkar, and Mr. Bala Sudalayandi for their valuable discussions and suggestions.

Finally, I would like to thank one and all for helping me in completing this work.

SUMMARY

In the present investigation, a MerlinTM Mid InSb MWIR infrared camera is used to observe chip and tool temperature fields during orthogonal machining of steel. A Valenite SECW-2.51.51 tungsten carbide tool insert is used at 15° rake angle to orthogonally machine SAE 1015 steel tube (156 mm outer diameter and 3.175 mm wall thickness) under orthogonal conditions at a feed rate of 0.2 mm/rev and different cutting speeds (from 26.9 m/min to 122.2 m/min) on a Vectrax 1660 lathe. The machining forces were measured using a Kistler 3-Component Piezoelectric dynamometer (Type 9257A). The temperature fields are recorded using Version 2.4.11 of ThermaGram Pro with Dynamite software. The temperature field data is then plotted using Version 9.2 of TecPlot software.

The experimental results are compared with the analytical model and Finite Element Method (FEM) results obtained using Version 4.4 of AdvantEdge software. The experimental tool face observations are found to be in reasonable agreement with FEM results. The study concludes that present infrared camera set-up can be effectively used to measure tool-face temperatures in orthogonal machining of steel.

TABLE OF CONTENTS

LIST OF TABLES

LIST OF FIGURES

Figure **Page**

LIST OF ABBREVIATIONS

A/D	Analog to Digital
AGC	Automatic Gain Control
ASCII	American Standard Code for Information Interchange
CCD	Charge Coupled Device
CFM	Cubic Feet per Minute
FPA	Focal Plane Array
FOV	Field of View or Field of Vision
GB	Giga Byte
GUI	Graphical User Interface
HDD	Hard Disk Drive
InSb	Indium Antimonide
IR	Infrared
LED	Light Emitting Diode
MB	Mega Byte
Mpixel	Mega (10^6) pixel
MWIR	Mid Wavelength Infrared
ND2	Neutral Density 2
NTSC	National Television System Committee
NUC	Non-uniformity Correction
PAL	Phase Alternation Line
RAM	Random Access Memory
RMS	Root Mean Square
ROIC	Readout Integrated Circuit
ROM	Read Only Memory
SAE	Society of Automotive Engineers
VBA	Visual BASIC for Applications

CHAPTER 1

INTRODUCTION

1.1 Introduction

The metal cutting process is a complex production process distinguished by: [1]

- Shear strains of the order of 2 to 5.
- Shear strain rates, typically of the order of 10^3 to 10^5 s^{-1}.
- The rubbing of the tool flank over a freshly generated nascent surface.
- Interaction between shear in the shear zone and friction on the tool face.
- Metallurgical parameters in the workpiece that can influence its response to the cutting tool.

In conventional orthogonal metal cutting, heat is generated by two mechanisms, namely (1) plastic deformation of the work material ahead of the tool and (2) friction between the chip and the rake face of the tool. This heat energy is dissipated into the chip, tool, and workpiece with an approximate distribution percentages being 80, 10, and 10, respectively [4].

The heating of the workpiece can cause subsurface deformation, metallurgical structural alterations in the machined surface, and residual stresses in the finished part. The workpiece temperatures also affect accuracy and precision of the workpiece. The cutting temperatures on the tool influence the life and performance of the tool. For example, the life of a cutting tool is determined by the maximum temperature on the tool

rake face or the clearance face of a cutting tool. Thus selection of optimum cutting conditions depends on the maximum temperatures in tool and thermal properties of tool, namely, thermal conductivity and thermal diffusivity.

It is possible to estimate the heat generated in metal cutting by calorimetric method as demonstrated by Count Rumford [5] in 1798. Since then the science of metal cutting and temperature measurement has made remarkable progress. However, temperature measurement generally is a challenging task. Several techniques have been developed over time for the measurement of temperature in metal cutting. They include: (1) calorimetric techniques, (2) thermocouple techniques, (3) infrared photographic technique, (4) optical and infrared radiation pyrometer technique, (5) thermal paints, (6) metallographic methods, (7) infrared camera technique.

Amongst the above methods the infrared camera technique is the most advanced technique used for the temperature measurement in metal cutting. Recent advances in commercially available infrared video technology dramatically improve the fidelity of infrared measurements for metal cutting. The most important advantage of an infrared camera is its ability to measure *in-situ* 2-dimensional temperature fields in non contact manner.

The thrust of the present study is to use an infrared camera for the measurement of cutting temperatures in orthogonal machining of steel and compare results with those obtained from analytical and numerical (using commercially available Finite Element Analysis software named AdvantEdge Ver.4.4) results.

In general, waveband of 8-13 μm is preferred for high-performance thermal imaging because of its greater sensitivity to ambient temperature objects and its better

transmission through mist and smoke. However, the waveband of 3-5 µm may be more appropriate for hotter objects, or if sensitivity is less important than contrast. The 3-5 µm-waveband also has the advantage that the diameter of the optics required to obtain a certain optical resolution is smaller, and that some detectors may be operated at a higher temperature than is usual in the 8-13 µm. In the present investigation, a Merlin Mid InSb MWIR infrared camera that operates in the waveband of 3-5 µm is used.

The infrared camera is used to observe chip, tool and workpiece temperature fields in orthogonal machining of steel. A 100 mm Si-Ge lens is used to obtain a field of vision that is 12.8 mm x 10.2 mm. A Valenite SECW-2.51.51 cemented tungsten carbide tool insert is used at 15° rake angle to orthogonally machine SAE 1015 steel tube (156 mm OD and 3.175 mm wall thickness) at a feed rate of 0.2 mm/rev and at five different cutting speeds from 26.9 to 122.2 m/min on a Vectrax 1660 lathe. The cutting forces are measured using a Kistler 3-Component dynamometer (Type 9257A). The temperature fields are recorded using Version 2.4.11 of ThermaGram Pro with Dynamite software. The temperature field data is then plotted using Version 9.2 of TecPlot software. The experimental results are compared with the analytical and Finite Element Method results obtained using Version 4.4 of AdvantEdge software.

1.2 Overview

This report on temperature measurement in orthogonal machining of SAE 1015 steel using an infrared camera consists of seven chapters. Chapter 1 gives an introduction to this report.

This is followed by Chapter 2 on Literature Review. In the literature review the works as early as that of Count Rumford, 1798 [5] have been reviewed. Temperature measurements methods, such as calorimetric techniques, thermocouple techniques, infrared photographic technique, optical and infrared radiation pyrometer technique, thermal materials, metallographic methods, have been reviewed briefly, whereas the infrared technique has been reviewed in greater depth.

The objectives of present investigation are given in detail in Chapter 3, Problem Statement. Chapter 4 is titled Equipment and describes in detail the equipment, namely the Merlin-Mid infrared camera which is used in the present investigation.

Chapter 5 provides the experimental procedure used for the present study. Chapter 6 deals with experimental results and discussion. The conclusions are listed in Chapter 7. The scope of future work is given in Chapter 8. A detailed list of references is provided in the end. In the Appendix-I, VBA code to convert data from pixel format into tabular format is given. In the Appendix-II, detailed calculation steps pertaining to analytical model (Shaw [37]) are given.

CHAPTER 2

LITERATURE REVIEW

Reference 4 presents an extensive review of the various experimental techniques used for the measurement of heat and temperature generated in machining. Much of the summary given in the following is based on that review by Komanduri and Hou [4].

The work to date in the field of experimental temperature measurement during metal cutting generally falls into one of these categories:

1. Calorimetric Techniques,
2. Thermocouple Techniques,
3. Infrared Photographic Technique,
4. Optical and Infrared Radiation Pyrometer techniques,
5. Thermal Paints and Powders,
6. Metallographic Methods,
7. Infrared Camera Technique.

2.1 Calorimetric Techniques

In 1798, Benjamin Thompson (Count Rumford) [5] in his pioneering work investigated the heat generated in the boring of a cannon and developed the concept of "mechanical equivalent of heat", the exact relation of which was established by Joule some 50 years later. Figure 2.1 shows the calorimetric method used by Rumford to

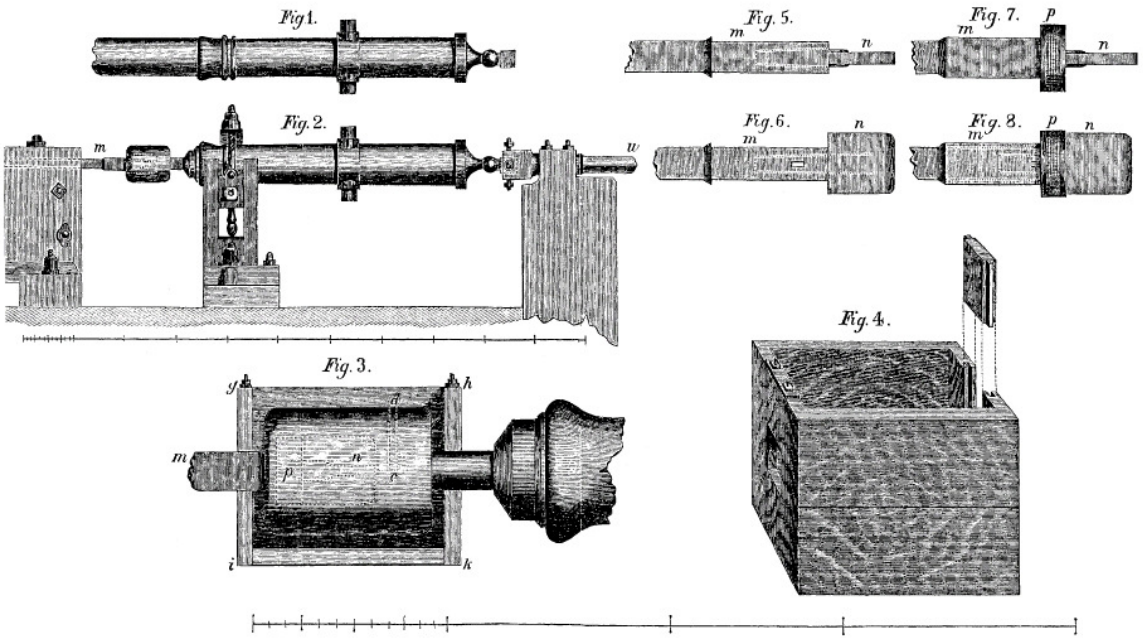

Fig.2.1 Schematic of the calorimetric setup to determine the heat generated in the boring of a cannon (after Rumford [5]). On the top is the cannon in the as-received state at the foundry. Below it is the experimental set-up used. The bottom figure is higher magnification of the calorimetric set-up showing the iron bar to the end of which a blunt boring tool is fixed, which is forced against the bottom of the bore in a cannon.

estimate the heat generated in the boring operation. Rumford conducted a systematic investigation to inquire into the source of heat excited by friction between a blunt boring bar rubbing against the bottom of the bore of a cylinder of cannon. This masterpiece study not only probed the source of frictional heat generated in the boring of cannon but also the very nature of heat during an era when heat was considered as either an igneous fluid or a material property [2,4].

Schmidt and Roubik conducted calorimetric studies to determine the amount of heat, which conducts into workpiece, the chip, and the tool at different cutting conditions, namely, the cutting speed and the in-feed rate [4]. They showed quantitatively for the first time that much of the heat generated in cutting was carried out by the chips (~70-80%) with ~10% entering the workpiece, and the remainder into the tool [4]. The calorimetric

technique gives the distribution of heat energy among chip, tool and work. However, it does not give actual temperatures or the temperature distributions.

2.2 Thermocouple Techniques

Thermocouples work on the principle known as the Seebeck effect: when two dissimilar metals are joined together to form two junctions and if these junctions are maintained at two different temperatures then an electromotive force (emf) exists across two junctions.

Thermocouples offer several advantages:

1. Simple and flexible construction
2. Remote measurement
3. Simple operation and signal processing.
4. Low initial and running costs

In metal cutting, two types of thermocouples have been used, namely, the embedded thermocouples and the tool-work or dynamic thermocouples.

2.2.1 Embedded Thermocouples

These are the earliest thermocouples used for estimation of temperatures in metal cutting. The embedded thermocouples have the following limitations [4]:

1. Generation of data for isotherms can be a tedious process
2. It is difficult to extend them to measurement of temperature at chip-tool contact.
3. Their placement can interfere with the heat flow

4. Surface gradients are steep, and it can be difficult to locate two thermocouples very close to each other
5. Embedded thermocouples have limited transient response due to their mass and distance from the points of interest.

2.2.2 Dynamic Thermocouples

This technique is also known as the Shore-Herbert-Gottwein thermocouple technique. It consists of tool-work and tool-chip junctions to measure interface temperatures.

The dynamic chip-tool thermocouple method is relatively simple to use but has the following limitations [4]:

1. The mean temperature is measured over the entire area between the chip and the tool including the wear land on the clearance face.
2. Misleading results may be obtained if a built-up edge is formed because then dissimilar metals do not exist over the entire area.
3. Calibration of the tool-chip thermocouple may affect the measurement of the temperature.
4. Separate calibration is needed for each tool-chip combination.
5. Workpiece and tool need to be insulated.
6. A rotating contact is required for the workpiece.

2.3 Infrared Photographic Technique

Boothroyd [6] developed an infrared photographic technique to measure the temperature distribution in the shear zone and at the chip–tool interface in machining.

The method involves photographing the workpiece, the chip, and the tool using an infrared (IR) sensitive photographic plate and measuring the optical density of the plate over the relevant field with a microdensitometer. A heated tapered strip mounted next to the tool and photographed simultaneously with the cutting process was used to measure the temperature distribution.

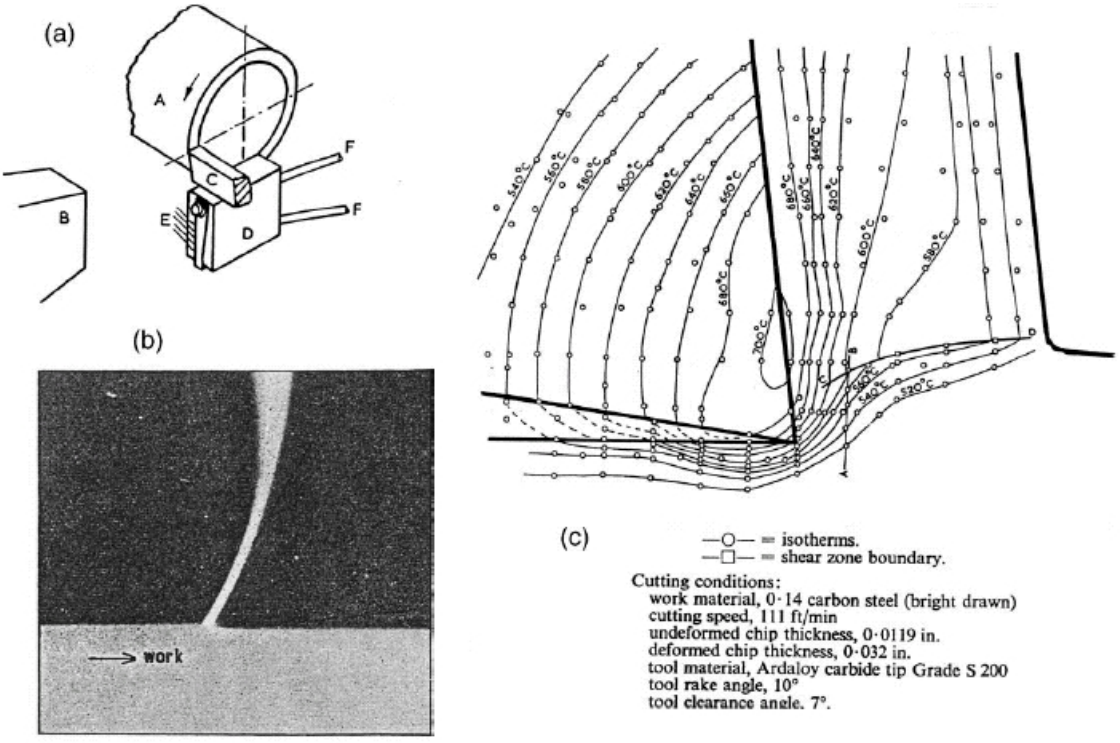

Fig.2.2 (a) Schematic of the experimental arrangement used for IR measurements of temperatures generated in the cutting process (after Boothroyd [6]); (b) infrared photograph of the cutting process (after Boothroyd [6]); (c) temperature distribution in the shear zone, chip, and tool during orthogonal machining of SAE 1014 steel (after Boothroyd [6]).

The radiating surfaces of the workpiece, the tool, and the calibration furnace were coated with lamp black to ensure the same value of emissivity. Figure 2.2(a) is a schematic of the experimental arrangement used for the infrared measurement of temperatures generated in the cutting process and Figure 2.2(b) is an infrared photograph

of the cutting process. Figure 2.2(c) shows the temperature distribution in the shear zone, chip, and tool during orthogonal machining. Some of the limitations of this technique include the following [4]:

1. The sensitivity of the infrared photographic plate was such that an exposure time of 10–15 s is required,
2. In order to obtain complete temperature patterns of the cutting process, it was necessary to preheat the workpiece between 350–500°C as the photographic film was not sensitive below this temperature.

Subsequently, Jeelani conducted a similar study using IR photography to measure the temperature distribution in the machining of annealed 18% Ni maraging steel in the cutting speed range of 0.406–0.813 m/s [4]. He built a special light-tight enclosure around the lathe to eliminate stray light. The thermal sensitivity of the high speed IR film used by Jeelani was better than that used by Boothroyd and hence it was not necessary to preheat the work material. A 30-gauge chromel–alumel thermocouple was used for calibration. It was heated electrically and photographed at various temperatures. The workpiece, the cutting tool and the calibration bead were all coated with carbon black to generate surfaces with similar emissivities. The IR film was developed and its density was read using a microdensitometer. He could not determine the temperature distribution below 400°C as the IR film is insensitive to temperatures below this value. He reported that the temperature on the machined surface is quite high (555°C at a cutting speed of 0.813 m/s) and decreases with the depth beneath the surface. In addition, the cutting temperature was found to increase with increase in the wear or dullness of the tool.

2.4 Optical and Infrared Radiation Pyrometers

Reichenbach [8] used a radiation technique with a PbS cell to measure the temperatures in cutting. The cutting tests were conducted on a shaper. The PbS cell was arranged to sight through a small hole drilled in the workpiece sensing radiation from the shear plane and clearance face of the tool. One of the limitations in using this technique to determine the temperature distribution in the shear zone was that the minimum temperature, which gave a useful reading, was 232°C.

Another limitation was that the fourth power radiation law gave such large variations in the readings that when the attenuation on the oscilloscope was set high enough to keep the maximum readings on scale, the low temperature regions could not be noticed.

Ueda *et al.* [9] used an optical pyrometer to determine the temperature on the rake face of a single crystal diamond tool in ultraprecision machining of aluminum. The infrared rays radiated from the chip–tool contact area, and transmitted through the diamond tool, were collected by a chalcogenide fiber and led to a two-color InSb and HgCdTe detectors.

The two-color pyrometer can measure the temperature regardless of the size of the object, when the temperature of the object is constant. When the object has a surface of known temperature distribution, it is possible to estimate the maximum temperature from the measured temperature.

Ng *et al.* [10] used infrared optical pyrometer to measure temperature in machining of SAE H13 hot work die steel. In 2002, M'Saoubi *et al.* [11] used pyrometer

along with an infrared-charge-coupled device (CCD) camera to measure temperatures in orthogonal cutting of low-alloyed carbon steel.

2.5 Thermal Paints and Powders

Use of thermal sensitive paints and powders is one of the simplest and most inexpensive techniques to estimate the temperature of a cutting tool during machining. It depends on the ability of a given paint to change its color due to chemical action at a given temperature. Different thermal sensitive paints respond to different temperatures. Much depends on the heating rate as well as the duration. Therefore, the application of this technique is generally limited to controlled heating conditions. Most researchers use this technique to estimate the temperatures in accessible surfaces of the tool or the workpiece.

The limitations of thermal sensitive materials technique are [4]:

1. Contours can be obtained only of those temperatures specific to a given material's melting point.
2. Tests need to be conducted for longer durations.
3. Only one temperature contour can be obtained in one experiment.

2.6 Metallographic Methods

The temperature near the rake face is determined either by observing the known microstructural changes in the high-speed steel (HSS) tool after cutting, or by measurement of changes in hardness using a microhardness test. Speeds (for example 180m/min) far higher than the normal speeds need to be used in this technique. At such

high cutting speeds the HSS tools can wear rapidly. By calibrating the microstructure of the HSS after heating at different temperatures and comparing it with the microstructure obtained after cutting, the temperature distribution can be determined. Only those materials that exhibit a change in microstructure with temperature, such as HSS can be used as tools in this technique. Several calibrations are required as the changes in the microstructure depend on the sufficient time for the transformation to take place completely and the rate of cooling period in addition to the cutting temperature. Also, the materials that do not show microstructural changes can not be used in this method.

It can be seen that among the various methods of temperature measurements some are quite simple (e.g. thermal paints) but may not be very accurate and can be subject to errors. Some techniques (e.g. metallographic technique) can be used only for specific materials where change in temperature leads to change in the microstructure (HSS). Some give average values under quasi-steady conditions (e.g. chip–tool thermocouples). While others require quite elaborate preparation (e.g. embedded thermocouples) and/or require expensive instrumentation (optical and infrared pyrometers). Some techniques can only provide a temperature at a given location or a given region (thermocouples) while others are capable of providing information on the temperature distribution (e.g. temperature distribution using PVD coatings of materials of known melting temperatures [4]).

The appropriate technique for temperature measurement depends on the application under consideration as well as the available tools for measurement. Optical and infrared radiation pyrometers require elaborate instrumentation and may require a special environment in some cases as can be seen from the literature review that follows.

2.7 Infrared Camera

Young and Chou [12] conducted orthogonal machining test to investigate the edge effect from measurement by non-contact infrared (IR) thermographic technique. Figure 2.3(a) shows the experimental setup used to measure chip back face temperatures during orthogonal machining of annealed SAE 1030 steel with tungsten carbide tool. The chip back face was displayed simultaneously on a color CRT as a frozen image through a high sensitivity infrared detector element. In this measuring system, the detector unit first detects infrared radiation and converts into electrical signals, which in turn is converted to obtain the corresponding temperature values. Tests were conducted at a cutting speed of 99 m/min for chip width to undeformed chip thickness ratios varying from 5.2 to 27.8. It can be noted from Figure 2.3 (b) that the temperatures on the back of the chip increase as chip moves away from the workpiece.

Figure 2.3(c) shows lateral temperature distributions on back surface of the chip observed at various values of chip width to uncut chip thickness ratio b/t. It can be seen

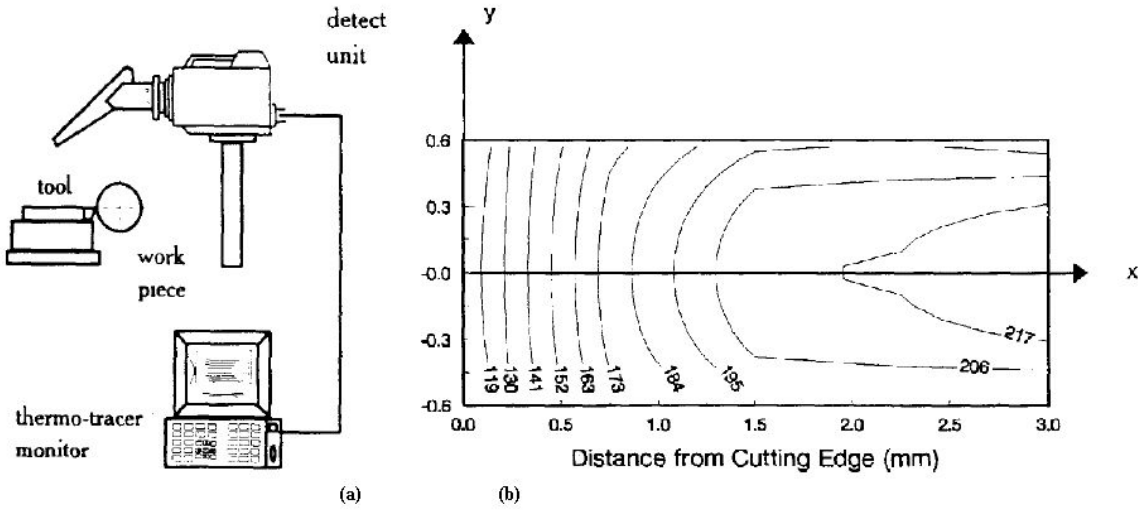

Fig.2.3 (a) Schematic of the experimental setup used by Young and Chou [12] (b) Typical chip-back temperature distribution observed in SAE 1030 Steel at 99 m/min cutting speed.

that for b/t ratios of 13 and 16.8 the temperatures observed at the edge of the chip are about 95% of those at the center of the chip. This temperature drop was observed to be less than 2% in the chip near the cutting edge. In the present investigation the b/t ratio is maintained at 15.9, thereby limiting temperature drop at the chip edge to about 5% of the center temperature.

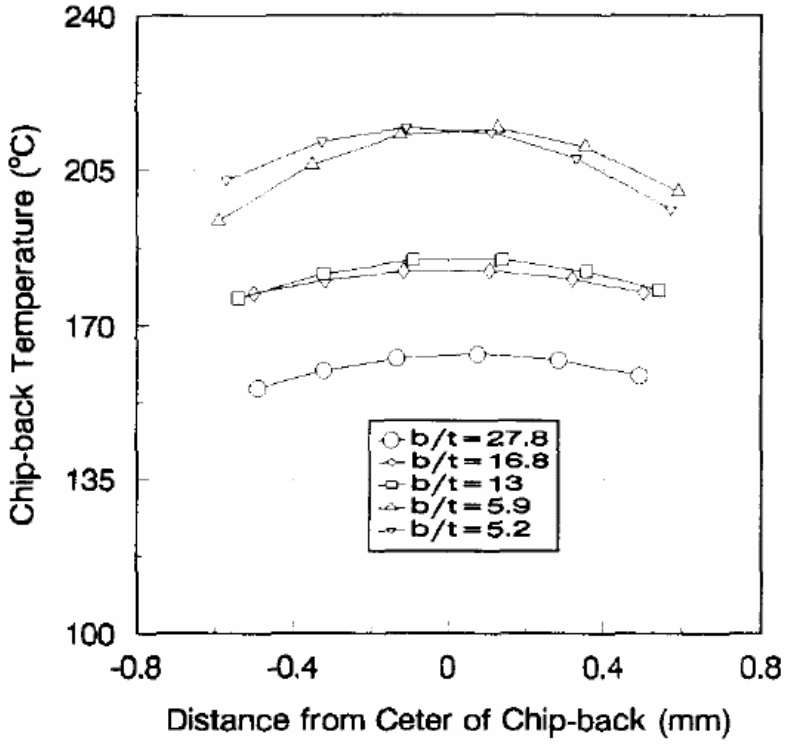

Fig.2.3(c) Lateral temperature distribution on back face of the chip in orthogonal machining of SAE 1030 Steel at a cutting speed of 99 m/min (after Young and Chou [12])

A set-up similar to that used in Ref 12 was used by Kwon *et al.* [16] to measure rake face temperatures [Figure 2.3]. They used IR 600 L of Inframetrics Inc. to measure the temperatures while machining hot rolled SAE 1045 steel and gray cast iron (GCI) (class 40 grade) using coated carbide tools. Images were obtained at a frequency of 30 Hz

and resolution of 165 μm/pixel. Tool inserts of grade C2-C4 had the back rake angle of 0°.

As shown in Figure 2.4, an aluminum fixture was built for the infrared camera, and was mounted on the carriage. The camera assembly on the fixture had a telescope and "downlooker" that focused the IR camera down on an insert. The whole assembly traveled with the carriage to obtain the IR images on the insert containing both spatial and temporal temperature data. Each frame of an IR image contains the spatial temperature information and the streams of IR images contained the temporal temperature information of the rake face of an insert. The IR images then were interpreted into the temperature information, which in turn were used to estimate the average chip–tool interface temperature.

Kwon *et al.* [16] performed dry-turning experiments. After cutting the material for a minimum of 76 seconds, the feed was stopped to allow an unhindered view of the

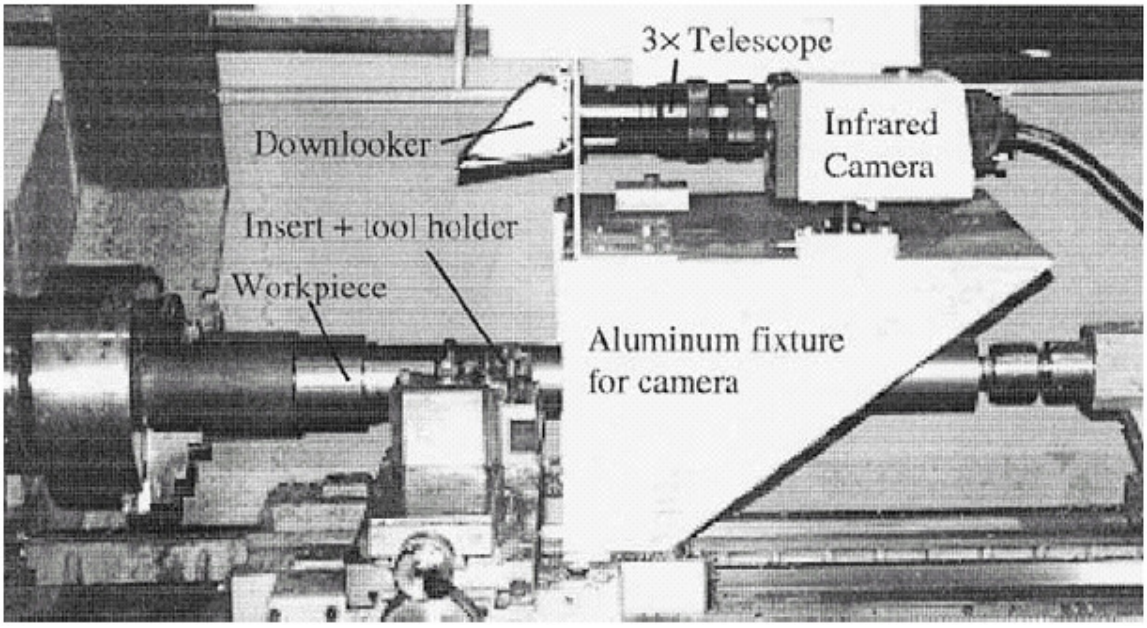

Fig.2.4 Machining set-up used to measure the rake face temperatures in machining of SAE 1045 (after Kwon *et al.* [16])

tool's rake face. It was impossible to measure the temperatures of the rake face of an insert during cutting owing to the adulterating effect of the flowing chips, whose temperatures are much higher than the tool surface. Hence, their investigation attempts to get the IR images after the feed was stopped. For all cuts, the depth of cut and the feed rate were kept constant at 2.54 mm and 0.51 mm/rev, respectively.

The IR images were recorded on a videotape, and analyzed subsequently using the software Image Pro Plus (IPP). The Multiframe Acquire feature was applied to select the first image right after the chip had left the field of view completely. It was also required to fix the origin at the boundary line of the interface. This problem bears a direct semblance to the difficulty experienced by Wang *et al.* [12] and in the present investigation.

One of the conclusions drawn by Kwon *et al.* [16] was that direct measurement of the chip–tool interface temperature using an infrared camera was not possible due to the flowing chips covering the chip–tool interface during cutting and the alteration in the local emissivity at the tool–chip interface due to adhesion of work material. Therefore, the IR images were obtained after the feed was stopped and the inverse estimation scheme had to be utilized.

Another observation from the interface temperature data was that the temperatures were lower for the gray cast iron (GCI) than for the steel. This conformed to the usual notion that materials with a lower specific work of plastic deformation, in general, exhibit lower interface temperatures.

Wang *et al.* [13] used an infrared (IR) imaging system (Inframetrics Model 600) to measure the transient temperature distribution within curled chips during dry

orthogonal machining of cold rolled SAE 1018 steel. Orthogonal cutting tests were conducted for dry turning under. The workpiece was prepared in the form of a circular disk (152 mm diameter and 3 mm thickness) and was mounted on a mandrel, with feed motion applied radially towards the axis of the disc. Figure 2.5(a) is a schematic representation of the setup. Machining tests were performed at a feed of 0.318 mm/rev and at cutting speeds of 134 m/min and 170 m/min. Since their IR imaging system could not use a variable emissivity during the experiments and the time to form a curled chip is about 100 ms, it was thought to be reasonable to assume a constant emissivity during the entire experiment.

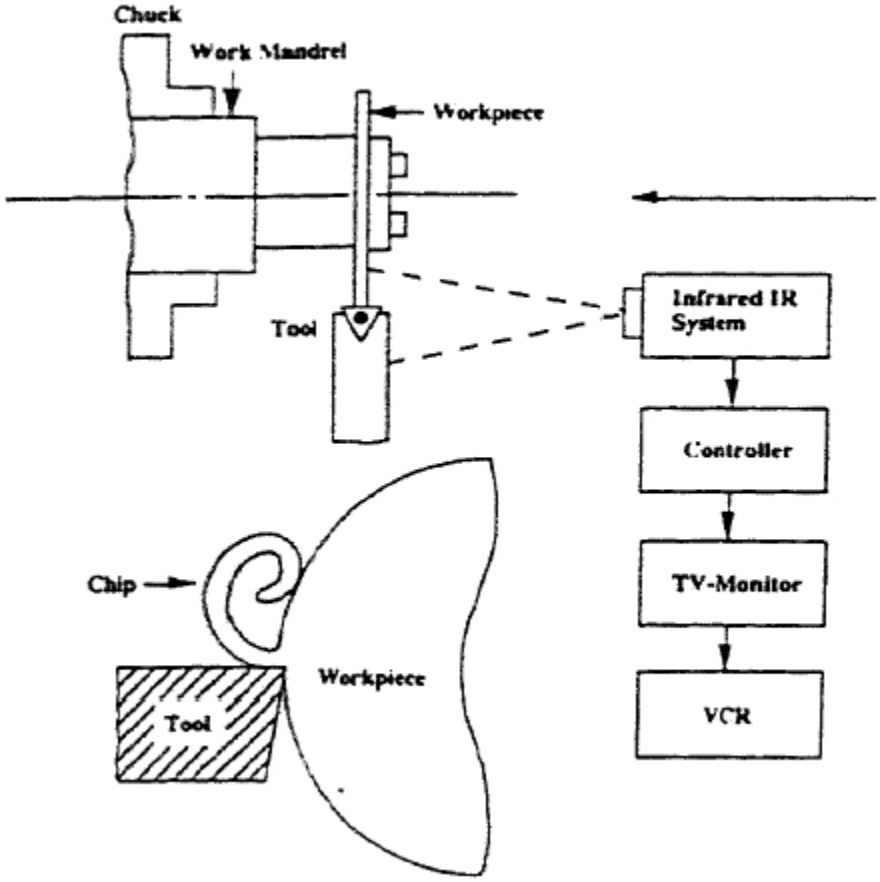

Fig.2.5(a) Schematic of the experimental setup used by *Wang et al.* [13] for machining SAE 1018 at a feed rate of 0.318 mm/rev and cutting speeds of 134 m/min and 170 m/min.

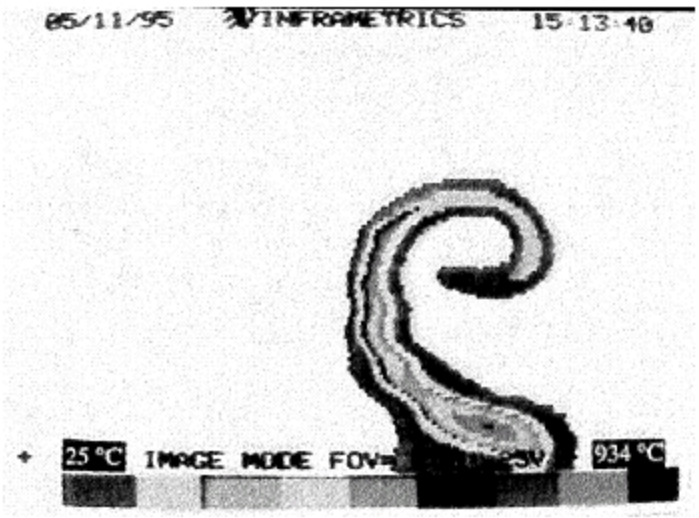

(CUTTING SPEED U = 134 m/min, FEED f = 0.318 mm/rev, WIDTH OF CUT w = 3 mm, WORKPIECE = COLD ROLLED STEEL AISI 1018.)

Fig.2.5(b) IR image showing temperature distributions within a curled chip (after Wang *et al.* [13])

An emissivity of 0.62 was used in the cutting test. The temperature range used in the camera was from 25° to 525°C. Due to heat convection and radiation at the outer surface of the chip, the temperature gradient is higher across the chip cross section than along the chip length.

Wang *et al.* [13] concluded that the temperature distribution within chips vary during their formation. The temperatures reach maximum value at the root of curled chip. This maximum value increases with cutting speed. The maximum temperature in SAE 1045 steel was reported to be higher than in SAE 1018 steel.

Dewes *et al.* [14] used Agema Thermovision 900 for temperature measurement in high-speed machining of hardened die steel (SAE H13) (hardness 52HRC). They used this system to find maximum temperatures and not the temperature contours.

Chandrasekar *et al.* [15] used the planning setup (Figure 2.6(a)) to measure tool-chip contact temperatures. The work material used was brass and a sapphire tool was

used as it is optically transparent in the wavelength region, 2-5µm, the operating range of IR camera. An Amber-Raytheon Radiance HS Modular snapshot IR camera at a sampling frequency of 100 Hz and integration time of 2 µs were used. This IR camera has 2-dimensional focal plane array (FPA) of 256 x 256 pixels and uses Si-Ge lenses.

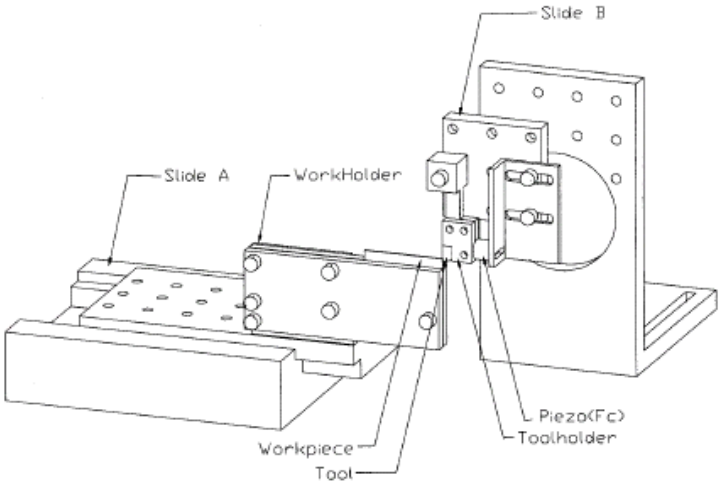

Fig.2.6(a) Schematic of the experimental planing set-up used for machining of brass at cutting speed 170 m/min, feed rate of 50 µm/rev, width of cut 2 mm (after Chandrasekar *et al.* [15])

They reported that the region of contact, (very close to the cutting edge) is much brighter in the image; the extent of this region is less than 200 µm. In a typical cutting experiment, about 150 IR images were acquired under steady state testing. Images obtained with the filters were paired with each other and each pair was used to obtain a full-field temperature contour of the rake face along the tool-chip contact.

Chandrasekar *et al*. [25] measured the temperature field at the tool-chip interface in machining using an optically transparent sapphire tool as shows in Figure 2.6(b). A Galileo IR camera (made by Amber-Raytheon) was used. It was a high-speed medium wavelength IR camera having 256 x 256, InSb focal plane array. The combination of the camera and associated optics, specially designed for the cutting experiments, provided a minimum field of view of 2.5 mm x 2.5 mm with a spatial resolution of 10 µm.

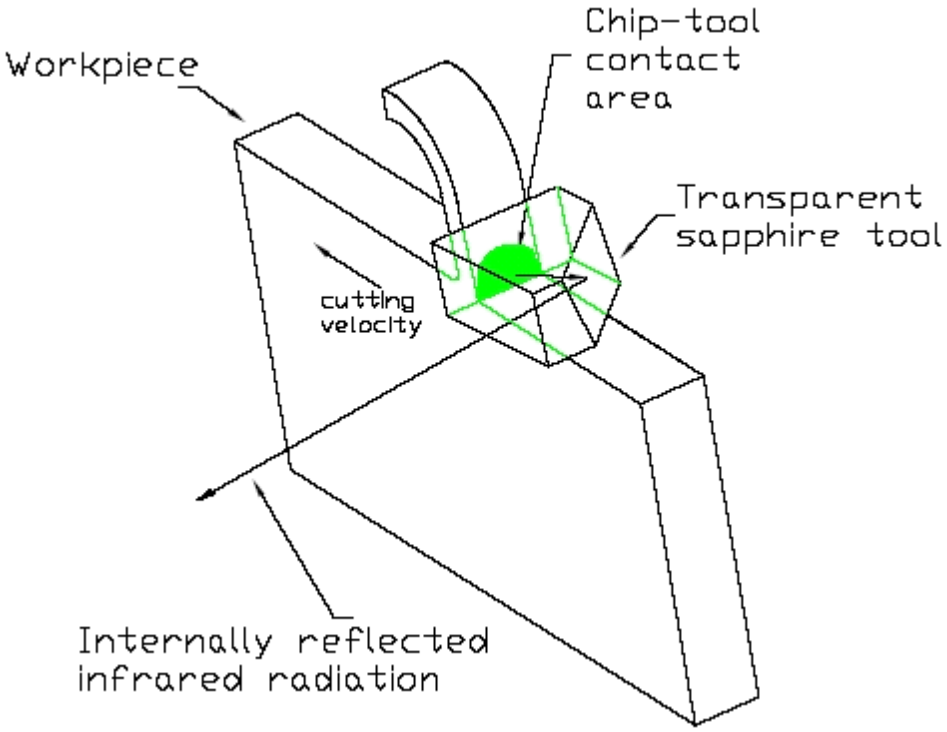

Fig.2.6 (b) Schematic showing transparent sapphire tool geometry (after Chandrasekar *et al.* [25])

Orthogonal cutting was done by turning a thin walled cold-drawn brass tube (Brass 332) (50 mm outer diameter and 1.65 mm wall thickness), with a sapphire tool having a rake angle of –5° and a clearance angle of 5°. The tool geometry and sharpness of the cutting edge enabled the entire tool-chip interface, including that near the cutting edge, to be optically resolved at high resolutions. The cutting conditions used were a feed rate of 50 µm/rev, depth of cut of 1.65 mm (equal to the tube wall thickness) and cutting speed in the range 50–200 m/min. The accuracy of temperature measurement by IR pyrometry was found to be limited, not by the camera but by the accuracy with which the emissivity of different regions of the chip-tool interface can be determined. The emissivity of ordinary mild steel surfaces is between 0.2 and 0.39 while the emissivity of highly polished steel surfaces can be as low as 0.066.

Figure 2.6(c) shows the measured temperature field along the rake face of a sapphire tool when cutting Brass 332 at 90 m/min. This temperature field is obtained by averaging 24 individual temperature contours that were generated in the manner described above. The cutting width is 2 mm and is represented by the entire horizontal axis on the plot. The temperatures of points at the same distance from the cutting edge are seen to be reasonably uniform across the middle of the contact region. However, some of the uniformity is lost near the lateral edges of the tool-chip contact because of the effects arising from stray radiation at the edges. Due to symmetry introduced by orthogonal cutting, observation of the lateral face of the tool can be interpreted as the temperature distribution in the median plane of the tool. Thus Chanrasekar *et al.* verified that, in spite of the fact that the cutting width is smaller than the tool width, the thermal loss due to a slight shift between the edge of the chip and the edge of tool is negligible.

Farther away from the cutting edge, a distinct zone of high temperature could be

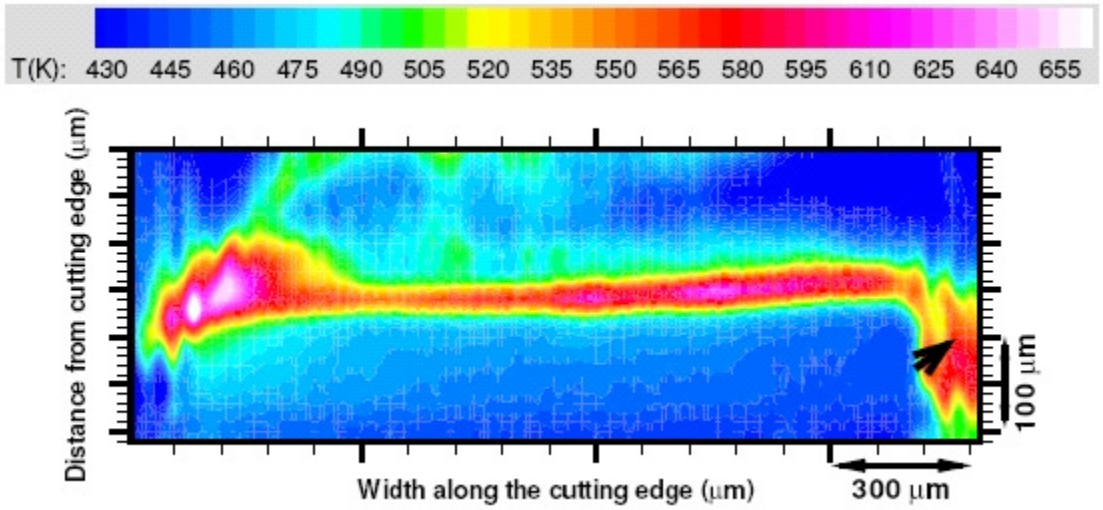

Fig.2.6(c) Rake face temperature field of the chip-tool contact region after machining Brass 332 at a cutting speed of 90 m/min, a feed rate of 50 μm (after Chandrasekar *et al*. [25])

observed along the rake face (Figure 2.6(c)). Similar zones of high temperature were also clearly visible along the lateral (or transverse) edges of the tool-chip contact in this figure. Chandrasekar *et al.* [25] found the temperature field to be relatively uniform, though temperature values were seen to increase slightly with distance from the cutting edge, in the zone of intimate, but retarded, sliding contact adjoining the cutting edge.

M'Saoubi *et al* [11] used an infrared charge coupled device (IR-CCD) camera to determine temperature distribution at the cutting edge of the tool. Experimental setup similar to Figure 2.5(a) was used. Special filters were used to cut the visible radiation range of 0.4-1.1 μm to 0.4-0.8 μm. The camera had 510 x 492 pixel array and 40 μs integration time. AFNOR 32CDV12 (HV270) steel was machined with a cermet tool for cutting speeds ranging from 100 m/min to 400 m/min and for feeds ranging from 0.15 mm/rev to 0.3 mm/rev. Rake angles of 0°, 8° and 10° and cuttings width values of 3 mm and 6 mm were used.

Figure 2.7 shows temperature distribution on the side of the cutting tool obtained as the cutting speeds from 100 to 400 m/min. The maximum temperature point is located on the rake face at the tool/chip interface. The morphology of the thermal map does not change significantly with cutting speed. However, a clear increase in temperature of the hot point is observed. This value reaches 750°C at 100 m/min to 850°C at 200 and 300 m/min and 950°C at 400 m/min.

Inframetrics Thermacam Model PM380E infrared camera was used by O'Sullivan and Cotterell [17]. The IR camera had 256 x 256 array PtSi detectors. Carbide inserts with a rake angle of 7° and a nose radius 0.35 mm were used. The workpiece used was an aluminum alloy (6082-T6) (150 mm diameter and 5 mm wall thickness). The workpiece

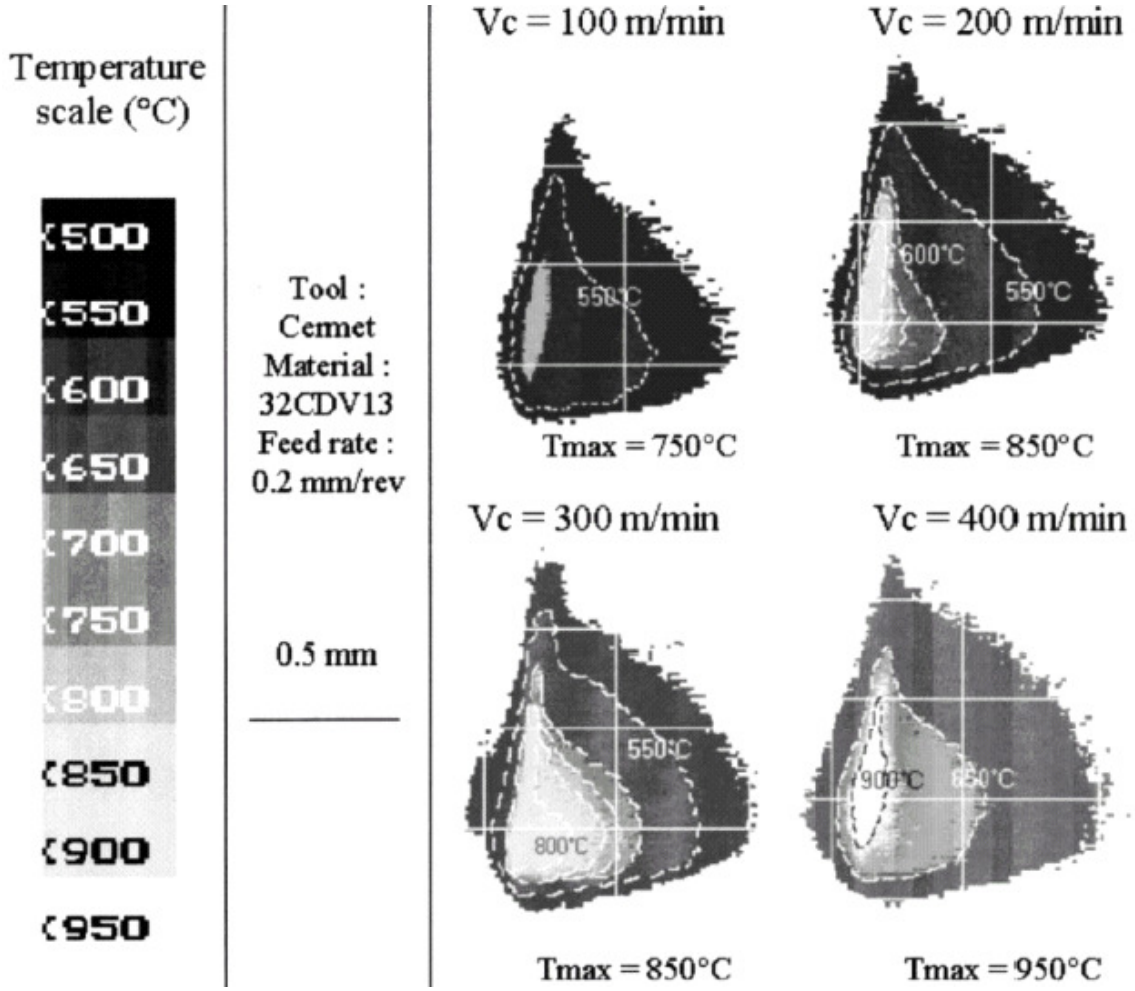

Fig.2.7 Influence of the cutting speed on the thermal map (32CDV13 steel, cermet tool) (after M'Saoubi *et al.* [11])

was painted with black matt paint of known emissivity 0.89. They used IR camera to measure temperatures of a newly generated workpiece surface. Figure 2.8 shows the schematic of experimental setup used by O'Sullivan and Cotterell [28]. The IR camera was placed on diametrically opposite side of the tool. They found that increased cutting speeds resulted in decreased cutting forces and lower workpiece temperatures.

Jaspers and Dautzenberg [18] and Jaspers *et al.* [19] used IR camera to measure temperatures during machining of SAE 1045 steel and aluminum AA6081-T6 in tubular form. SAE 1045 was machined at feed rates of 0.1, 0.2 and 0.4 mm/rev, and cutting

speeds of 2 m/s and 4 m/s. Cutting width was kept as 4 mm. The spatial resolution of the camera was 350 µm. The chips produced were continuous and straight. The IR camera was placed straight above the rake face of the tool to measure the temperature on the free side of the chip. Images were selected out of continuous film for each experiment.

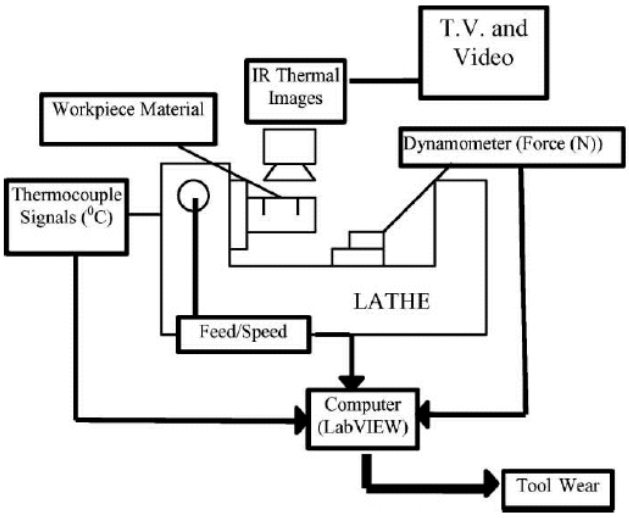

Fig.2.8 Schematic of machining setup (after O'Sullivan and Cotterell [17])

Davies *et al.* [20, 21] used a custom built infrared imaging microscope with a 0.5 mm square target area, and having a spatial resolution of less than 5 µm to measure the temperature fields at the tool-chip interface during the steady state, orthogonal machining of SAE 1045 steel tube. The camera had an Indium Antimonide (InSb) 128 x 128 focal plane array with an all-reflective microscope objective. The experiments were conducted on diamond turning lathe. Figure 2.9(a) shows experimental system used by Davies *et al.* [20]. The workpiece used was 101. 5mm diameter and 1.5 mm thickness.

The cutting speeds used by Davies *et al.* [20] were 192 m/min and 222 m/min the feed rates were varied from 266 µm/rev to 554 µm/rev and the uncut chip thickness from 23 µm to 48 µm. The rake angle was kept 0°. The image shown in Figure 2.9(b) was generated from fifty frames measured at approximately 0.25 seconds intervals during a

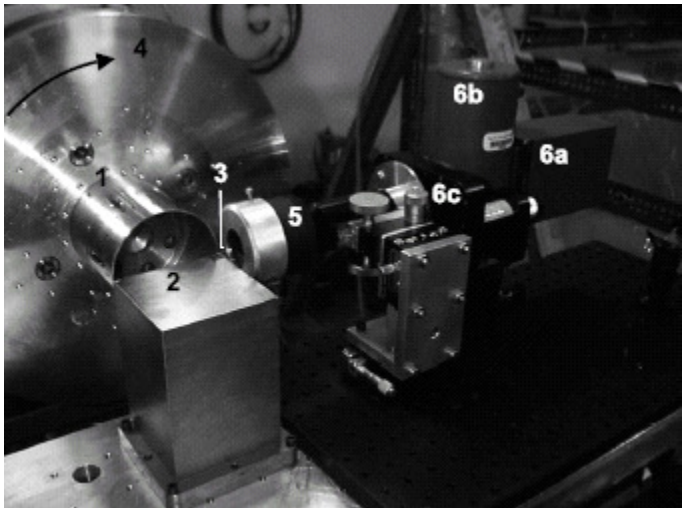

Fig.2.9(a) Experimental system for measuring machining temperatures in orthogonal cutting
1. polished SAE 1045 steel tube; 2. monolithic steel tool post; 3. tungsten carbide cutting tool insert; 4. diamond-turning class air-bearing spindle; 5. 15x reflecting objective; 6. thermal imaging camera consisting of focal plane array (a), nitrogen container (b) and wavelength notch filter (c) (after Davies *et al.* [20])

single experiment. Nine of these fifty frames were corrupt due to passage of a burr through the cutting region.

Figure 2.9(b) shows the mean of these 41 temperature measurements. The high temperatures shown in the region bounded by the workpiece and chip free surfaces are the result of imaging of the ‘‘free’’ surface of the chip. Such an effect could result from: 1. bulging of the back side of the chip during machining, 2. slight misalignment between the tool cutting edge and the optical axis of the microscope, and 3. stray and reflected light. This hypothesis is consistent with the apparent ‘‘kinks’’ in the isotherms, which indicate a transition from the side image of the chip to the back surface image. The heat transfer is dominated by conduction in the tool and mass transfer in the chip. Hence, the magnitude of the thermal gradients is much greater in the chip than in the tool. Ten such

independent measurements were made at each set of conditions, the mean temperatures of which are shown in Figure 2.10.

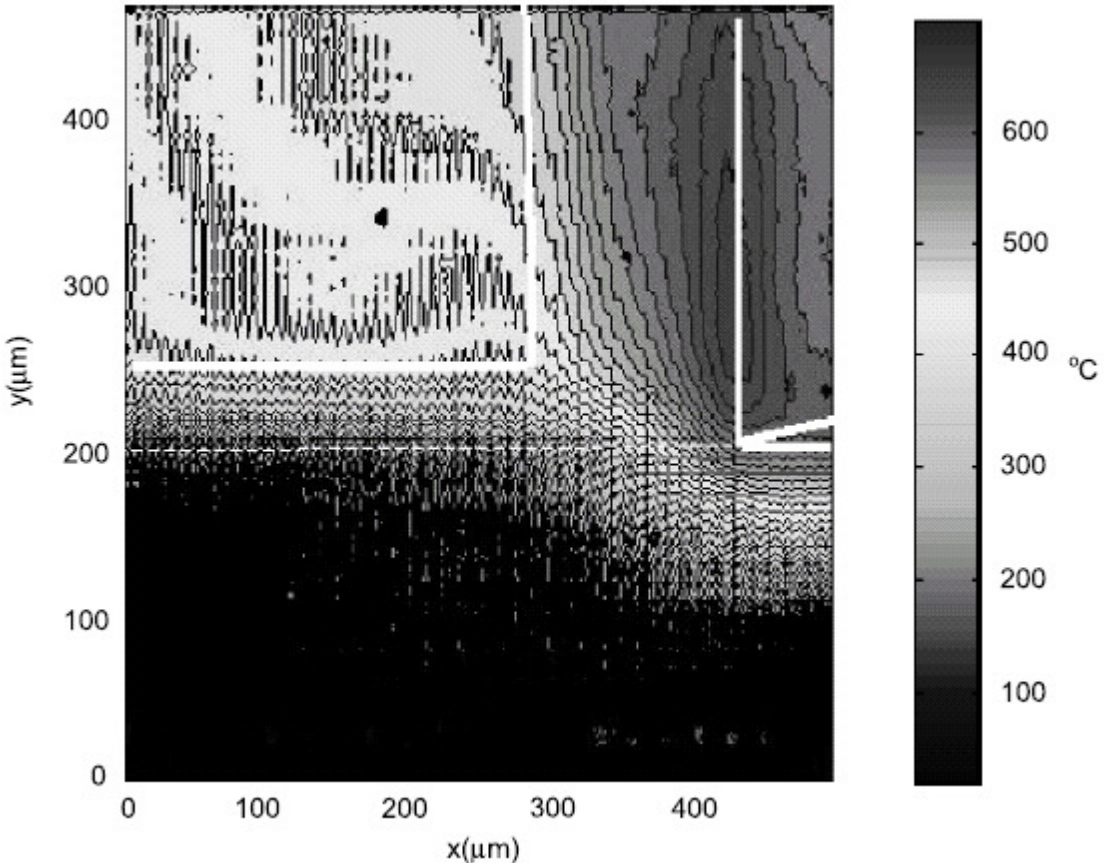

Fig.2.9(b) Mean of 41 thermal measurements of steady-state machining of SAE 1045 Cutting conditions: feed: 341 µm/rev, uncut chip thickness: 37 µm, cutting speed: 3.2 m/s, chip width: 1600 µm (after Davies *et al.* [20])

Miller *et al* [22] measured temperatures in orthogonal machining of SAE 1025 steel with a 15° rake tool having a chip deflector. A continuous rectangular chip was produced for all tests conducted. The feed rate used was 0.102 mm/rev, depth of cut was 0.102 mm, and cutting speeds were varied from 1.78 m/s (106.8 m/min) to 3.40 m/s (204 m/min). The IR camera was set on broader band spectrum, 3-14 µm and was set normal to the target surface. The cutting tools were preheated in a furnace over 500 °C to uniformly darken the target surface and prevent any emittance change during the test. The

imaged were recorded on VHS at a rate of 30 Hz and the contact length of the chip was measured using the video microscope.

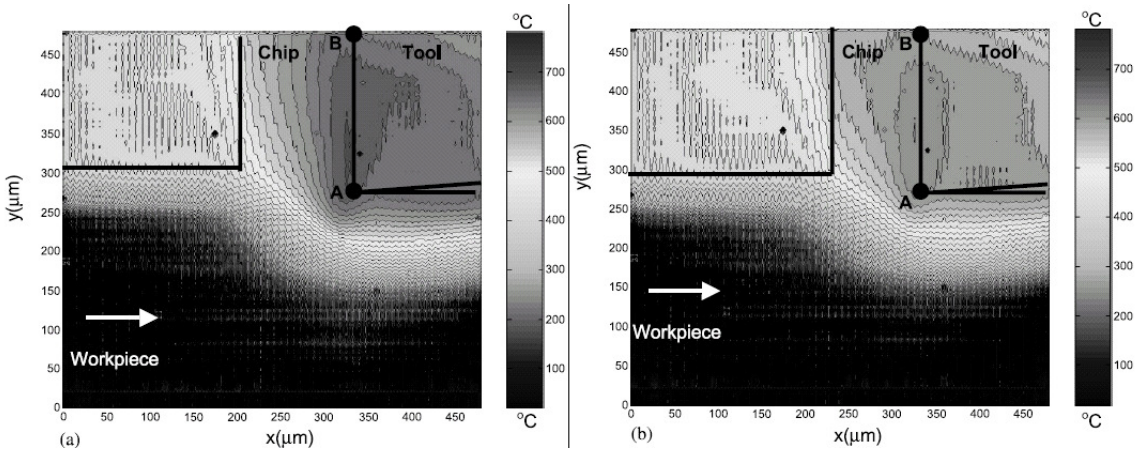

Fig.2.10 Mean of 10 independent thermal measurements of steady-state machining of SAE 1045. Cutting conditions:
(a) Feed: 358 μm/rev, uncut chip thickness: 31 μm, cutting speed: 3.7 m/s, chip width: 1500 μm;
(b) Feed: 266μm/rev, uncut chip thickness: 23 μm, cutting speed: 3.7 m/s, chip width: 1500 μm (after Davies *et al.* [20])

A random sample of images was chosen from each segment of the tape between 1.0 and 5.4 seconds after the start of the test and averaged to create a matrix of temperature values. Each numeric element of the averaged data matrix corresponds to a single pixel within the image. The tool outline was superimposed on isotherm image using CAD software. Figure 2.11 shows thermal measurement machining of SAE 1025 steel at a feed rate of 102 μm/rev, cutting speed of 1.78 m/s, and chip width of 4670 μm. Figure 2.11 shows "fiducial" marks as used by Miller *et al.* [22] so as to assist location of the tool tip.

Miller *et al.* [22] concluded that IR camera technique as applied to orthogonal dry machining offers the potential to study cutting zone temperature distributions and hence

may be used to optimize many critical cutting tool parameters, such as rake angle, edge preparation, surface roughness, and coatings.

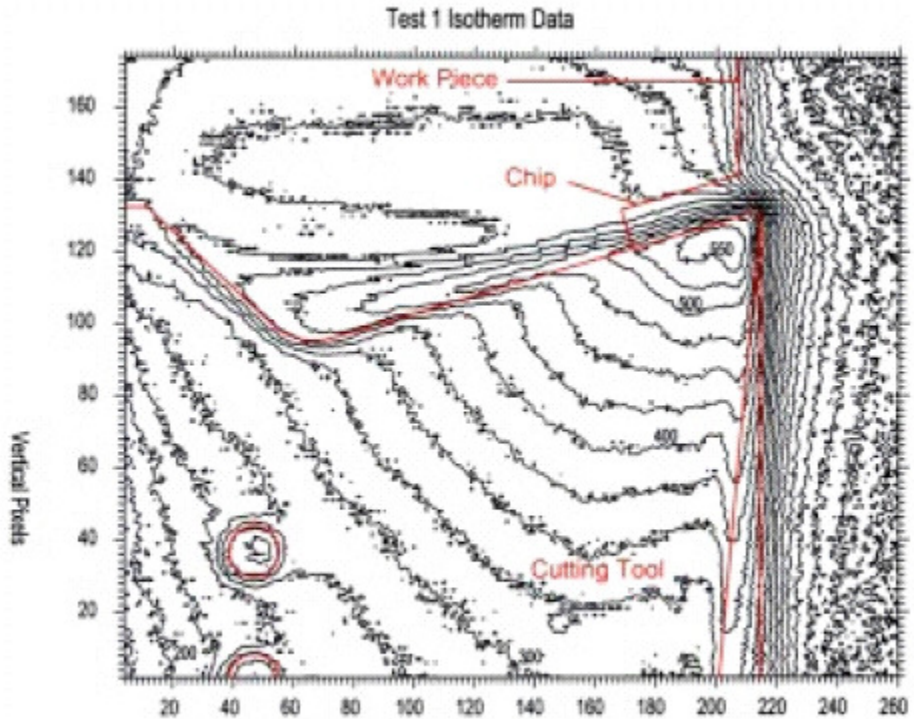

Fig.2.11 Thermal measurements of machining of SAE 1025 at a feed of 102 µm/rev, cutting speed: 1.78 m/s, chip width: 4670 µm (after Miller *et al.* [22])

Ivester and Whitenton [23] used a novel experimental approach to thermal measurement of machining by combining a high-speed infrared video camera with an infrared/visual beam splitter and a high-speed visual spectrum visual camera, as shown in Figure 2.12(a). The beam splitter enabled simultaneous imaging through the same magnification optics. They machined 7075-T651 aluminum alloy at cutting speeds of 1, 2.5 and 5 m/s, and feeds of 0.04, 0.05 and 0.06 mm/rev. The maximum and minimum temperatures for each experiment were obtained by average of the frames of infrared video for each of the experiments and then finding the maximum and minimum temperature within the field of view. These temperatures were found to be significantly different from the maximum and minimum values for the entire video of the experiment

as there was considerable variability during the cutting operation for most of the experiments. It was also noted that as the surface departs from the focal plane, the radiative intensity diminishes and temperature gradient becomes more difficult to distinguish.

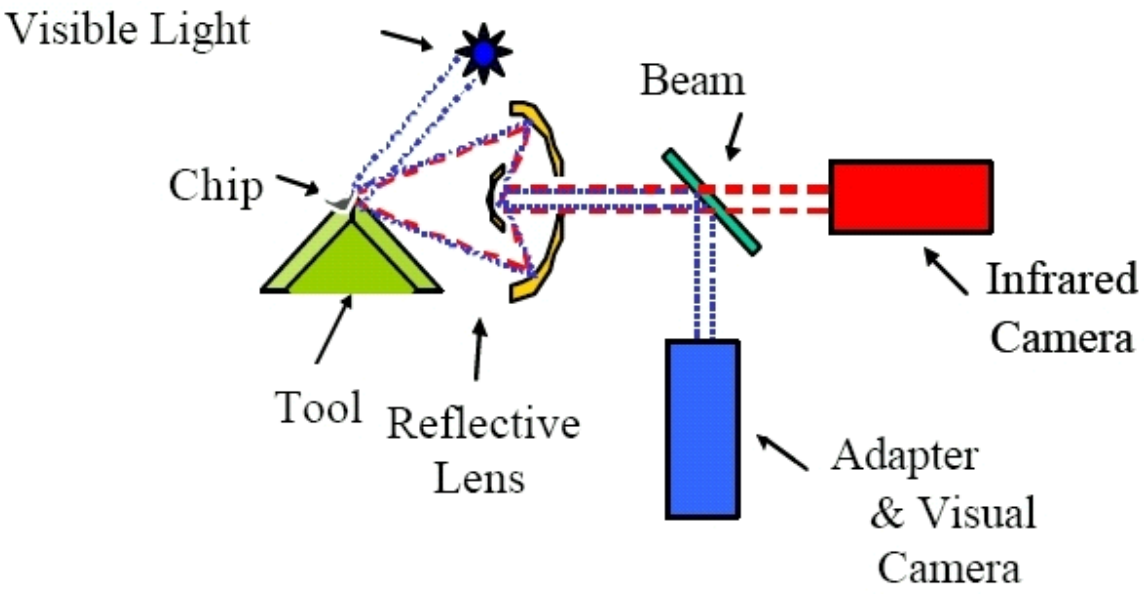

Fig.2.12(a) Schematic of the optical setup (after Ivester and Whitenton [23])

The effect of any localized features moving at workpiece speed across the field of view, such as a burr or edge or irregularity were removed by averaging the frames together. Figure 2.12(b) shows some of the temperature isotherms obtained by Ivester and Whitenton [23].

Ivester and Whitenton [23] concluded that the fidelity of the thermal profiles improved with increase in cutting speeds and feeds. The contours for many of the frames from the lower speed experiments differed significantly from their respective averages and from general expected shape. The decrease in fidelity of the thermal contours with decreasing feeds suggests that lower chip thickness lead to more rubbing, smearing and greater burr formation.

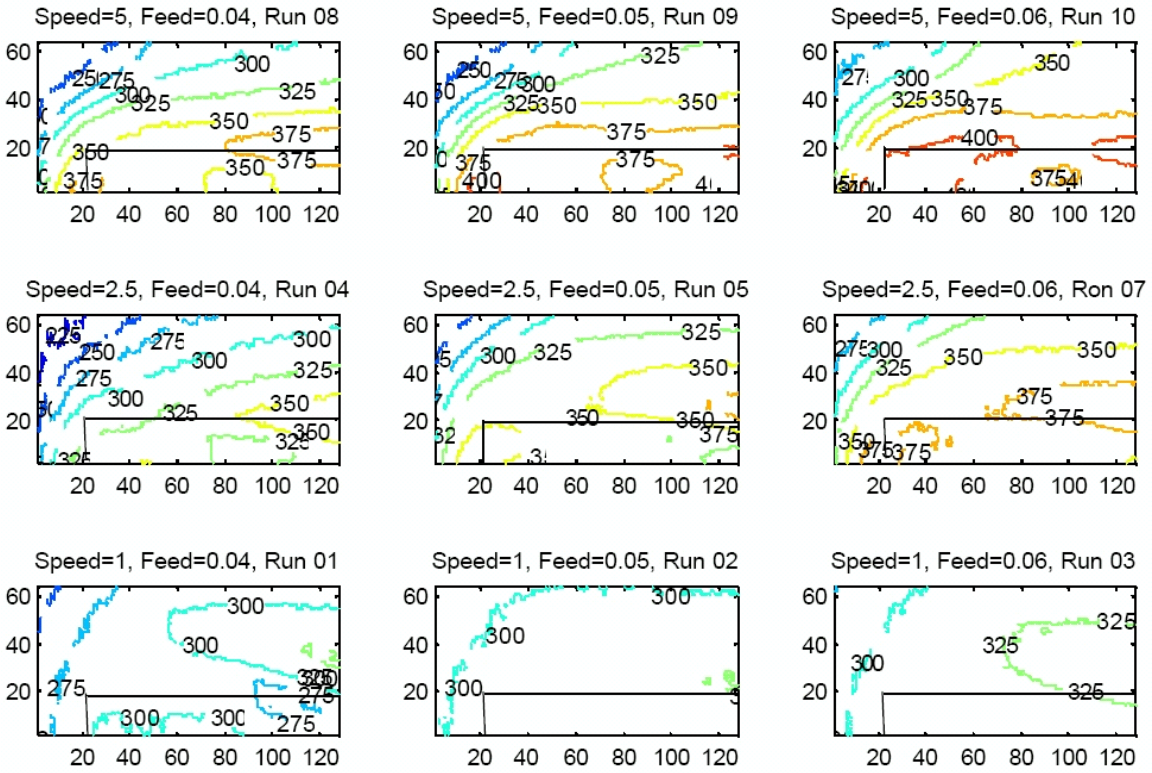

Fig.2.12(b) Thermal contours in °C with X and Y axes in µm for given speeds in m/s and feeds in mm/rev observed in machining of 7075-T651 (after Ivester and Whitenton [23].)

Vernaza-Pena *et al.* [24] used a stationary, focused, linear array of high speed HgCdTe infrared detectors to measure temperature distribution at the surface of 6061-T6 aluminum alloy and SAE 1018 steel at cutting speeds of 10 to 100 m/s. Orthogonal machining was achieved by using a modified Hopkinson bar as shown in Figure 2.13(a). The width of cut was 10.1 mm and length of cut was 10.1 mm. The cutting tools had rake angles of –5, 0, 5, 10 and 15° and width of 14.3 mm, which made them slightly wider than the specimens and ensured orthogonal cutting conditions. Figure 2.13(b) shows the temperature field for SAE 1018 steel, -5° rake angle, 0.26 mm depth of cut, 2.43 mm width of cut, and 29.8 m/s cutting speed. Sutter *et al* [26] used an experimental setup similar to Figure 2.13(a) for machining experiments on 42CrMo4 workpiece with a TiCN coated cemented carbide tools.

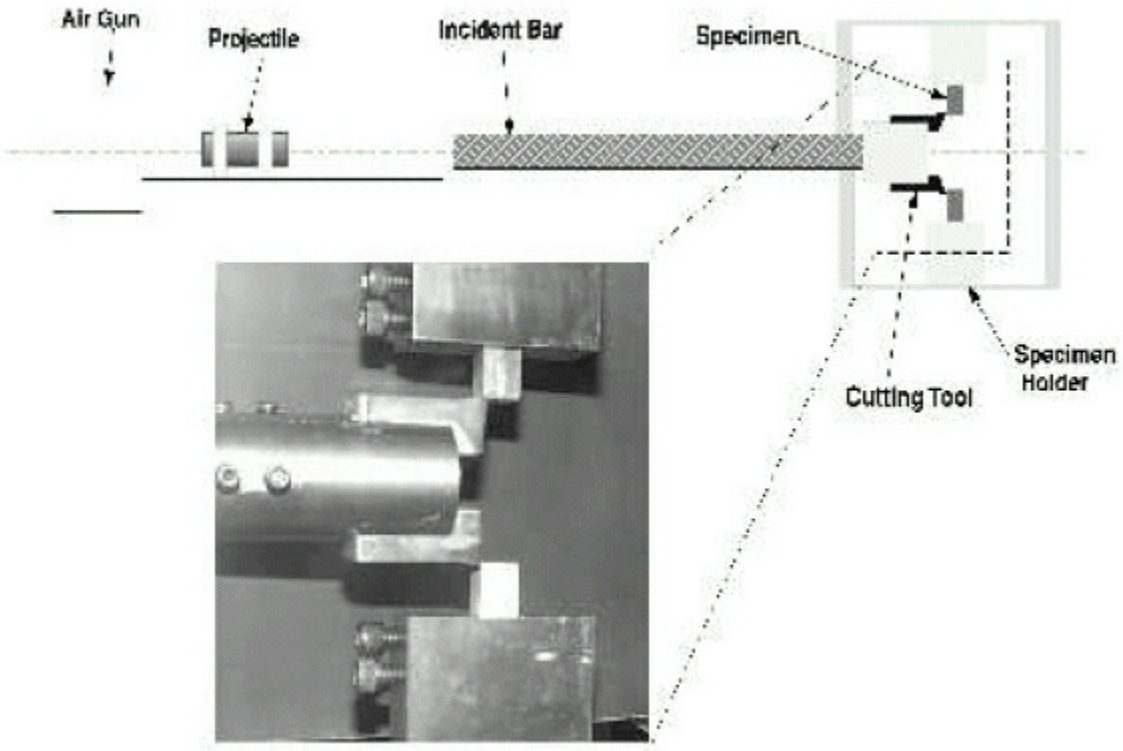

Fig.2.13(a) Schematic and a photograph of the orthogonal machining using a modified Hopkinson bar apparatus (after Vernaza-Pena *et al* [24])

Figure 2.14 shows schematic of experimental setup used by Rech *et al.* [27]. 42CrMo4 (SAE 4142H) workpiece was dry machined at a cutting speed of 200 m/min, a feed rate of 0.15 mm/rev. Radial orthogonal machining setup was used for the purpose.

M'Saoubi and Chandrasekaran [28] machined SS2541 workpiece with a cemented carbide tool having 6° rake angle to investigate the effect of tool geometry. Cutting speeds were in the range of 100-400 m/min and feeds in the range of 0.05 to 0.2 mm/rev. The tests were conducted for durations of 10-15 s.

A series of images of the lateral face of the parting tool were recorded during the test from the time-based acquisition software that monitors the IR-CCD camera. Measurements were restricted to steady state temperatures. The tool temperature map on the lateral face of the insert was plotted off-line.

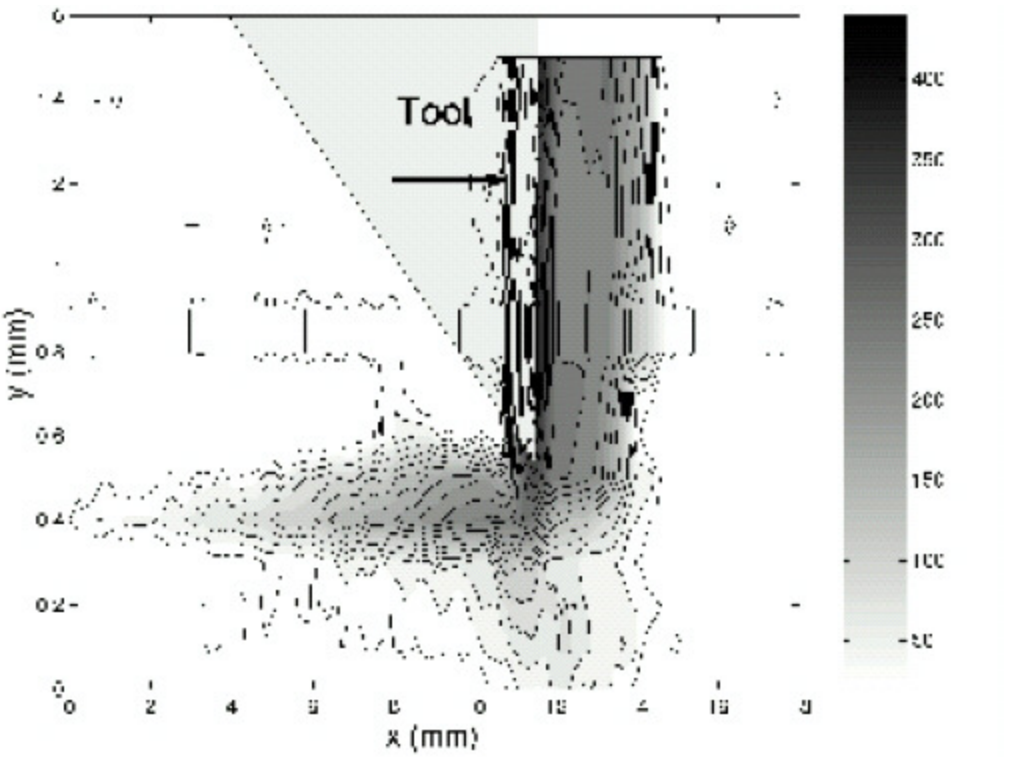

Fig.2.13(b) Temperature field for SAE 1018 steel. Cutting conditions: -5° rake angle, 0.26 mm depth of cut, 2.43 mm width of cut, and 29.8 m/s cutting speed (after Vernaza-Pena *et al* [24])

The appropriate technique for a machining problem depends on the situation under consideration, such as the ease of accessibility of the sensor to the location of the subject, spot size, dynamics of the situation, accuracy needed, cost of instrumentation, advancements in sensor technology, and data collection and analysis.

As can be seen from above literature review IR cameras of several types were used in several ways to measure temperatures in orthogonal machining. Mostly a turning operation was used for machining experiments although use of shaper-like [15] arrangement and modified Hopkinson bar [24] have also been reported.

The workpiece material used was mostly mildsteel (for example SAE 1018 steel) [13, 24] or aluminum (for example 6082-T6 [17]), although some studies were performed

on alloy steels (for example SAE H13) [10] and (SAE 4142H steel) [26, 27] and Brass [25].

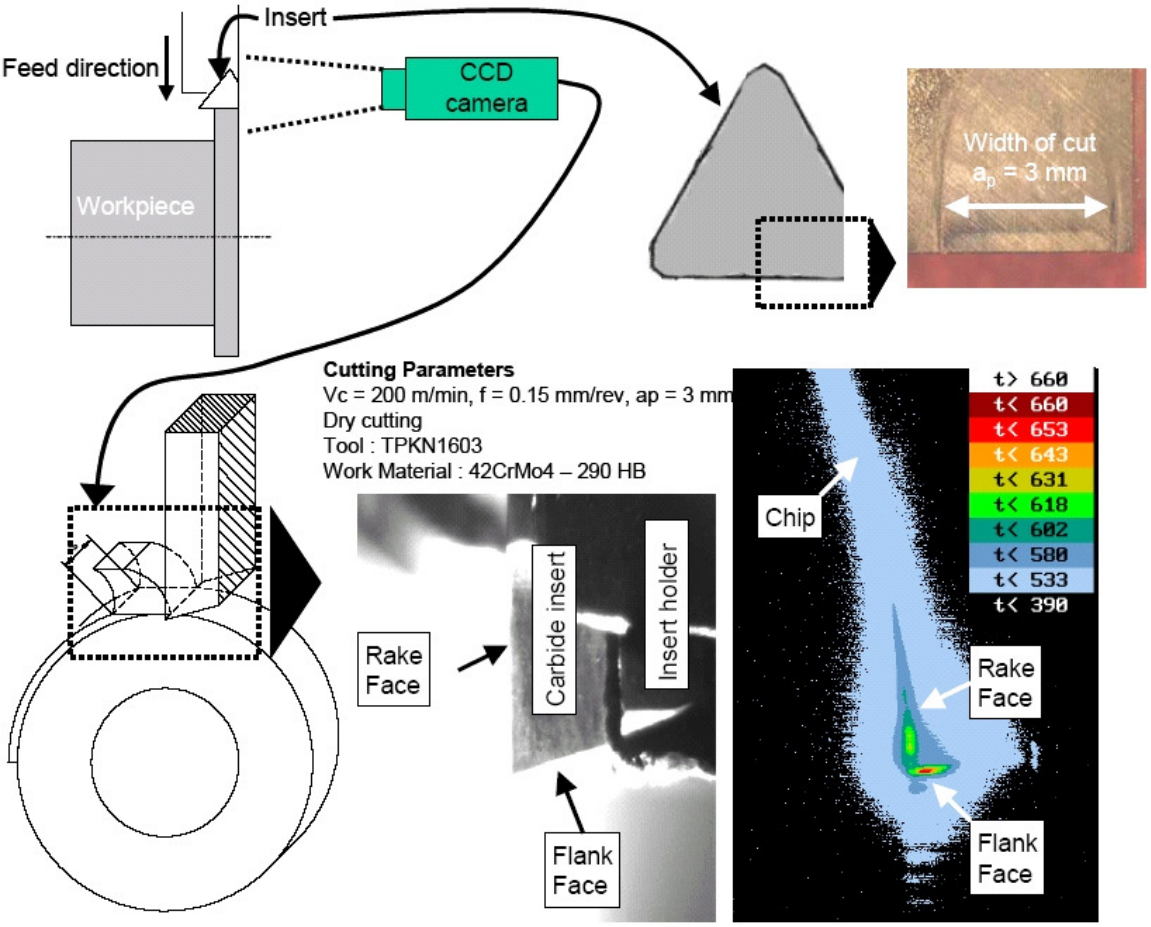

Fig.2.14 Schematic of Tool-chip interface temperature measurement and output obtained thereof (after Rech *et al* [27])

The orthogonal machining setup similar to the one as used by Boothroyd [6] [Figure 2.2(a)] was used in most other experiments. Cutting velocities in turning were used in the range from 50 m/min to 400 m/min depending on the stability of the machining system and ability of the temperature recording system. Cutting feed rates were used in the range of 0.05 mm/rev to 0.554 mm/rev. Feed rates were kept low, typically 0.05 mm/rev, in ultraprecision machining. Width of cut was found to be 2 mm to 10 mm, but was typically kept at 2 mm to 5 mm. Rake angles were varied from –30° to

20° were used. Tests were typically conducted for durations of 5 s to 15 s. The smallest resolution used was 2 µm.

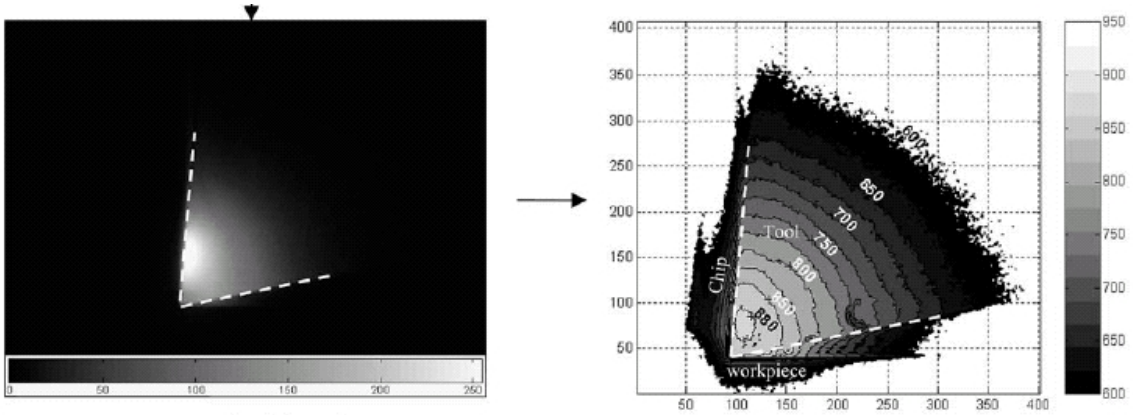

Fig.2.15 Thermal map in machining SS2541 workpiece at 200 m/min and feed 0.15 mm/rev (after M'Saoubi and Chandrasekaran [28])

Sapphire can be effectively used in the wavelength region of 2-5 µm because it is optically transparent to IR [25]. Integration times used for IR camera were in the range of 2 to 40 µs, and images were recorded at frequencies of 4 to 1500 Hz. Focal Plane Arrays were found to have minimum size of 64 x 128 and maximum of 752 x 582. In almost all the cases, the data and images obtained from the camera were post processed to obtain temperature maps. This involves averaging of multiple images, emissivity compensation, and superimposition of tool chip geometry and generation of temperature contours.

2.8 Advantages and Limitations of Infrared Camera Technique

Infrared camera is used by recent investigators because

1. It is a completely passive technique, requiring no external source of illumination.

2. Ideal for detection of areas of different values of emissivity in the same scene.
3. It is real-time, rapid response and remote sensing technique.
4. It facilitates 2D data acquisition.
5. It can be used to cover a large temperature range.
6. The experimental setup is relatively simple and portable.
7. The output can be obtained as video signal.

It should, however, be noted that thermographic cameras measure "radiated" energy from the solid surface only (~25.4 μm deep). So, practically, all infrared cameras measure and record only the radiation from the surfaces in the field of vision. Thus in case of the chip the camera measures the temperatures on the side of the chip. As verified by investigation of Young and Chou [12] the temperatures on the side of the chip are about 5% lower than temperatures at mid section of the chip.

Another limitation of using infrared camera is the presence of infrared "halo" in images. This halo is due to presence of the infrared radiation. The presence of this halo becomes more predominant with increasing temperatures. This poses practical difficulties in locating the actual physical boundaries of the object being viewed; more about this is written in Section 6.2.

There exists one more limitation of using infrared technique (film or camera). The infrared measurements can be done in pre-selected range of temperatures. Temperatures lower and higher than this range are not sensed by the infrared device. Hence, before post processing the data, tests are required to be conducted on more than one temperature

ranges. And the images with best temperature resolution for selected condition are used for analysis purpose.

CHAPTER 3

PROBLEM STATEMENT

The first objective of the present investigation is to use an infrared camera to observe, record, and analyze temperature fields generated in orthogonal machining of steel on a lathe. This includes fabrication of the camera mounting fixture, machining sapphire mounting window and tool holders and measurement of the workmaterial emissivity, developing procedures for post processing the temperature field data obtained using the camera. The present infrared camera setup has a coarse (40μm) spatial resolution which is inadequate to measure shear zone temperatures and hence this investigation specifically focuses on temperature fields in the tool and the chip.

The second objective is to perform orthogonal machining tests on a steel workmaterial at different cutting speeds and record temperature isotherms using an infrared camera.

The third objective is to measure forces, using a three component dynamometer, in orthogonal machining of steel. This includes machining a mounting block for the dynamometer and a tool clamping plate for measuring forces at different cutting speeds.

The fourth objective is to compare the experimental results with those obtained using an analytical model and simulations using a commercial FEM software (AdvantEdge) to develop a certain level of confidence in the infrared camera experimental technique.

CHAPTER 4

EQUIPMENT

4.1 Introduction

In 1800 Fredrik William Hershel accidentally discovered infrared radiation [32]. Figure 4.1 shows the infrared region at high wavelength end of the visible electromagnetic radiation spectrum.

Infrared region (Figure 4.1) is broadly divided into three parts: the near infrared (0.7-1.5μm), the middle infrared (3-5μm), and the thermal infrared (far, >5.5). The sources of infrared can be divided into three groups, based on their mass:

1. Subatomic particles, such as electrons whose "jumps" supply most of the radiation in the near infrared.
2. Atomic particles whose movements produce the intermediate (mid) infrared.
3. Molecules whose vibrations and rotations generate radiation in the far infrared.

All particles continually emit radiation at a rate and with a wavelength distribution that depends upon the temperature of the object and its spectral emissivity.

4.2 Merlin^{TM} Mid Camera

Merlin Mid is a mid-wavelength infrared (MWIR) high-performance camera manufactured by Indigo Systems Corporation (See Figure 4.2 and Table 4.1 for details).

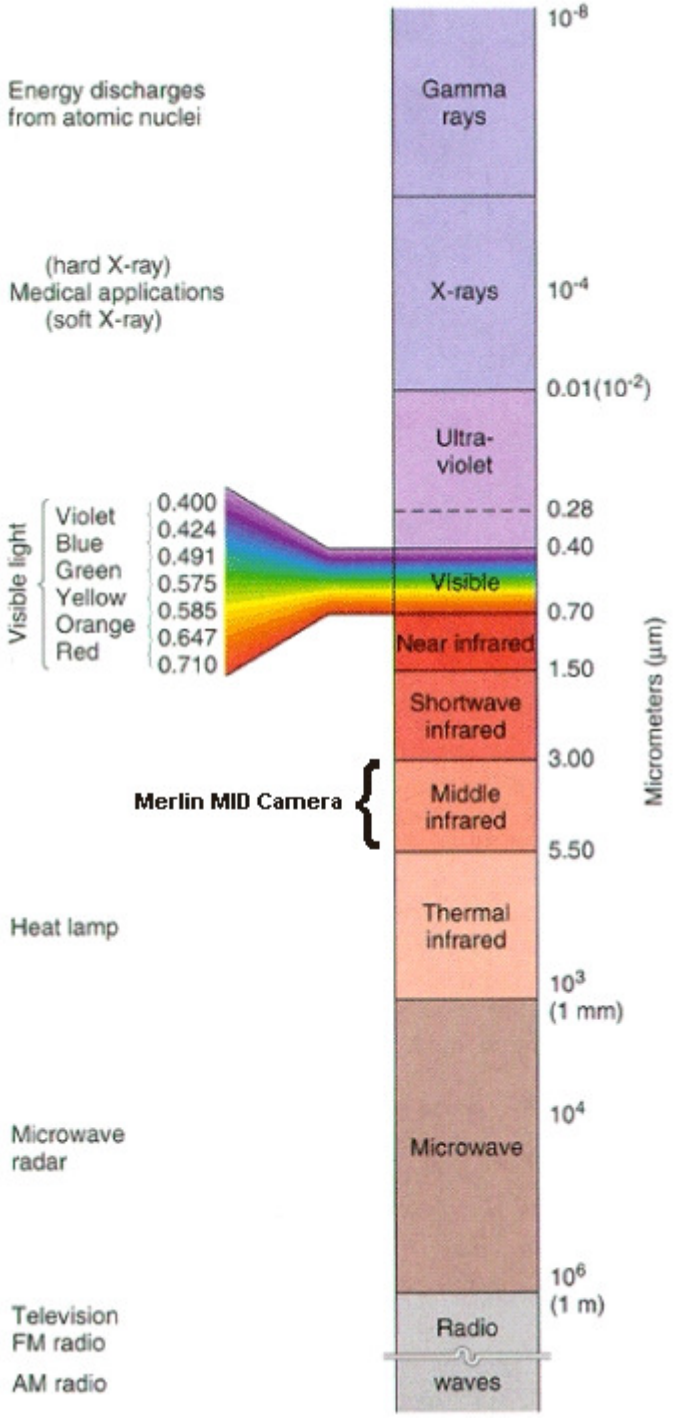

Fig.4.1 Electromagnetic Radiation wavelengths and regions

The Merlin-MID (as compared to other IR cameras in the family) can detect minute temperature changes within a scene. Temperature differences as small as 0.018 °C are easily distinguished by the indium antimonide sensor in the Merlin Mid. Higher signal-to-noise ratio in reduced frame rate modes of 30 or 15 Hz, integration times as long as 33 and 66 ms, respectively, can be achieved.

Table 4.1 Merlin Mid MWIR Camera Specifications [40]

Detector Type	InSb (Indium Antimonide)	
Spectral Range	1 - 5.4 µm (3 - 5 µm set by cold filter)	
Detector Size	30 x 30 µm	
Array Format	320 x 256	
Integration Time	5 µs - 16.5 ms	
Camera f/#	2.5 or 4.1	
Cooling Type	Integral Stirling	
Analog Video	NTSC @ 30 Hz (PAL @ 25 Hz optional) S-Video	
Digital Video	60Hz (50 Hz PAL), 12-bit	
Remote Control	Button Panel & RS-232	
Size	140mm H x 125mm W x 250mm L	
Weight	4Kg	
Temperature Measurement		
Standard	0-350°C	
Extended	300-2000°C	
Accuracy	2°C or 2%	
	Temperature Range (°C)	Integration Time (µs)
NUC 0	2 to 68	2000
NUC 1	44 to 123	400
NUC 2	111 to 231	80
NUC 3	221 to 425	10
NUC 4 (ND2)	380 to 765	200
NUC 5 (ND2)	600 to 1600	20

Fig.4.2 Merlin^{TM} Mid InSb Mid Wave Infrared Camera, Ref.[40]

The camera consists of a Stirling-Cooled Indium Antimonide (InSb) focal plane array (FPA) built on an Indigo systems' ISC9705 Readout Integrated Circuit (ROIC) using indium bump technology.

To achieve maximum thermal sensitivity, a two-dimensional array of detectors is used, with sufficient number of detectors to give a one to one correspondence with the desired number of picture points in the scene. Such an array is called staring array.

The FPA is 320 x 256 matrix or staring array of detectors that are sensitive in the 1.0 µm to 5.4 µm range. The standard camera configuration incorporates an inbuilt cold filter that restricts the camera's spectral response to the 3.0-5.0 µm band. The FPA is enclosed in an all-metal evacuated dewar assembly cooled by a closed-cycle Stirling cryocooler, and is thermally stabilized at a temperature of 77K [40].

Merlin's signal processing electronics control the FPA, create timing and bias signals, perform analog-to-digital (A/D) conversions, non-uniformity correction, replaces bad pixels, automatically controls the brightness and contrast of the display video when commanded (including histogram equalization for image display enhancement), output and analog video data and perform interface functions with external camera components. By design, Merlin is operated by a remote button panel. The camera chassis supports

quick connect/disconnect optics. A real-time, 60Hz, 12bit digital data stream is one of the camera's standard output formats.

The camera operates on a single power input of 24 V DC, which is provided by an external power supply that plugs into a wall socket. The camera consists of [30]:

- Detector/Dewar/Cooler Assembly
- FPA Support PCB
- Camera Controller PCB
- Power supply PCB
- Back Panel PCB
- Externally Mounted Remote Button Panel
- Calibration Flag Assembly

4.3 Optical Interface: Lens

Ordinary optical glass does not transmit beyond 2.5 µm in the infrared region i.e. it is opaque to the waveband of 3 to 5 µm in which Merlin Mid camera operates. It can be seen from Table 4.2 that barium fluoride, lithium fluoride, magnesium fluoride, silicon, sapphire, silicon nitride, zirconium oxide, yttrium oxide are potentially useful infrared transmitting materials.

Magnesium fluoride and alumina are used as coatings in 3 to5 µm waveband, whereas semiconductor silicon is used as lens material. Germanium is used for lenses in the 8 to 13 µm region. In the case of Merlin Mid lens, germanium has been used to color correct silicon optics as silicon/germanium doublet objective.

It can be seen that from Table 4.3 silicon has higher Knoop hardness and lower refractive index than germanium.

Table 4.2 Infrared transmitting materials (after Burnay *et al.*[31])

Type of material	3-5µm	8-13µm
Alkali halides	-	KCl, NaCl, CsI
Other Halides	BaF_2, LiF, MgF_2	KRS_5, PbF_2, ThF_4
Semiconductors	Si	Ge, GaAs, InP, GaP
Chalcogenides	-	ZnS, ZnSe, CdS, CaLaS
Others	Al_2O_3, SiN, SiC, ZrO, Y_2O_3	-

Being a semiconductor, silicon develops charge carriers and become opaque at elevated temperatures. So, it is necessary to take enough care so that the lens temperature is maintained about 295K (21°C) [31].

Table 4.3 Physical Properties (after Burnay *et al.*[41])

Material	Knoop Hardness (kg/mm^2)	Refractive index (10µm)
Ge	692	4
Si	1000	3.4
Sapphire, Al_2O_3	1370	1.59
Diamond	8000	2.4

The lens to camera interface is shows in Appendix A. The standard dewar f/number for the Merlin Mid camera is f/2.5, and the aperture is 10.52 mm in diameter.

In this investigation 100 mm Si-Ge lens (JTI-40496) manufactured by Janos Technology is used. The normal-incident reflectivity R of a non-absorbing dielectric

surface is given by R= [(n-1)/ (n+1)]², where n is the refractive index of the reflecting surface. Silicon has a refractive index of 3.4, so that 29.75% of all incident radiation is reflected by each uncoated silicon surface. It is, therefore, essential to put an antireflection coating on all silicon lenses. Hence the transmission for the lens used (3 to 5 µm) is 92%. These coatings also improve the scratch resistance and chemical durability of silicon optics. A set of four extender rings is used to focus the camera on a 12.8 mm x 10.2 mm area around the tool tip.

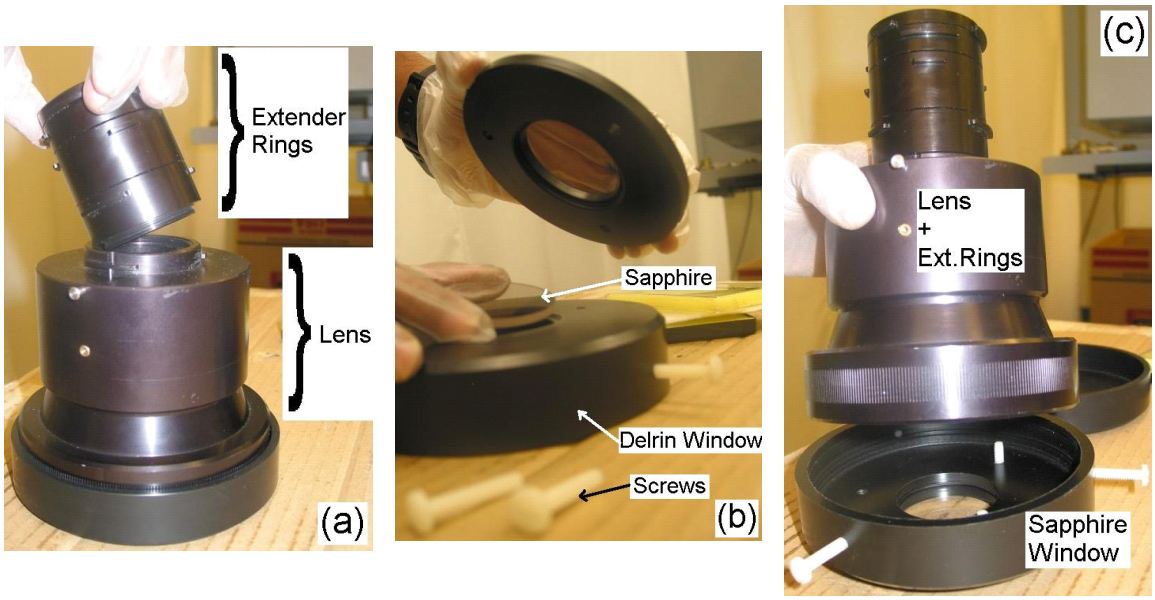

Fig.4.3 (a) Fitting extender rings on the lens, (b) Fitting sapphire in the delrin window, (c) Fitting sapphire window on the lens.

4.4 Optical Interface: Neutral Density Filter

An neutral density (ND) filter, is a type of filter designed to decrease the intensity of the input light without affecting the color (or spectral) distribution. Neutral density (ND) filter simply blocks a certain percentage of light from passing through. In other words, it is a darkening filter. The “neutral” refers to the fact that a proper ND filter does not color the light inadvertently or does not introduce any color cast to the image. Due to

this neutral characteristic, the filters appear gray in color. ND filters are typically designated by their optical density (OD). The transmission for an ND filter is given as $T=10^{-OD}$, where OD is the optical density of the ND filter. Alternatively, optical density is the log of the opacity of the filter. In the present investigation, a neutral density filter of 2 as its optical density is used (ND2). Thus by using the above formula the transmission of the ND2 filter is 0.01 or 1%. In other words, a ND2 filter blocks 99% of incident radiation and allows only 1% radiation to pass through.

ND filter in this work is used to decrease light consistently over the infrared spectrum and to protect the FPA from excessive intensity, especially for temperatures higher than 400°C. This ND filter whenever used is fixed between the extender rings and the FPA.

4.5 Optical Interface: Sapphire Window

Machining on a lathe invariably produces chips. Some of the chips dislodge and fly away from workpiece in a disorderly manner. To avoid any damage from such flying chips to the expensive lens, a protective window is required. For this purpose sapphire is considered appropriate because of its transparency to wavelengths in the Mid-IR range, (see Table 4.2).

The use of sapphire in infrared applications is confirmed by previous applications such as by Chandrasekar et al [25]. A 50 mm diameter sapphire flat with commercial optical finish on both sides is used. A mounting disc is machined from a 125 mm rod of Delrin. This disc is mounted on the camera lens using three Nylon screws.

4.6 Non-Uniformity Correction (NUC)

Infrared detectors vary in their individual response to thermal or photon energy. This variation is referred to as detector "non-uniformity". Unless some type of compensation is made, this variation in response of the individual detectors will result in a non-uniform image. Non-uniform images appear "grainy" and unclear with possible black and/or white pixels apparent.

Over time, there is a gradual change in detectors from a uniform to a non-uniform state. In most cases, where camera parameters have not been changed, it is only necessary to perform an occasional offset correction, referred to as a one-point correction, to achieve a uniform image. This is done by filling the field of view of FPA with a uniform source of illumination. The term one-point refers to performing this correction as single temperature reference point, internally updating only the offset correction coefficients. The one-point correction can be applied internally as well as externally.

The internal flag is kept disabled during external correction. External one-point correction is used in this work. It is necessary to apply correction every time NUC is changed. When one-point correction command is executed, the camera collects data from several successive image frames of the uniform source placed in the field of view. (Refer to Users Manual Section 2.3.1.3 for detailed instructions [30]). This correction is lost every time the Non-uniformity correction (NUC) table is changed.

4.7 Integration Time

The INTG_TIME function is used to change the FPA integration time, which can be varied from 10 μs to 16.6 ms. <NUP> and <NDN> buttons are used to change the

value. The integration time is not permanently stored in FLASH unless a one-point or two-point correction is performed.

The camera used in the present investigation is a microbolometer type camera. Microbolometer cameras are different from cameras that detect individual photons through photovoltaic or photoconductive means. In a microbolometer camera, individual pixels receive different amounts of thermal radiation from the scene and heat up different amounts with respect to the bolometer array substrate. The part of each bolometer that heats up is thermally isolated from the substrate so that a very small amount of input IR power results in a measurable change in the bolometer's temperature. By selecting the thermal conductance to the substrate and also selecting the thermal mass (heat capacity) of the thermally isolated bolometer, the bolometer's thermal time constant is determined. The array substrate is held at a very stable and uniform temperature so that the bolometer heats up to a specific temperature for a specific amount of input IR radiation from the scene. The amount of heating of each pixel (and thus the intensity of the IR scene) is determined by passing a known current or known voltage through a resistive element in the thermally isolated section of the bolometer. The resistive element is made from a material that changes resistance significantly with temperature. If a known voltage is applied across the bolometer's resistor for a short time, the current generated will be related to the resistance of the resistors, which in turn is related to the temperature of the bolometer, which is a direct measure of the incident IR radiation.

The length of time that the measurement (integration) current is allowed to flow through the bolometer and be collected on some type of integrating mechanism (like an integration capacitor) is the camera's integration time. Clearly, the amount of signal

collected at an integration capacitor will be proportional to the length of integration time and also the size of the current. Since higher currents result from hotter scenes, then a shorter integration time will allow hotter scenes to be imaged without saturation of the integration capacitor. Similarly, colder scenes will generate more signals on the integration capacitors if their currents are integrated longer. The reason that integration time is kept in the range of microseconds is that current passing through the resistor of the bolometer results in temporary heating of structure that is desirable to minimize. Also, the passing current for time durations allowed by the camera generates an appropriate amount of signal. This definition of integration time is fundamentally different from the integration time of a photon detector where the current to be integrated is generated directly from absorbed photons and the length of time that the photocurrent is allowed to collect on an integration capacitor is the integration time.

Unlike a camera based on a photon detector, the bolometer camera always receives input power from the scene. At the time the temperature of the bolometer is sampled by the integration current, the bolometer will have been viewing the scene for the full frame time (1/60 seconds). The bolometer's temperature right before the application of the integration current will be the result of heating that occurred over the last 16 ms. So, from the point of view of a photon detector camera, the bolometer camera "integrates" its input signal for the full frame time. Perhaps a better term for this is "Sampling Time".

The application of the integration current occurs on a row-by-row basis, not on the whole FPA. So, Merlin Mid is a rolling-mode device, not a snapshot.

4.8 Temperature Data Acquisition

The signal from the camera is received by GRAM^{TM} card fitted on a stand alone computer. The computer has Pentium III processor, 256MB RAM, 40GB HDD and Windows 2000 operating system.

In addition to the computer, a video display is used. This display is used to view the camera settings as the field of vision of the camera. The display unit receives video signal through a video cable. The display unit is equipped with a VCR so that, if need be, a video recording can be obtained.

Version 2.4.11 of ThermaGRAM Pro software with accessory Dynamite IR, developed by Thermoteknix Systems Limited is used for data acquisition from the IR camera. Dynamite IR allows full image capture of a sequence of thermal images from the infrared video camera connected to a PC of suitable specification. Dynamite IR controls the capture process and allows replaying, editing, and saving the sequences.

The recording is started manually or automatically by a trigger to an input on the GRAM card but the use of a cyclic buffer means that images arriving before the trigger can be included at the beginning of the recording. The precise number that can be included depends on the size of the buffer available.

The sequences are stored in Thermoteknix Sequence files with extension ".tdw". A recording can be made to play forwards or backwards, jump to any point in the recording or stop or pause the replay at any point and then step forwards or backwards one frame at a time. One can save a complete sequence, which can be reloaded into Dynamite IR, or individual images, which can be loaded into ThermaGRAM. An individual image is stored in TherMonitor Image format files with extension ".tgw".

ThermaGRAM is used to analyze an IR image or a series of IR images. Temperature data can be extracted using various tools. The most commonly and effectively used tool for this study is “Rectangle Tool”.

4.9 Lathe

All the experiments are performed on VECTRAX 1660 Lathe (Figure 4.4). The specifications of the lathe are given in the Table 4.4. The tool insert is secured in a custom made tool holder. The tool holder is machined from a 19 mm square bar of hot rolled SAE 1045. The rake angle is 15° and the relief angle is 5°.

A clearance angle is required so that the newly machined surface of the workpiece does not rub on tool. The clearance angle of 5° is selected because a higher angle weakens the mechanical support to the insert. The rake angle of 15° is selected because at this rake angle the chip, before separating from the tool, slides on the rake face for a distance such that it can be guided with a screw driver. This is further explained in

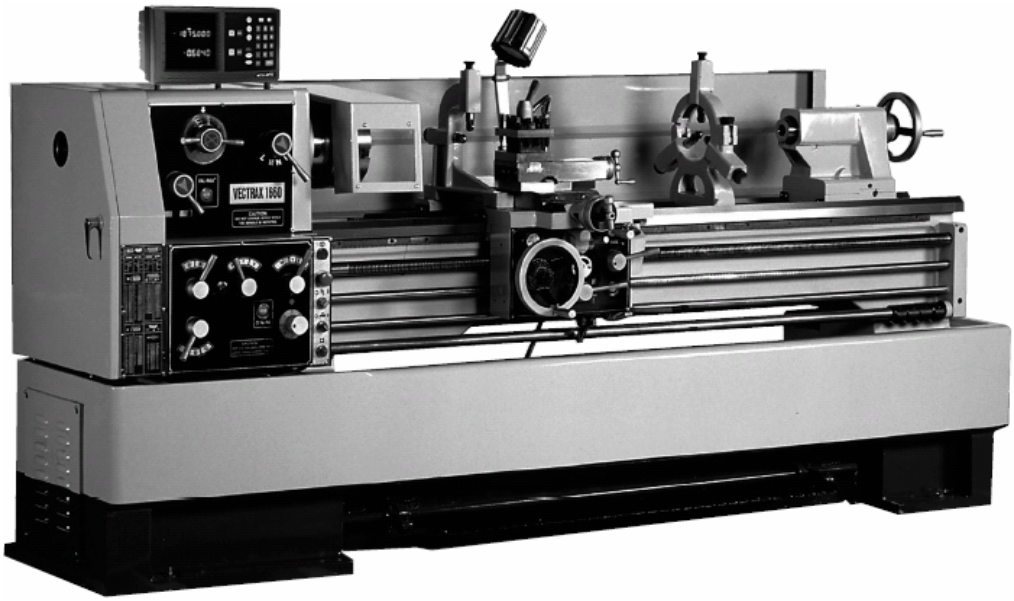

Fig.4.4 Vectrax 1660 Lathe

Section 5.6. The insert is held in place using a screw and a nut. At 15° rake about half the nut is required to be removed by grinding to maintain the clearance angle. A higher rake angle needs further grinding of the nut, which results in practically grinding the complete nut.

Table 4.4 VECTRAX 1660 Lathe Specifications

Swing over crosslide	255 mm
Number of spindle speeds	12
Range of spindle speeds	36-2000 rpm
Number of feed rate changes	32
Longitudinal feed range	0.05 - 1.5 mm/rev
Main Drive Motor Horsepower	5.6 kW (7.5 HP)

An in-house custom made tool holder is preferred over the purchased one because of the flexibility. Also, it is economical and fast to machine a new combination of rake and relief angles, which proves beneficial in the initial stages of experimentation.

The insert used is a steel grade Valenite (SECW-2.51.51) cemented tungsten carbide; the detailed specifications of which are given in Table 4.5. The choice of insert is limited due to the requirement of a square insert having a hole and no chip breaker.

An insert without chip breaker is necessary so that the chip slides some distance on the flat rake face. This condition is assumed by the analytical models used for comparison and the chip contact length remains an important input parameter. A hole is required to secure the insert in the custom made tool holder. A square insert is necessary because the camera can be used to measure temperatures on a face exactly perpendicular to the cutting edge. This face is parallel to the plane in which temperatures are predicted by the analytical and numerical methods.

Table 4.5 Specifications of SECW 2.51.51 insert

Shape	S	Square
Clearance	E	20°
Tolerance	C	+0.0127 mm -0.0254 mm
Type	W	With Hole and No Chip Breaker
Width	5/16in	7.938 mm
Length	1/4in	6.350 mm
Thickness	5/32in	3.969 mm
Nose Radius	1/64in	0.397 mm
Coating	TiN	Titanium Nitride
Grade	C5	Steel Roughing
Grade C5 Specifications [33]		
Tungsten Carbide, WC	72%	
Titanium Carbide, TiC	8%	
Tantalum Carbide, TaC	11.50%	
Cobalt, Co	8.50%	
Grain Size	Medium	
Density g/cm3	12.6	
Hardness, RA	90.7-91.5	
Transverse Rupture Strength	1.72 GPa	
Elastic Modulus, E	558 GPa	
Impact Strength	0.9 m-N	
Compressive Strength	5.17 GPa	
Relative Abrasion Resistance	13 /cm^3	
Thermal Conductivity	0.12 cal/s.°C.cm	

4.10 Dynamometer

Forces are measured using a Kistler three-component piezoelectric dynamometer (Type 9257A) (Table 4.6). It is a piezoelectric transducer for measuring forces in three components perpendicular to each other [34].

The force to be measured is introduced through the top plate and distributed between 4 three-component force elements arranged between the top and base plates. In these four force elements the force applied is broken down into its three components.

Thus for each of the three forces components a proportional electrical charge is setup in the measuring platform. These charges are lead into 5010B dual mode charge amplifiers where they are converted into proportional voltage which can be displayed or recorded, as required. The dual mode amplifier can be used with either charge mode or voltage mode. In the present investigation the amplifier is used in the charge mode [35]. The amplified signal is then received by Keithly input card fitted on a stand alone computer. The computer used for data collection has a Pentium processor, 64MB RAM, 10GB HDD and Windows 98 operating system.

Table 4.6 Specifications of 3-Component Dynamometer (Ref.[44])

Maximum measuring range Fx, Fy	-5 to 5 kN
Maximum measuring range Fz	0-10 kN
Sensitivity, Fx, Fy	-7.5 pC/N
Sensitivity, Fz	3.5 pC/N
Rigidity, Fx, Fy	~1 kN/µm
Rigidity, Fz	~2 kN/µm
Natural frequency, Fx, Fy, Fz	>4kHz
Operating Temperature	0-70 °C
Weight	6.9 kg

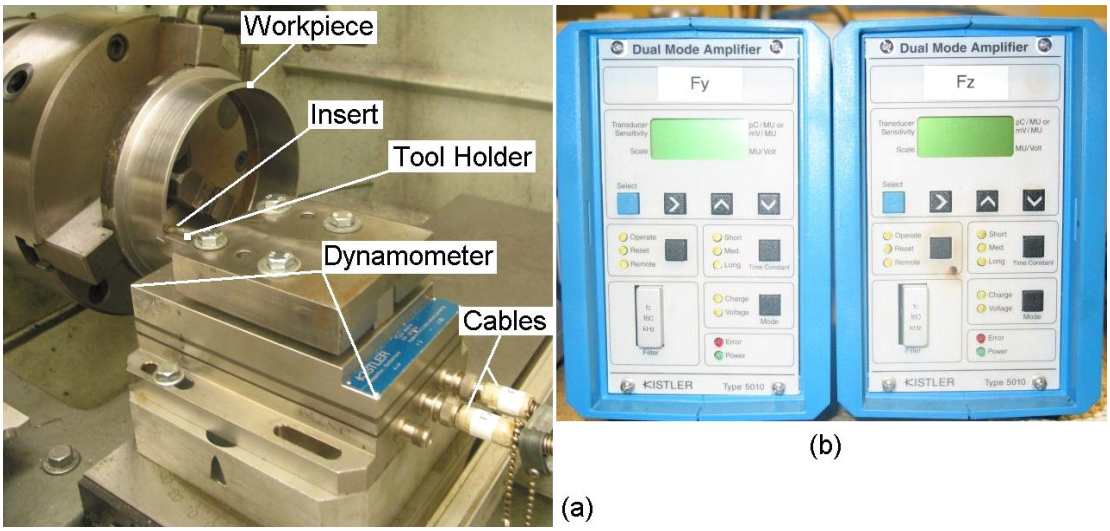

Fig.4.5 (a) Dynamometer fitted on to lathe, (b) Dual mode amplifiers used to convert electrical charges into voltage.

4.11 Radiation

Conduction, convection, and radiation are three modes of heat transfer based on their action mechanism. Thermal radiation is independent of temperature gradients and presence of a medium. It is emitted by the atomic excitation of a substance, and the radiant energy travels at the speed of light, even through vacuum, until it reaches another substance where it may be absorbed, reflected, or transmitted through the medium.

The rotational and vibrational movements of the atomic and subatomic particles within the matter produce radiation. Since atomic and subatomic particles are always in motion, physical matter always emits thermal radiation. This is true at all temperatures above absolute zero. Thermal radiation is necessarily a form of electromagnetic radiation and hence travels at the speed of light, c, given by

$$c = \nu\lambda$$

where, c = velocity of light in vacuum (2.99792458 x 10^8 m/s), υ = frequency, and λ = wavelength.

Electromagnetic waves are observed over broad range of wavelengths from 10^{10}μm for radio waves to 10^{-10} μm for cosmic rays. Thermal radiation has wavelengths in the range of 10^{-1} to 10^3 μm. Of particular interest to this experimental study is the infrared range i.e. 1 to 10^3 μm.

4.11.1 Blackbody Radiation

The radiant energy emitted by any body at any temperature varies continuously over a range of wavelengths. A blackbody is a perfect emitter and a perfect absorber of radiant energy, and is characterized as follows:

1. It has unit emissivity and absorbs all incident radiation, regardless of wavelength and direction,
2. For a given wavelength and temperature no surface can emit more energy than a blackbody, and
3. Radiation emitted by a blackbody is a function of wavelength and temperature; it is independent of the direction.

Work of Stefan (1879) and Boltzmann (1884) showed that a black surface emits radiant energy at a rate proportional to the fourth power of the absolute temperature of the surface. Radiant energy E_b of a black surface with area A is given by

$$E_b = \sigma A T^4$$

where, σ = Stefan-Boltzmann Constant (5.67051 x 10-8 W/m^2K^4) and T is the absolute temperature of the surface. Blackbody is the standard against which all real radiating surfaces can be compared.

4.11.2 Emissivity

Real surfaces are non-black and emit radiation at less than maximum. Thus

$$E = \varepsilon E_b = \varepsilon \sigma A T^4$$

The dimensionless parameter ε is called the emissivity of the surface and varies between zero and unity. A real surface has emissivity always less than unity. Studies have shown that emissivity varies with temperature [36] as well as surface characteristics, such as roughness, texture, color, degree of oxidation, wavelength, and presence of coatings [36]. An ideal material with constant emissivity is called a graybody.

The present study involves measuring temperatures using infrared radiation of real surfaces. Hence, emissivity becomes an important consideration. The temperature readily recorded by a camera is different from the real temperature of the object. The relation is given by

$$T_{camera} = \varepsilon_{object}.T_{object} + (1-\varepsilon_{object}).T_{background}$$

Since the emissivity of a real surface is always less than unity, the temperature readily recorded by the camera is always less than the real temperature of the object. To overcome this, it is necessary to recalculate the temperature using the following formula

$$T_{object} = \frac{T_{camera} - (1-\varepsilon_{object}).T_{background}}{\varepsilon_{object}}$$

While using ThermaGram this recalculation is done internally by the software after emissivity of the surface is applied to the corresponding region in the image. Whereas in the present work the temperatures recorded by the camera are extracted to a MS Excel file and temperatures are recalculated using a VBA code.

This need for recalculation necessitates the measurement of emissivity of the tool, chip and workpiece. The tool is painted with high temperature black paint having constant emissivity of 0.95. In the following chapter, on Experimental Work, more is written about the emissivity measurements of workpiece.

4.12 Calibration

The calibration of the camera was performed at National Institute of Standards and Technology, Gaithersburg, MD in cooperation with Dr. Ivester of NIST.

Before using the camera for experiments it is necessary to check the calibration of the camera so that certain level of confidence can be achieved in the temperatures measured by the camera.

A graybody with a constant emissivity of 0.99 is heated in steps from a temperature of 30°C to a temperature of 1050°C. The temperature is measured using the

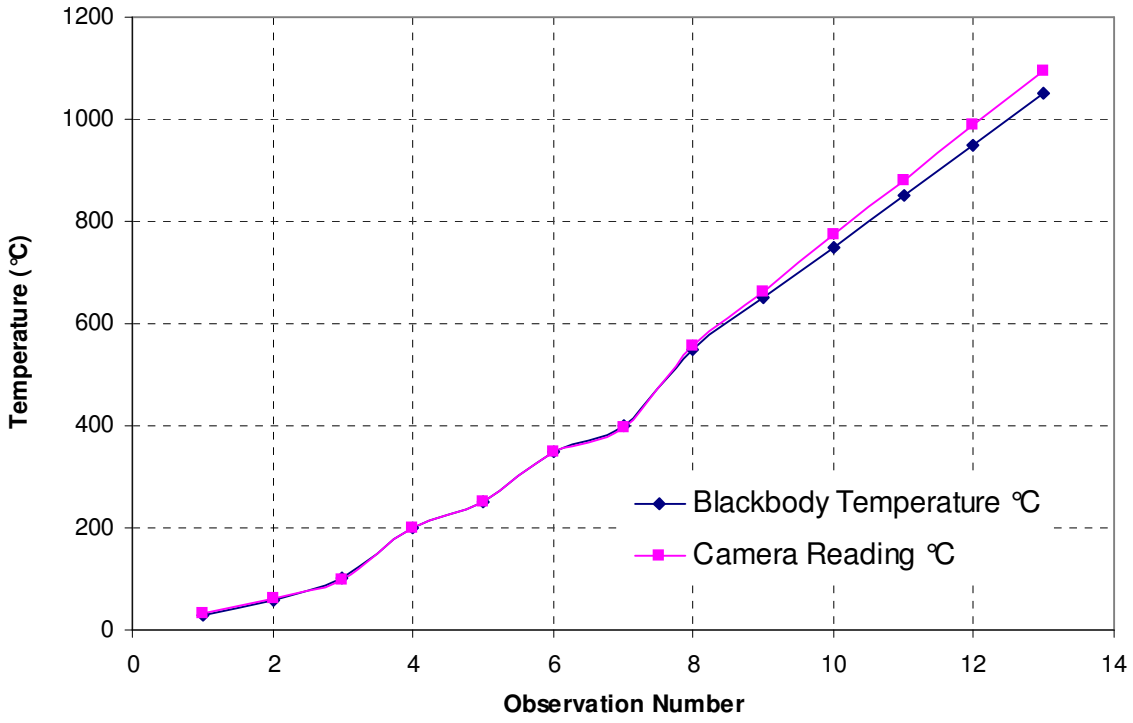

Fig.4.6 Camera Calibration plot using 100 mm lens using machining optical setup.

camera. Figure 4.6 shows the plot of graybody temperature and temperature measured by the camera. It can be noted that the temperature measured by the camera is in close agreement with that of the graybody. But at higher temperatures, the camera indicates a higher temperature. So, for temperatures higher than 600°C, a separate calibration curve was obtained in terms of the signal generated by the camera sensors. The calibration plot for higher temperatures is shown in Figure 4.7.

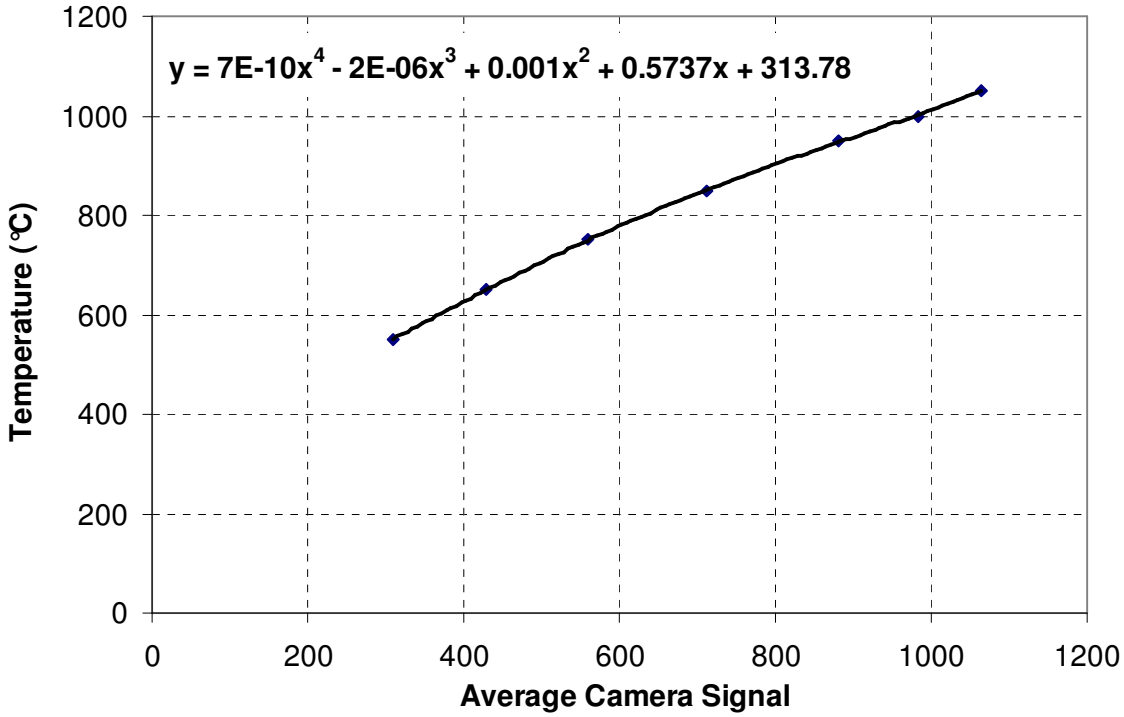

Fig.4.7 Camera Calibration plot using 100 mm lens, ND2 filter at 100 µs integration time using optical setup for machining.

CHAPTER 5

EXPERIMENTAL WORK

In the present investigation, workpiece selection is a preliminary step which involves the selection of workpiece material, type (rod or tube), outer diameter, length, and tube thickness. It can be noted from the literature review that the material most commonly used for temperature measurement in metal cutting is plain carbon steel, that too low and medium carbon steels. Also end turning of the tube is the simplest and the most effective means of performing orthogonal machining on a lathe. It was observed that for tubes having diameter greater than 165 mm the jaws extending beyond the chuck foul with the camera mounting bracket. Considering the local availability it was decided to use SAE 1015 steel tube with outer diameter of 165 mm and 12 mm wall thickness.

Another aspect of workpiece selection is the choice of wall thickness. A chip width to uncut chip thickness ratio (b/t) greater than 10 is desirable to have plain strain conditions. The thickness of 3.175 mm combined with feed rate of 0.2 mm/rev is observed sufficient to generate a quantifiable amount of thermal energy, while it is not so thick to deflect the tool or to cause the workpiece to be pulled from the jaws of chuck. In case of orthogonal machining of a tube the workpiece is necessarily free in order to be in contact with the cutting tool forcing the tube to be cantilever. It is observed during initial phase of experimentation that workpiece lengths beyond 65 mm cause severe deflection and vibration of workpiece due to absence of any support from tailstock.

5.1 Overview of experimental procedure

The flow chart of the experimental procedure is given in Figure 5.1. The experimental procedure is divided in to the following steps:

1. Setup workpiece on lathe
2. Setup infrared (IR) camera
3. Perform experiments to record force data
4. Perform experiments to record IR data
5. Post process and plot IR and force data
6. Perform finite element analysis of experiments using AdvantEdge to determine temperature fields and forces
7. Compare results\

5.2 Setup workpiece on lathe

A three jaw self-centering chuck is used. For rigidity workpiece in the form of a SAE 1015 steel pipe (wall thickness of 12 mm, outer diameter 165 mm and about 65 mm length) is secured in the external jaws. The workpiece is then turned and bored to obtain experimental workpiece having wall thickness of 3.175 mm and 156 mm OD. Boring is necessary so as to obtain uniform wall thickness. This is done at 105 rpm, feed of 0.02 mm/rev and 1 mm to 2 mm depth of cut. Figure 5.1 shows before (a) and after (b) views of the workpiece. The workpiece is not removed from the jaws until the machined length is completely used. This approach of not removing the workpiece reduces vibrations.

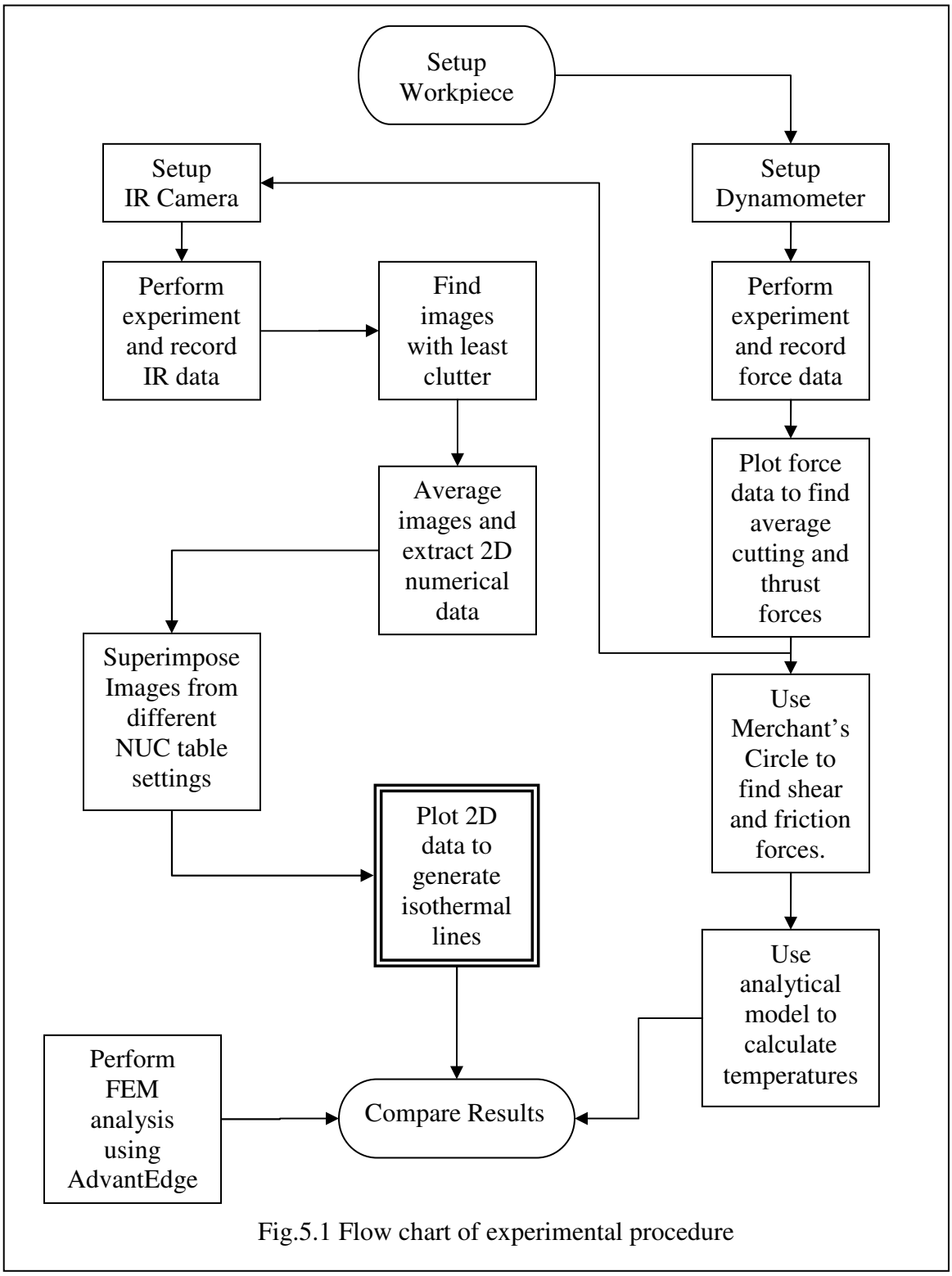

Fig.5.1 Flow chart of experimental procedure

5.3 Setup machining tool

After the workpiece is machined to a wall thickness of 3.175 mm and outer diameter of 156 mm, the four way tool post and the compound slide are removed. The dynamometer is mounted on a 43 mm thick machined aluminum block using 5/16 in screws. A tool insert holder is machined from 19 mm square bar of hot rolled SAE 1045 steel. The rake angle is 15° and end relief angle is 5°. The custom made tool holder is secured on the top plate of the dynamometer by means of a machined clamping plate using M8 screws as shown in Figure 5.1(b).

5.4 Perform experiments to record force data

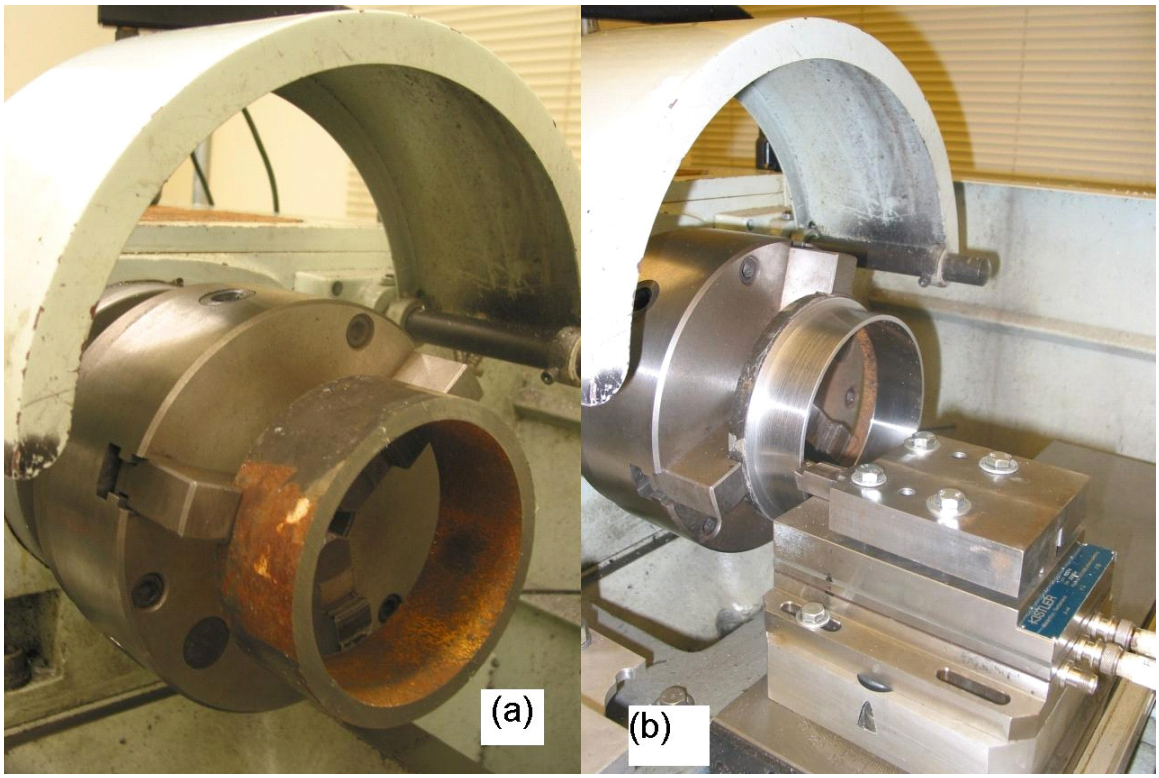

Fig.5.2 (a) Workpiece mounted on the lathe using a three jaw chuck,
(b) Workpiece machined to a tube having wall thickness of 3.175 mm. Also seen is a tool mounted on a dynamometer.

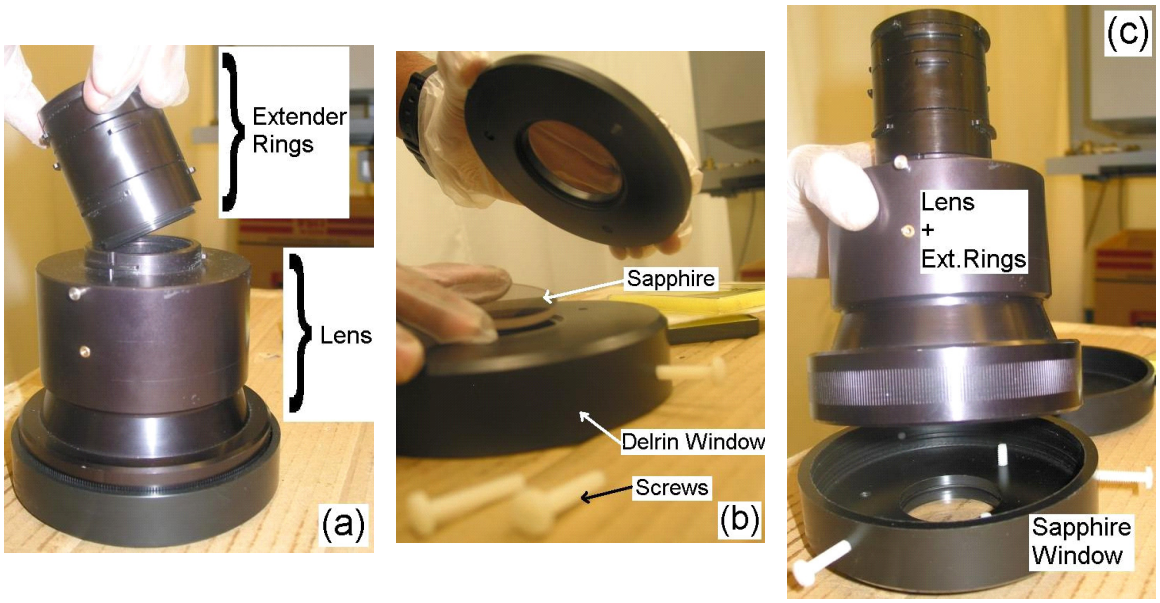

Fig.5.3 (a) Fitting extender rings on the lens, (b) Fitting sapphire in the delrin window, (c) Fitting sapphire window on the lens.

The tool overhang is kept shorter than 10 mm as recommended by manufacturer of the dynamometer (Kistler) [34]. The compound slide and tool post are removed from the cross slide. A machined aluminum block is fixed upon which the 3-componenet measuring platform is fixed using four 5/16 in bolts. Figure 5.1(b) shows the experimental setup for force measurement. One cable for each force component is connected to the dynamometer to carry the charge signals to the dual mode amplifiers.

Firstly, machining is done to measure the force in the lateral direction, Fx. This is to confirm that the machining operation is orthogonal. Under ideal conditions this force should be zero. In the present investigation a careful attempt is made to keep this force at minimum or negligible. The sensitivity of the dual mode amplifier is kept at 7.5 pC/N and the scale factor at 500.

Before conducting any machining experiments the workpiece is rotated at the desired speed without engaging the tool so as to record vibrations generated. This vibration data is later used to normalize the force data. Machining experiments are then

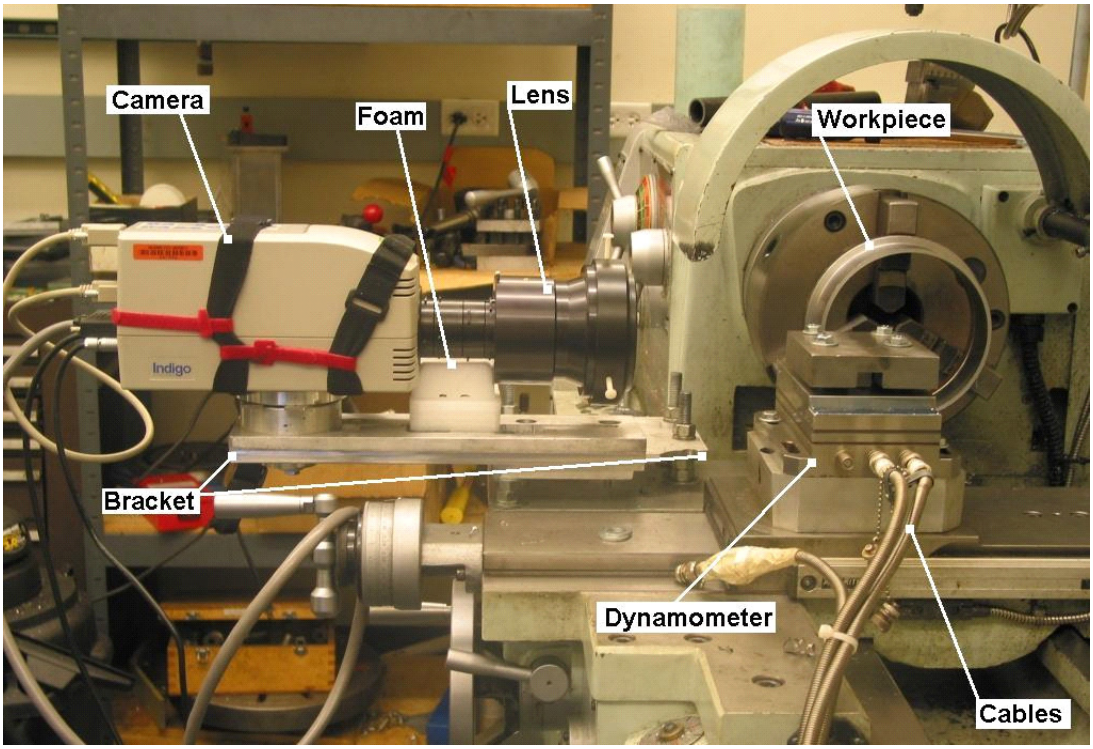

Fig.5.4 (a) Temperature measurement setup showing the camera, camera mounting bracket, workpiece, foam and dynamometer.

performed to measure cutting force, Fz and thrust force, Fy. Three experiments with the same set of machining conditions are performed to gather three data sets of machining force (Fz) and thrust force (Fy). The sensitivities of the dual mode amplifiers used for cutting force (Fz) and thrust force (Fy) are kept at 3.5 pc/N and 7.5 pC/N respectively, whereas the scale factors maintained at 2000 for both.

5.5 Setup infrared camera

A camera mounting bracket (Figure 5.3(a)) is built in-house. It has a steel plate which is mounted on the lathe carriage by two 5/ 8in bolts. An adjustable aluminum plate assembly is mounted on this plate and is held by four bolts. The IR camera is secured on

this aluminum plate assembly by a single 5/16 in bolt. This arrangement allows for changing height, distance, and glancing angle of the camera.

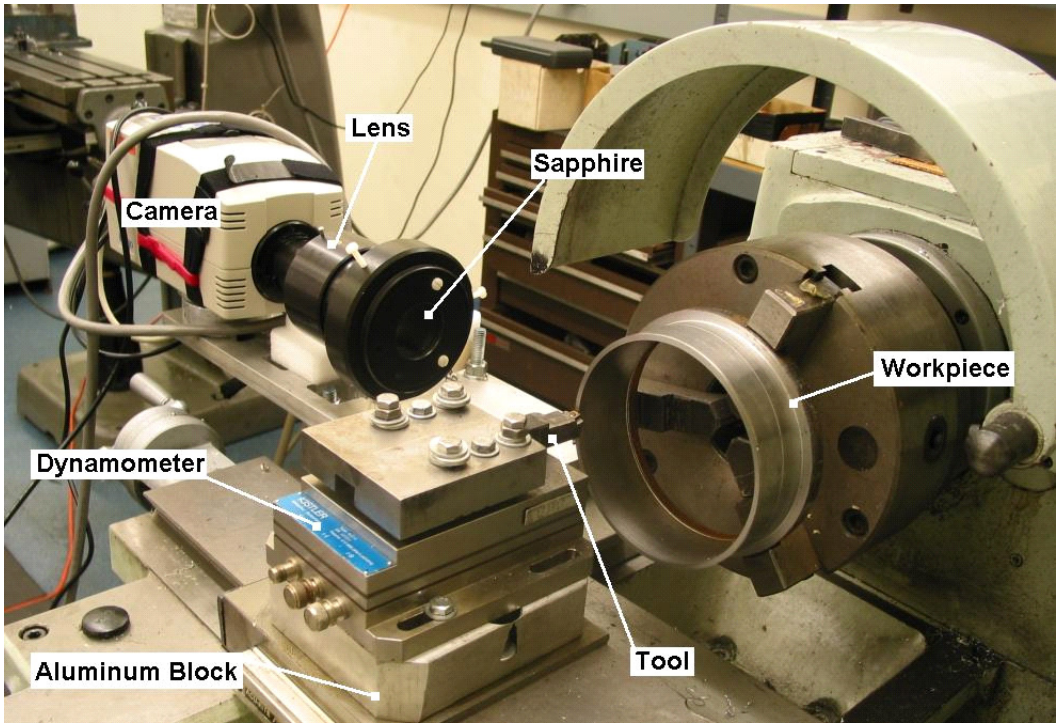

Fig.5.4 (b) Another view of the temperature measurement setup showing the camera, lens, sapphire, workpiece, tool, dynamometer and aluminum block.

The set of four extender rings is attached to the lens (Figure 5.2(a)). The sapphire plate is fixed in the delrin window (Figure 5.2(b)) and the window is then attached to the lens (Figure 5.2(c)). If previous observations indicate that the temperatures are higher than 300°C then neutral density filter is fixed in the farthest extender ring.

Power, data, remote control and video cables are connected to the camera and the camera is switched on. To completely cool the sensor array (as recommended by the manufacturer) the camera is not used for 15 minutes after switching on. Lens was mounted after removing the front protective cover. The lens was then fitted with a protective sapphire window. Dynamite software was started and was made ready to

receive data from IR camera. Figures 5.3(a) and (b) show the complete experimental setup.

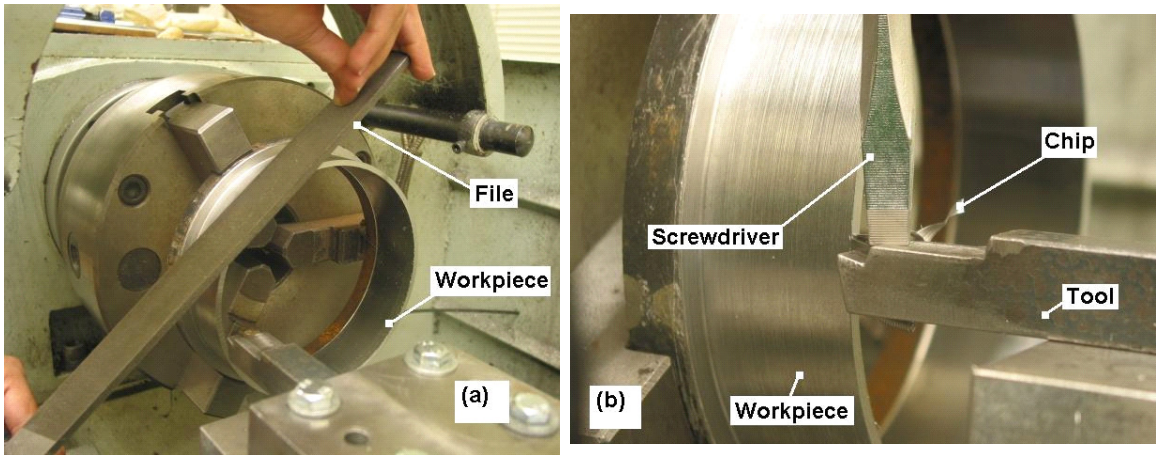

Fig.5.5 (a) Removing side flow using a file, (b) Guiding chips using a screwdriver.

5.6 Perform experiments to record infrared data

Experiments were conducted at cutting speeds of 26.9, 51.3, 63.5, 90.4, and 122.2 m/min and feed rate of 0.2 mm/rev. Machining test was performed for a duration of 20 s and the IR sequence was recorded. The images for the sequence are recorded at 30 Hz frequency. The workpiece and tool are allowed to cool down to room temperature between two consecutive experiments naturally. Generally it takes about 15 minutes for the workpiece to cool down.

Implementation of the experimental measurement trials in the present work is not without some mechanical difficulty. Several unforeseen issues arise. One such issue is that the orthogonal machining and ductility result in the side flow of work material. It is observed that the side flow is negligible when the tube thickness is greater than 2 mm for tube having outer diameter of 156 mm and when the outer cylindrical surface of the tube is machined rather than as received. It is necessary to eliminate the side flow because it

blocks the camera's view of the tool tip. Furthermore care is taken to remove the very small amount of side flow between two consecutive runs. The side flow is removed by rotating the workpiece at 105 rpm and pressing a bastard file on the machined edge of the workpiece (Figure 5.4(a)). Thus, the hindrance because of side flow is eliminated completely.

Another phenomenon that blocks camera's field of view is curling of chips in between camera and the tool. To combat this difficulty an assistant is employed to prevent chips from coming in between the tool and the camera with the help of a screw driver (Figure 5.4(b)). A similar method was used by Shaw *et al* [39].

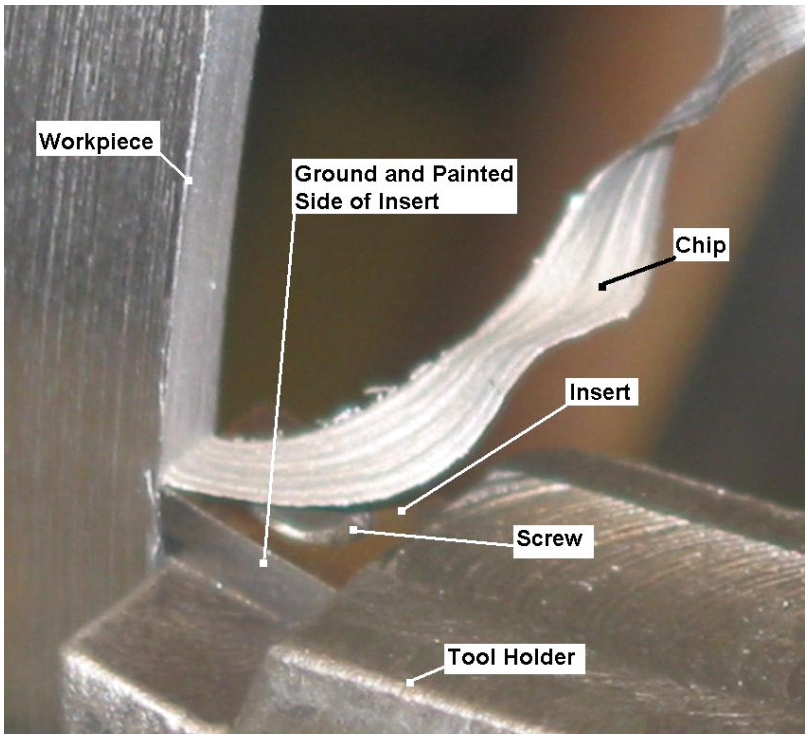

Fig.5.5(c) Close up showing relative arrangement of chip and insert. Notice the distance between chip edge and side edge of the tool. The left side of the tool is ground and painted with a black paint of emissivity of 0.95.

The tool is positioned such that the distance between the painted side of the machining insert viewed by the camera and corresponding edge of the chip is about 0.5 mm (Figure 5.4(c)). This is necessary to perform the machining experiments under

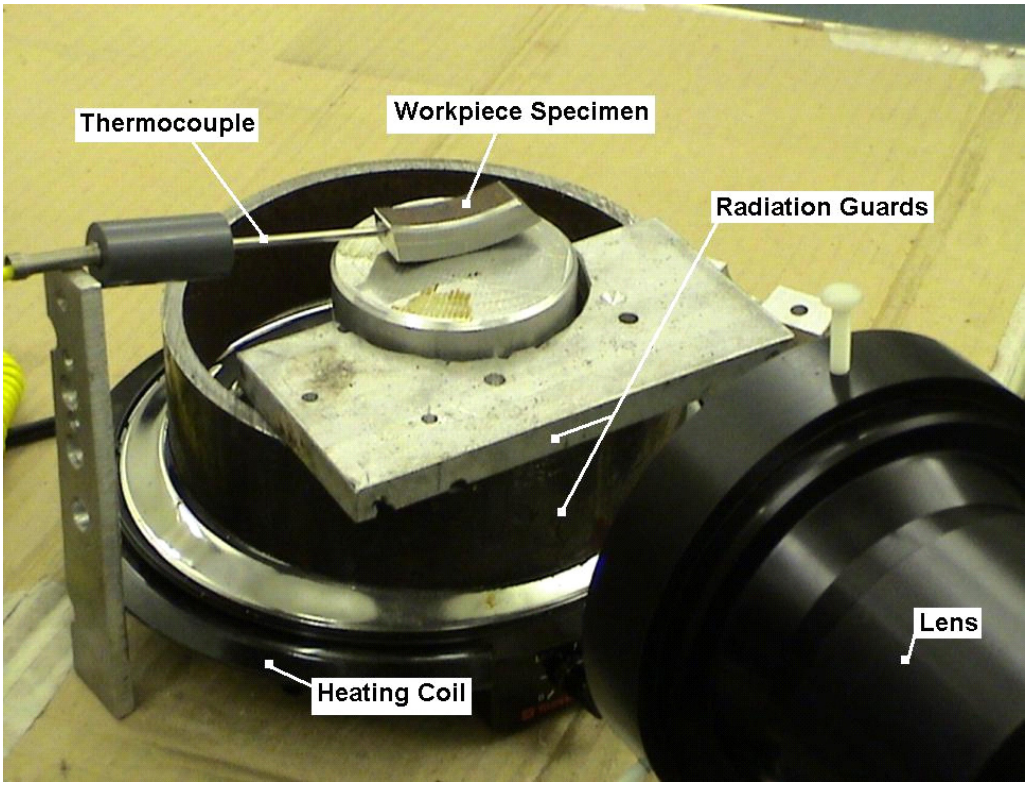

Fig.5.6 Experimental setup to measure emissivity of the workpiece showing workpiece specimen, thermocouple, heating coil and radiation guards.

orthogonal conditions because the insert has a nose radius of 0.397 mm. This distance is kept to a minimum to reduce the error in temperature measurement. For every set of machining conditions it is necessary to take two complete sets of measurements. During one set of experiments the camera is focused on the workpiece and during the other set it is focused on the painted side of the machining insert. To facilitate focusing, the side of the tool to be viewed by the camera is ground to generate a vertical face.

5.7 Emissivity measurement

As discussed in Section 4.11.2 of Chapter 4, emissivity of a real surface plays a vital role in correct measurement of temperature. Hence, it is necessary to measure emissivity of chip, tool, and workpiece.

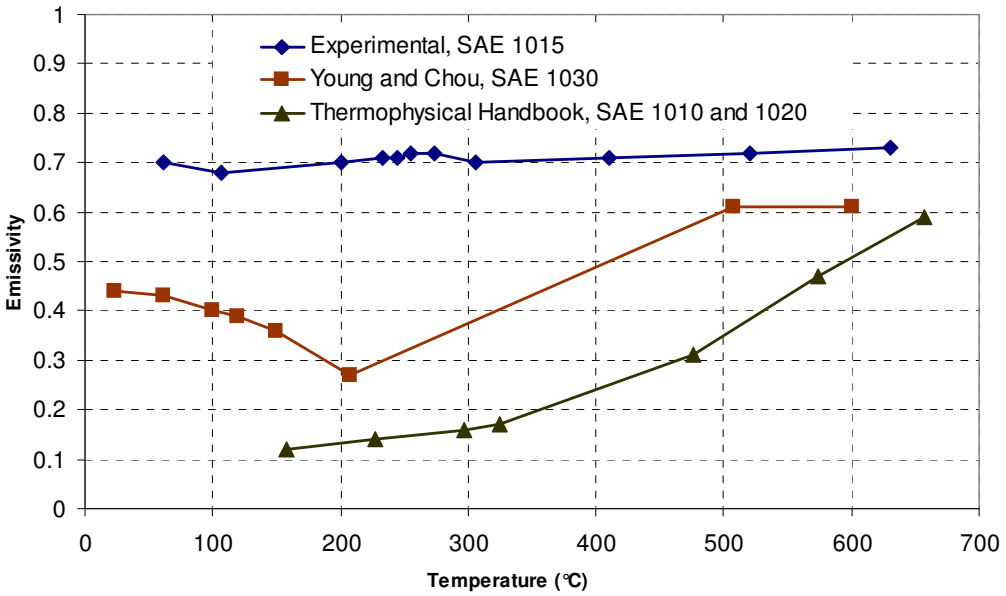

Fig.5.7 Measured emissivity of the workpiece compared with Handbook [36] data and work of Young and Chou [12]

Initial approach used is to paint the workpiece and tool with a paint of known emissivity of 0.95. This method was also used by Boothroyd [6] and O'Sullivan and Cotterell [17]. The painting approach gives satisfactory results with tool. But in case of painted workpiece while machining tiny paint flakes separated and formed sticky buildup on tool. This buildup of paint was on outer side of the workpiece, i.e. between the chip edge and the camera hindering the visibility. Another shortcoming of the paint method is that the paint though heat resistant can get heated to a temperature higher than that of workpiece and tool to introduce significant error in the workpiece and chip temperature measurement.

It is, therefore, necessary to use workpiece in unpainted condition and also to measure its emissivity. A piece is cut out of as machined tube and is used for emissivity measurement. It is heated using an electric heater coil. To avoid "glow" of heated coil when viewed by an IR camera radiation guards are used as shown in Figure 5.6.

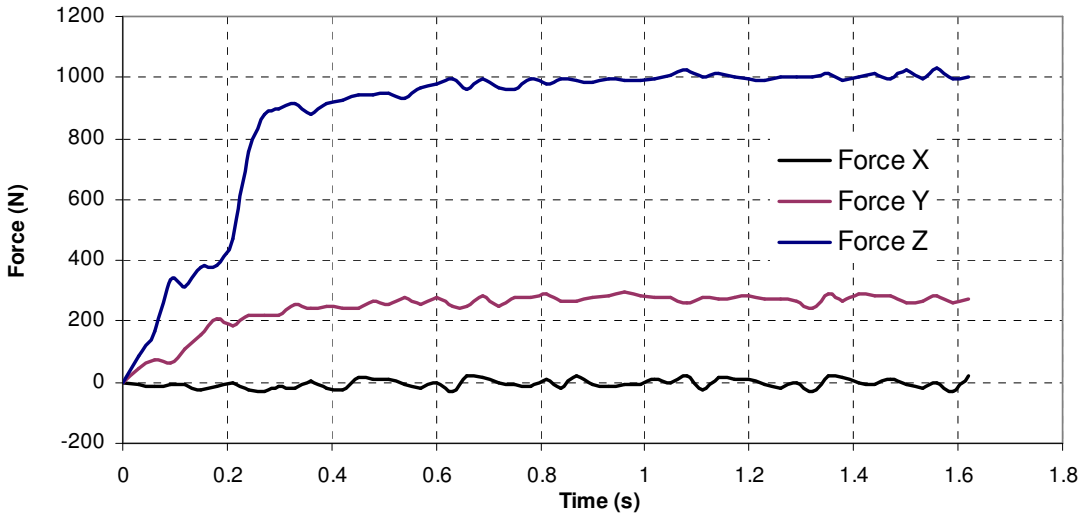

Fig.5.8 Typical plot of forces measured while machining 3.175 mm thick tube of SAE 1015 at a cutting speed of 122.2 m/min, feed of 0.2 mm/rev and rake angle of 15°.

To heat the specimen without abrupt temperature changes it is placed on 50mm long 50 mm diameter aluminum block. The temperature is then slowly increased in steps of 50°C and is measured simultaneously using the infrared camera and a K type thermocouple. A hole of exact size of the thermocouple is drilled in the specimen. The thermocouple is pressed inside this hole so as to maintain maximum contact. The same optical setup as that used in the experiments is used. The temperature as indicated by the camera is compared with the temperature indicated by the thermocouple. If the temperatures are different then emissivity value used by the camera is changed. This procedure is repeated till the temperature indicated by the camera matches with that indicated by the thermocouple. The emissivity value when both the temperatures match is the emissivity of the workpiece at that temperature. This method is used to find emissivity of the workpiece at all temperatures from room temp of 22°C to 650°C. The plot of the measured emissivity of the workpiece compared with Handbook [46] data and work of Young and Chou [22] shown in Figure 5.7. Another important consideration is that the same emissivity value of 0.7 is used for the workpiece and chip as the area used

for analysis purpose is about 2 mm x 2 mm and the emissivity changes in this region can be assumed to be negligible. The force data was plotted using Microsoft Excel®. Figure 5.8 shows a typical plot of cutting and thrust forces obtained during experiments.

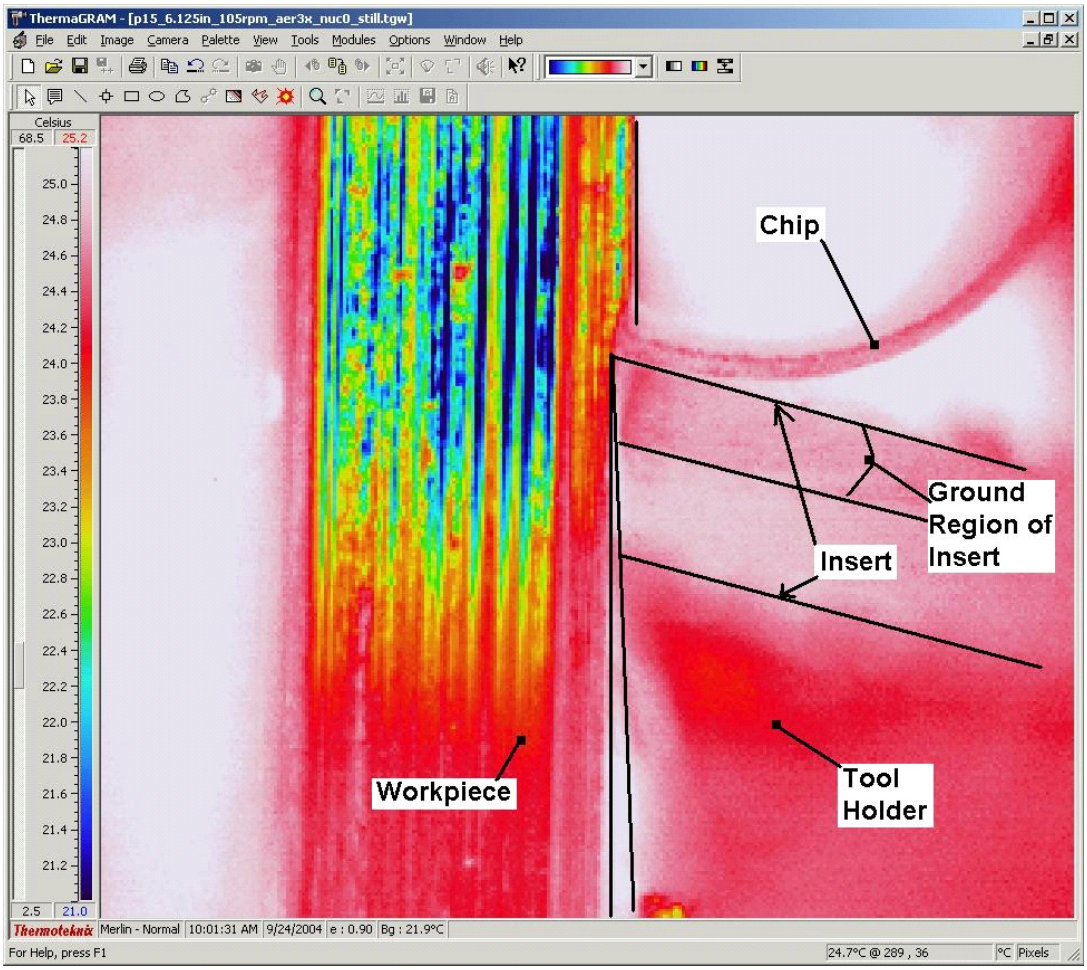

Fig.5.9 Typical infrared image obtained using the IR camera. Chip, tool and workpiece. The different appearance of the ground region of insert can also be seen.

5.8 Post process and plot force and IR data

It is necessary to find images which are free from any flying chips or small metallic particles. It is observed that such particles are generally not in the focal plane of the camera and hence distort the view of the camera as well as the temperature field measured by the camera. Five such images corresponding to half a second duration after

the forces get stabilized are collected from a sequence. These images are then averaged using ThermaGram to reduce effect of instantaneous temperature rise, if any. A typical image obtained using ThermaGram is shown in Figure 5.9.

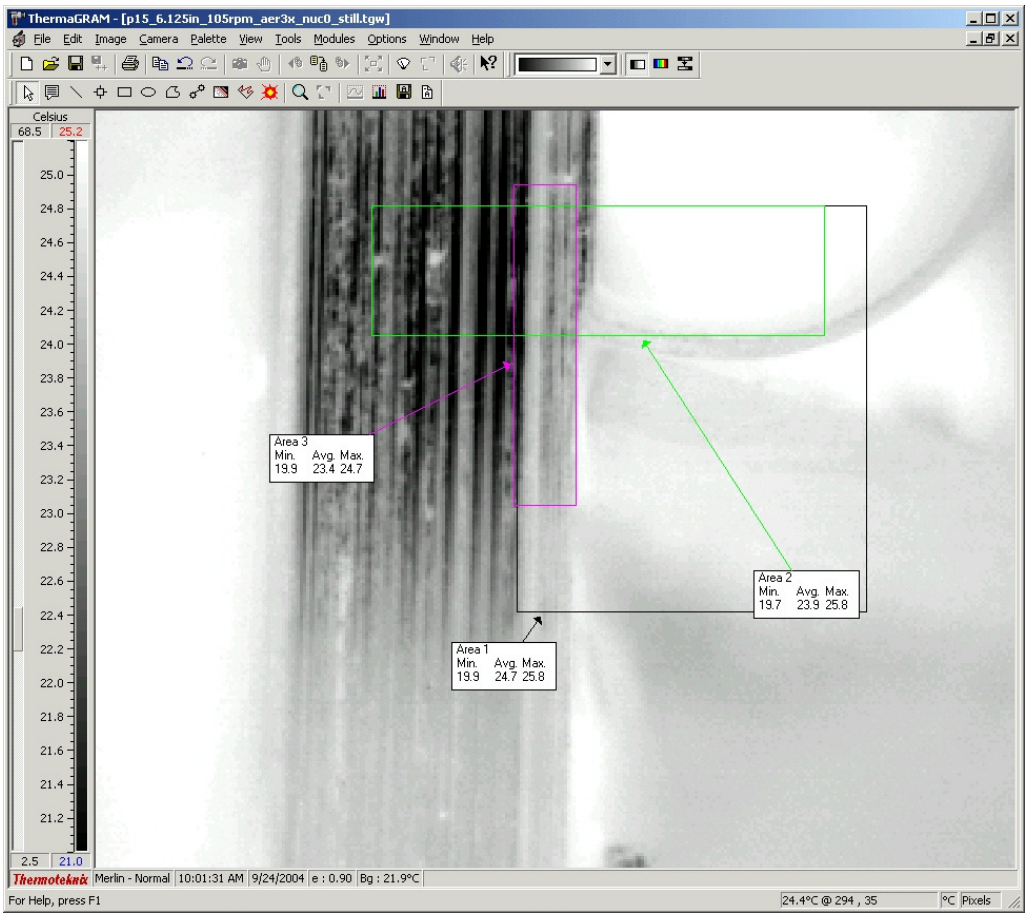

Fig.5.10 Typical infrared image marked with three "Rectangle" tools using ThermaGram. "Area 2" and "Area 3" help locate the tool tip.

This image is then marked with three "Rectangle Tools" as shown in Figure 5.10. The rectangle named "Area 1" corresponds to total plotting area. Rectangles "Area 2" and "Area 3" correspond to the location of tool tip with respect to the top left corner of "Area 1". Rectangle "Area 2" gives number of rows of pixels between the top edge of the plotting area and the tool tip, whereas "Area 3" gives number of columns between the left edge and tool tip. These values of number of rows and number of columns are used to

locate the tool tip and calculation of the field coordinates because while plotting temperature fields the distances are measured with respect to the tool tip.

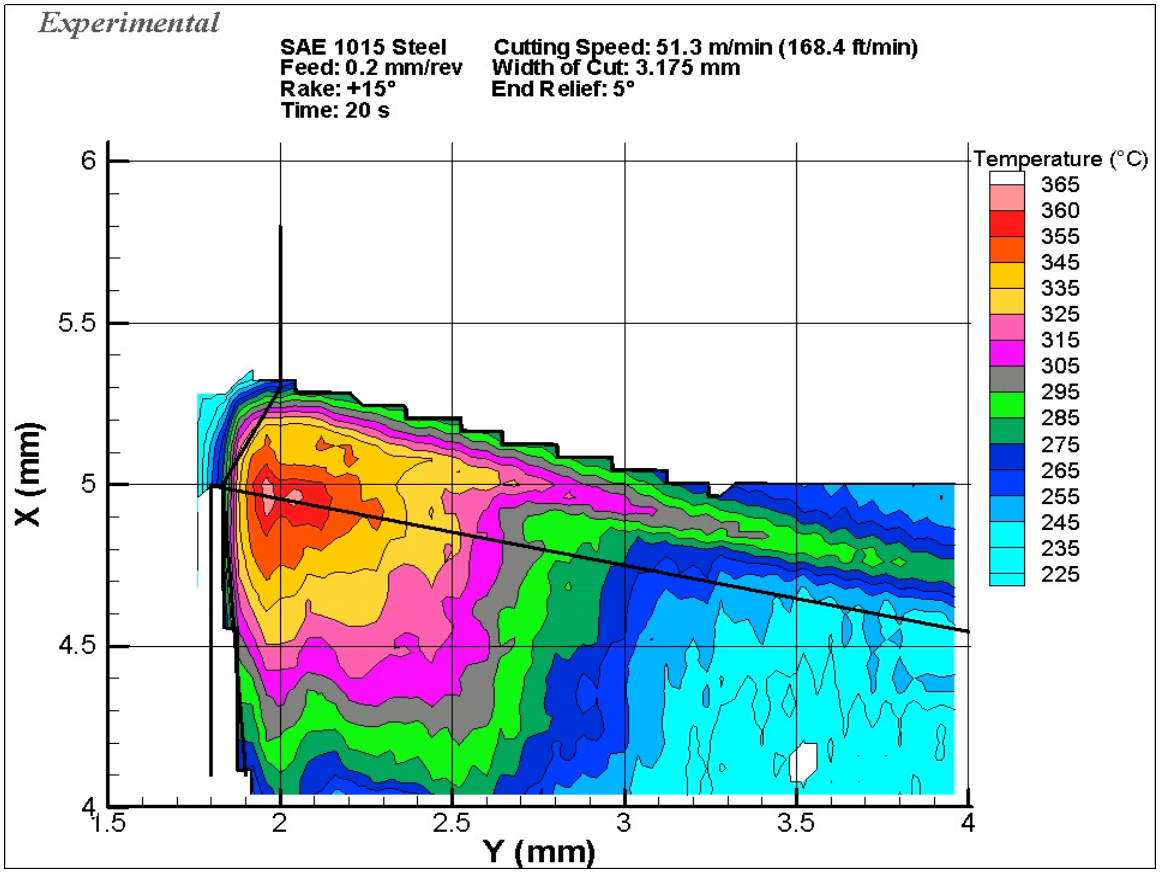

Fig.5.11 Typical experimental cutting temperature (steady state) field plot obtained after using TecPlot for plotting IR data for cutting speed of 51.3 m/min; feed rate of 0.2 mm/rev, width of cut 3.175 mm, 15° rake, and 5° relief angle in machining of SAE 1015 after 20 s duration.

The temperature data from these images is then taken to Microsoft Excel® using "Copy ASCII" tool in ThermaGram. These data is in pixel format and is required to be converted into tabular format of X-co-ordinate, Y-co-ordinate and temperature. This is done using a Microsoft Excel® with VBA program. While converting the data from pixel format, it is also divided into three regions, namely chip, tool and workpiece. The corresponding emissivity values are applied. The data now in tabular format are plotted using version 9.2 of TecPlot software so as to generate isotherms.

5.9 Perform finite element analysis

Finite element analysis is performed using a commercially available software – AdvantEdge. It is a Lagrangian explicit finite element code. The material model and properties as provided within the software are used. FEM code is not modified or appended in anyway. The material selected for this purpose is SAE 1020 as it is the closest material available to the experimental material used (SAE 1015).

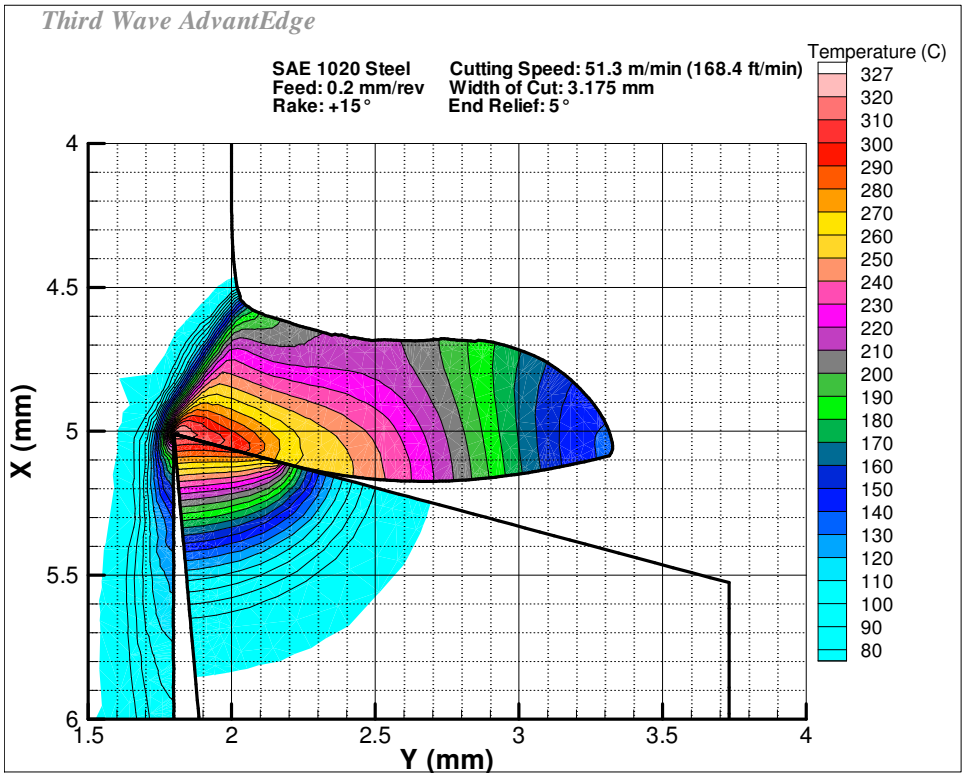

Fig.5.12 Typical cutting temperature (steady state) field plot obtained after using AdvantEdge FEA software for the similar conditions of machining of SAE 1020 as shown in Figure 5.11. (cutting speed 51.3 m/min; feed rate 0.2 mm/rev, width of cut 3.175 mm, 15° rake, 5° relief)

The machining conditions same as those in experiments are used for the analysis with the only known difference of edge radius. In finite element analysis an edge radius of 0.005 mm is used whereas in the tests no such radius is provided. This radius is required in FEM model so as to avoid an error in execution of finite element code. The

feed rate (0.2 mm/rev) is 40 times that of this edge radius hence the effect of radius in FEM can be considered negligible. Figure 5.12 shows a typical plot obtained using AdvantEdge.

From Table 5.1 it can be seen that the mechanical properties of SAE 1015 and SAE 1020 are comparable, whereas thermal properties of the two materials are almost identical. Hence it is reasonable to compare experimental results of SAE 1015 with FEM results of SAE 1020.

Table 5.1 Properties of SAE 1015 and SAE 1020 (Ref. [40])

	SAE 1015	**SAE 1020**
Components		
C, Wt%	0.13-0.18 (0.16*)	0.17-0.23
Mn, Wt%	0.3-0.6 (0.4*)	0.3-0.6
P, Wt%	Max 0.04 (0.1*)	Max 0.04
S, Wt%	Max 0.05 (0.012*)	Max 0.05
Fe, Wt%	99.13-99.58	99.08-99.53
Shear Modulus, GPa	80	
Machinability**	60	70
Thermal Properties		
CTE, linear 20°C, µm/m-°C, from 0-100°C	11.9	11.7
CTE, linear 250°C, µm/m-°C, from 0-300°C	13	12.8
CTE, linear 500°C, µm/m-°C, from 0-500°C	14.2	13.9
Heat Capacity, J/g-°C	0.486	
Thermal Conductivity, W/m-K	51.9	
*Actual values from material test report provided by the steel tube manufacturer		
**Machinability ratings are from the percentage of cutting speed for 1212 steel at 50 m/min		

Furthermore, the FEM model used generates results under steady state conditions. The experiments are conducted for about 20 s durations. When the temperature contours and the highest temperature in the field of vision do not exhibit any significant change the

steady state is said to be achieved. These results of steady state (16 s duration) condition are compared with FEM.

CHAPTER 6

EXPERIMENTAL RESULTS AND DISCUSSION

Table 6.1 lists the cutting conditions at which temperature measurements in orthogonal machining of SAE 1015 steel are made using the infrared camera.

Table 6.1 Experimental machining conditions

Workpiece Material	SAE 1015
Workpiece OD, mm	155.6
Wall Thickness, mm	3.175
Workpiece Hardness, HRB (BHN)	74 (131)
Machining Insert	Valenite SECW-2.51.51
Rake Angle	15°
End Relief Angle	5°
Chip Type	Continuous
Cutting Speeds, m/min	26.9, 51.3, 63.5, 90.4, 122.2
Cutting Fluid	-None- (Dry Machining)

6.1 Orthogonal Machining

The thrust force, and cutting force values obtained at various cutting speeds are given in Table 6.2 and the same are plotted in Figure 6.1.

Table 6.2 Experimental values of cutting and thrust forces

Cutting Speed (m/min)	**Cutting Force (N)**	**Thrust Force (N)**
26.9	1403	730
51.3	1389	700
63.5	1289	679
90.4	1310	593
122.2	1191	511

The force measurement confirms the orthogonal nature of the cutting operation. A study of results given in Figure 6.1 and Table 6.2 permits the observation that cutting force and thrust force decrease with increase in cutting speed.

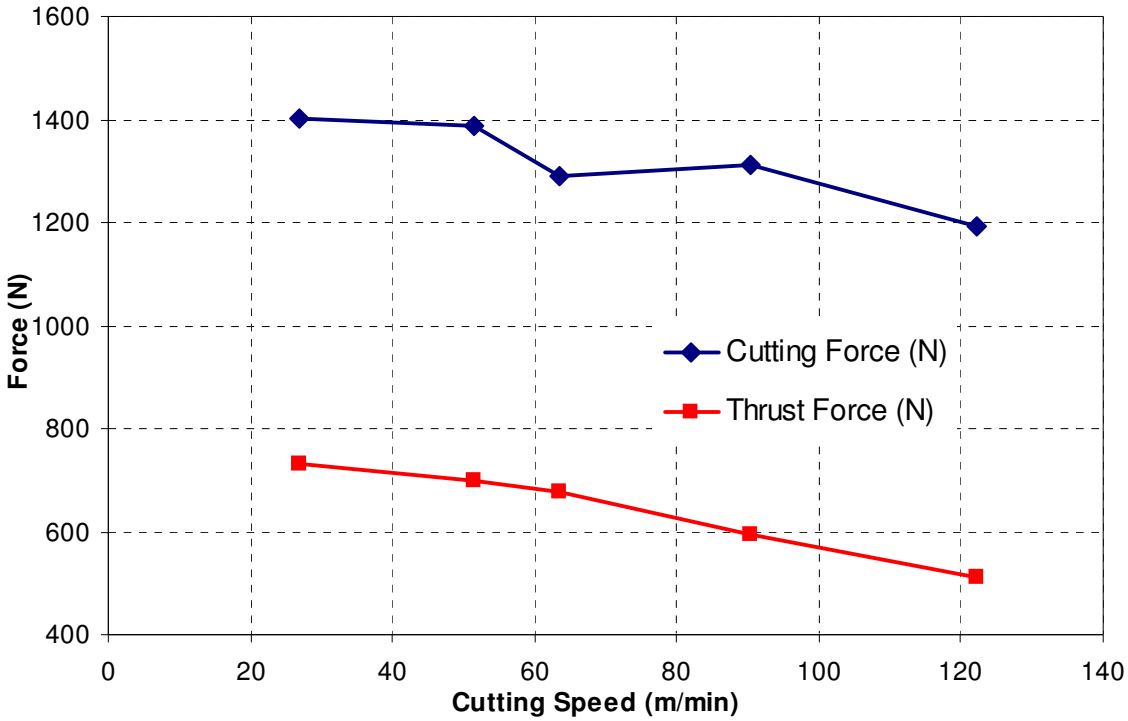

Fig.6.1 Cutting and Thrust force values at various cutting speeds in machining of SAE 1015 at feed rate of 0.2 mm/rev and width of cot of 3.175 mm.

6.2 Temperature Measurement

Table 6.3 lists the appropriate non-uniformity correction (NUC) table provided within the camera, which are used during the experiments.

Table 6.3 Non-Uniformity Correction tables used

Cutting Speed (m/min)	NUC Table Used	Temperature Range (°C)
26.9	NUC2	111 to 231
51.3	NUC3	221 to 425
63.5	NUC3	221 to 425
90.4	NUC3	221 to 425
122.2	NUC4	380 to 765

6.2.1 Transient and Steady State Conditions

Temperature contour plots at six time steps during machining of SAE 1015 steel at cutting speed of 51.3 m/min are shown in Figure 6.2. It can be noted that the maximum temperature in the field of vision increases from about 295°C at 1 s (Figure 6.2(a)) to about 365°C at 9 s (Figure 6.2(e)).

Furthermore, it can be seen that the maximum temperature in the field of vision, the temperature distribution, and temperature gradients at 9 s and 20 s are almost the same. Thus, it can be inferred that, at this cutting speed, the steady state condition has reached in ~9 s after initiating the cut.

It can also be noted that the distance of the maximum temperature spot, from the cutting edge, is almost the same at all time steps regardless of the fact that maximum temperature increases in the transient state and remains unchanged in the steady state. We see that the maximum temperature spot is observed to be distributed between the chip and the rake face in both transient and steady state conditions.

The shape of the 295°C contours in Figure 2.6(a); 325°C in Figure 2.6(b); 345°C in Figure 2.6(c); 355°C in Figure 2.6(e); 355°C in Figure 2.6(f); are the same. Thus the shape of the contours surrounding the maximum temperature spot is the same in the transient or the steady state condition.

Figure 6.3 shows the maximum rake face temperature at different time steps and at cutting speeds of 51.3, 63.5, 90.4, and 122.2 m/min. We see that the maximum temperature on the rake face increases with an increase in cutting speed. The higher the cutting speed, the higher the maximum temperature on the rake face, in both the transient and steady state condition. Also, the time to reach the steady state condition is different

for each cutting speed, e.g. it is ~ 6 s for 51.3 m/min and ~12 s for 122.2 m/min (Figure 6.3(c)).

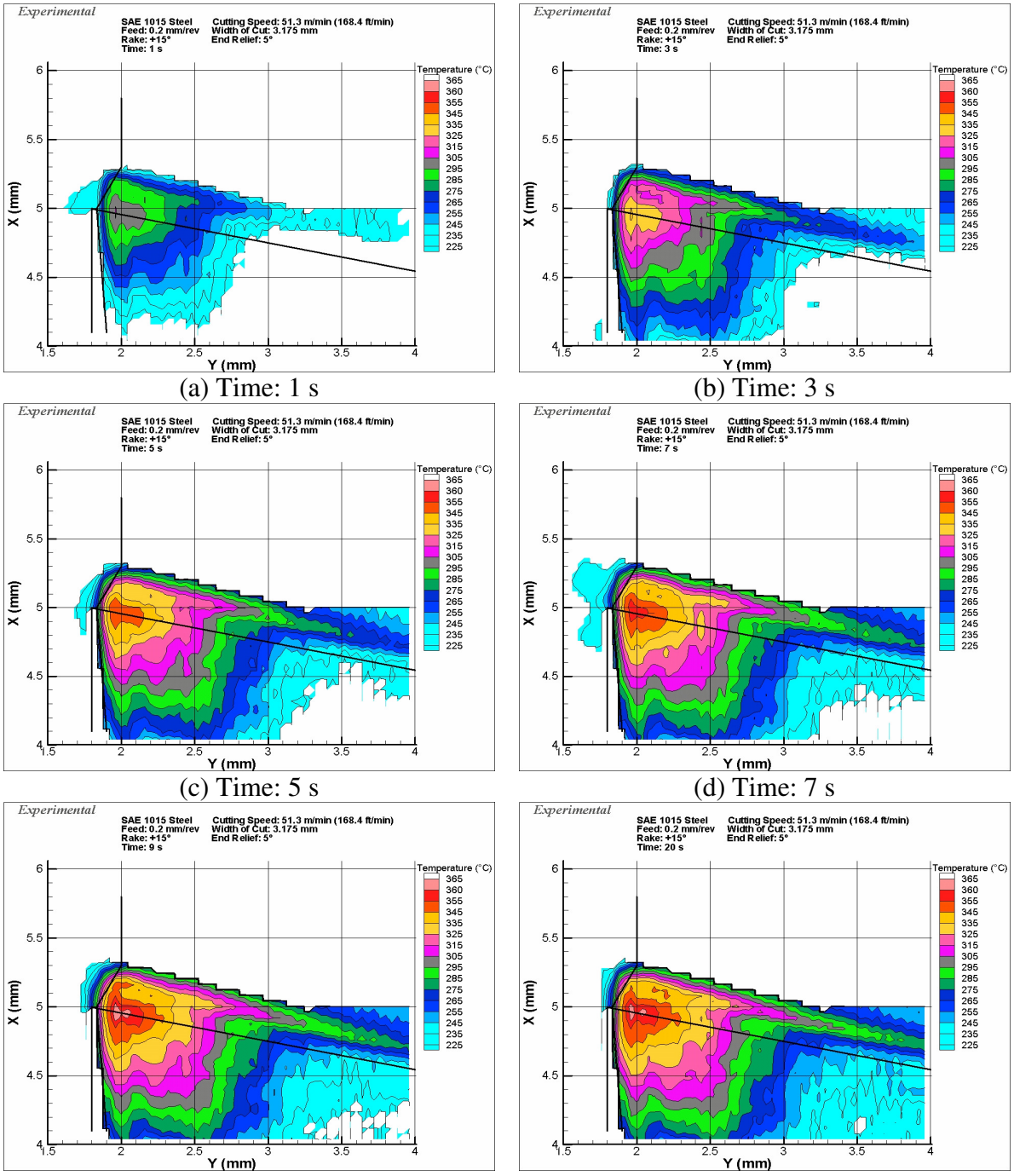

(a) Time: 1 s (b) Time: 3 s

(c) Time: 5 s (d) Time: 7 s

(e) Time: 9 s (f) Time: 20 s

Fig.6.2 Temperature contour plots depicting transient to steady state transformation while machining SAE 1015 at cutting speed of 51.3 m/min and feed rate of 0.2 mm/rev.

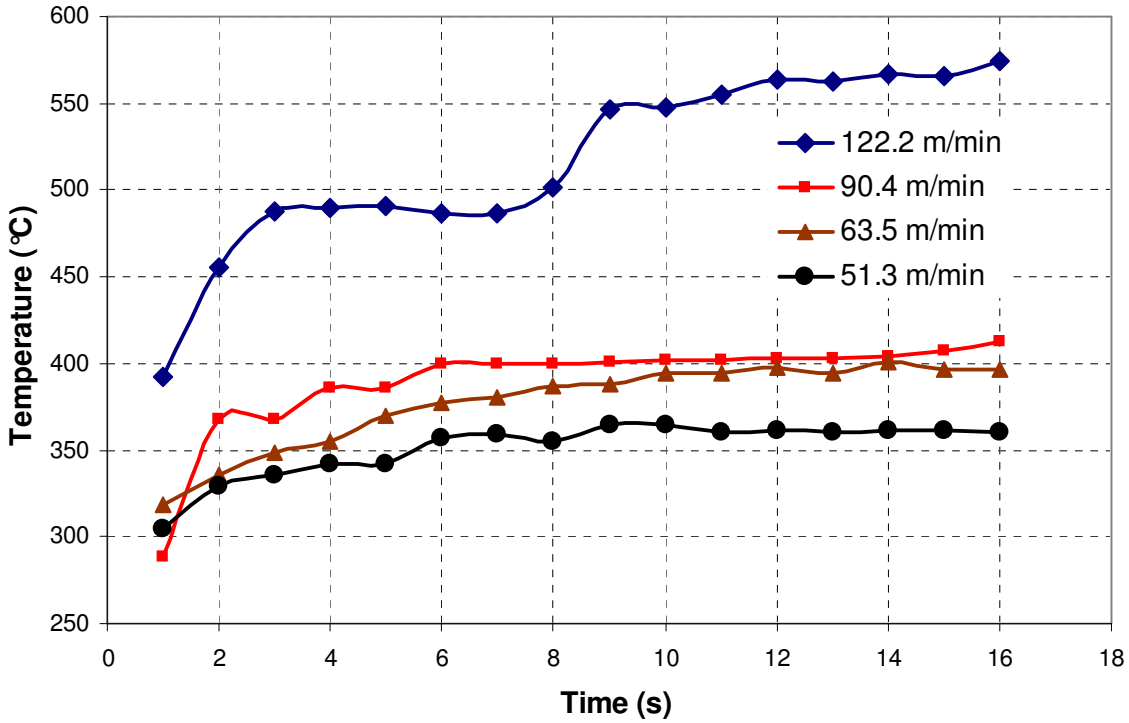

Fig.6.3(a) Maximum rake face temperature at different time steps and at cutting speeds of 51.3, 63.5, 90.4, and 122.2 m/min respectively

6.2.2 Chip-tool Contact Length

From Figures 6.4(a) and 6.4(b) it can be seen that the chip-tool contact length observed experimentally is different from that obtained using FEM. At a cutting speed of 26.9 m/min the experimental chip-tool contact length is 1.2 mm and that obtained using FEM is 0.5 mm. This is due to the contact conditions considered in FEM are different from the experimental contact conditions. In the case of FEM, it is observed that the cutting forces and, hence, the coefficient of friction is constant for all cutting speeds. Whereas, from Figure 6.1, it can be seen the cutting forces and, hence, the coefficient of friction reduces with an increase in cutting speed. This is further supported by the fact that the chip-tool contact length is observed to increase with increase in cutting speed (Figure 6.3(b))

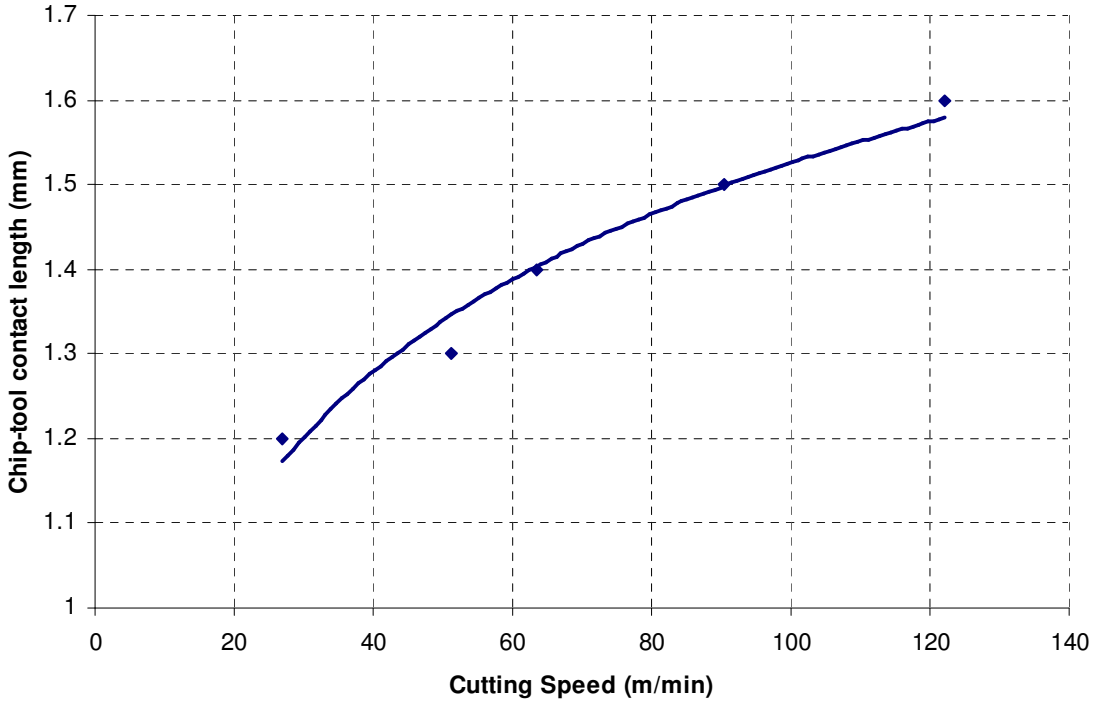

Fig.6.3(b) Chip-tool contact lengths in machining of SAE 1015 at different cutting speeds.

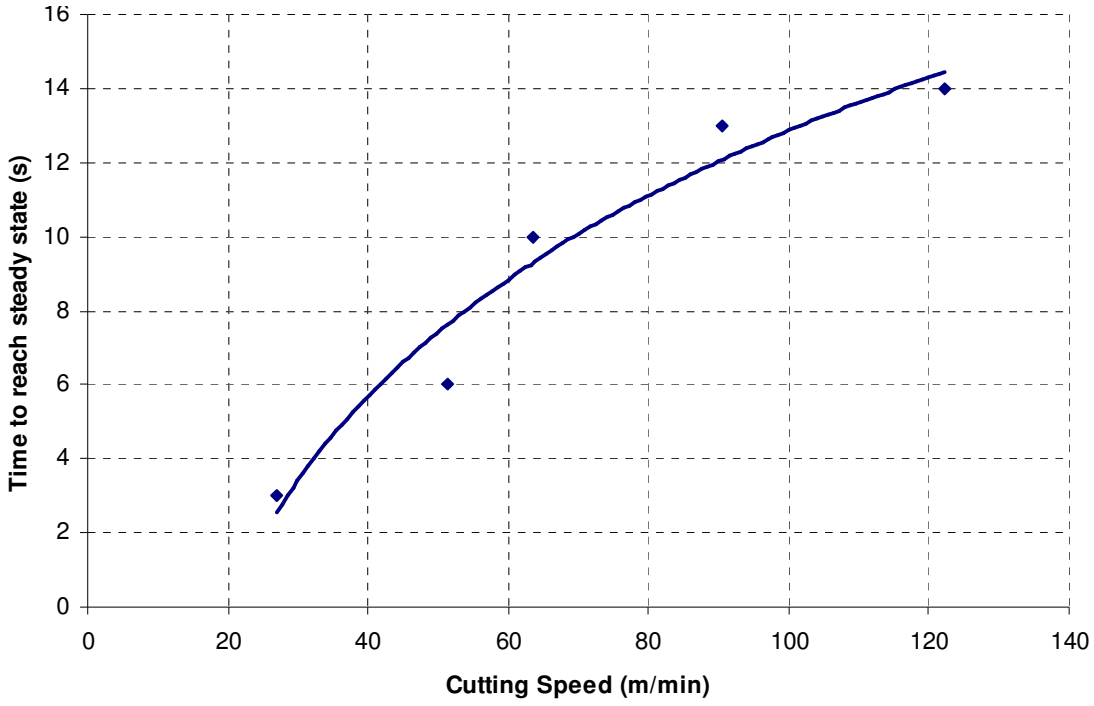

Fig.6.3(c) Time to reach steady state in machining SAE 1015 at different cutting speeds.

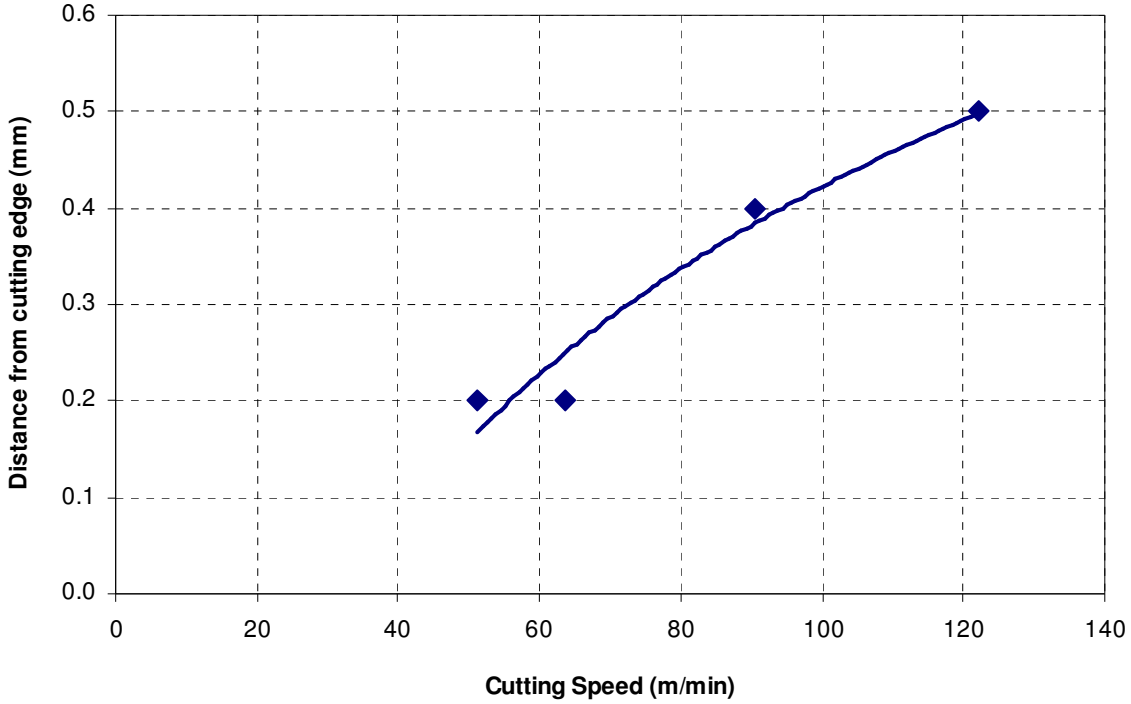

Fig.6.3(d) Distance of maximum temperature spot on rake face from the cutting edge at different cutting speeds.

6.2.3 Temperature Fields

In Figures 6.5 though 6.9, temperature contour plots obtained using infrared camera and those estimated using FEM are shown. It is observed that the time to reach steady state increases as the cutting speed increases. At a cutting speed of 122.2 m/min, it takes ~12 s to reach the steady state and, hence, infrared images corresponding to 16 s are used for comparison with FEM.

The chip produced is of continuous nature for higher cutting speeds of 180.9 and 308 m/min. Also, higher speeds need more time to reach steady state. Hence, a large amount of hot continuous chip is generated in short duration of time. Thus there is practical difficulty of chip handling so as to get a clutter free view of the tool tip. Hence the results for cutting speeds higher than 122.2 m/min are not presented here.

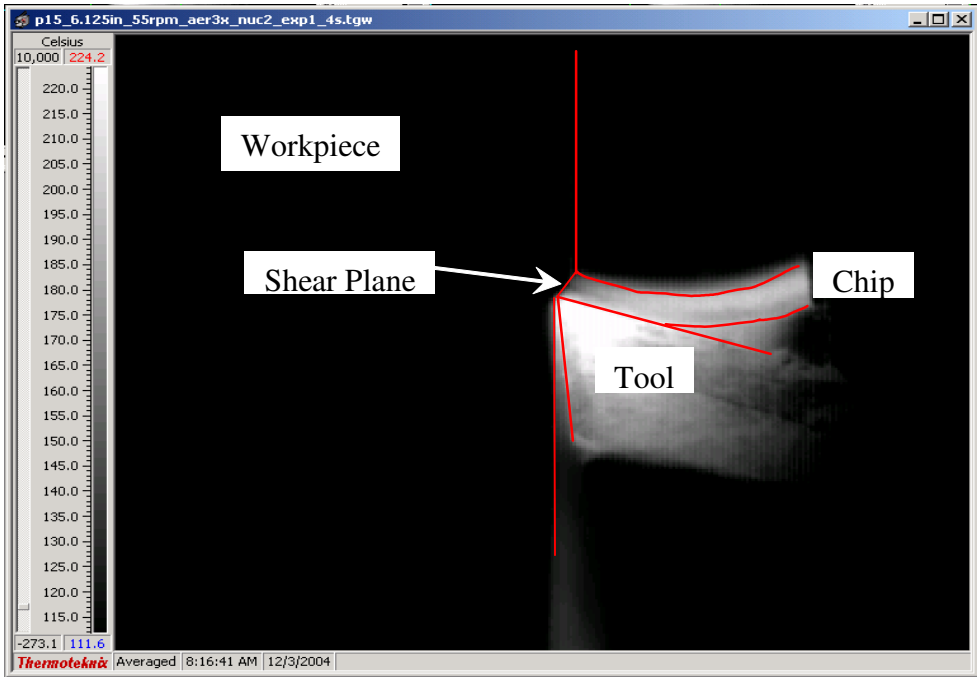

Fig.6.4 (a) Experimental chip-tool contact length (1.2 mm) at cutting speed of 26.9 m/min.

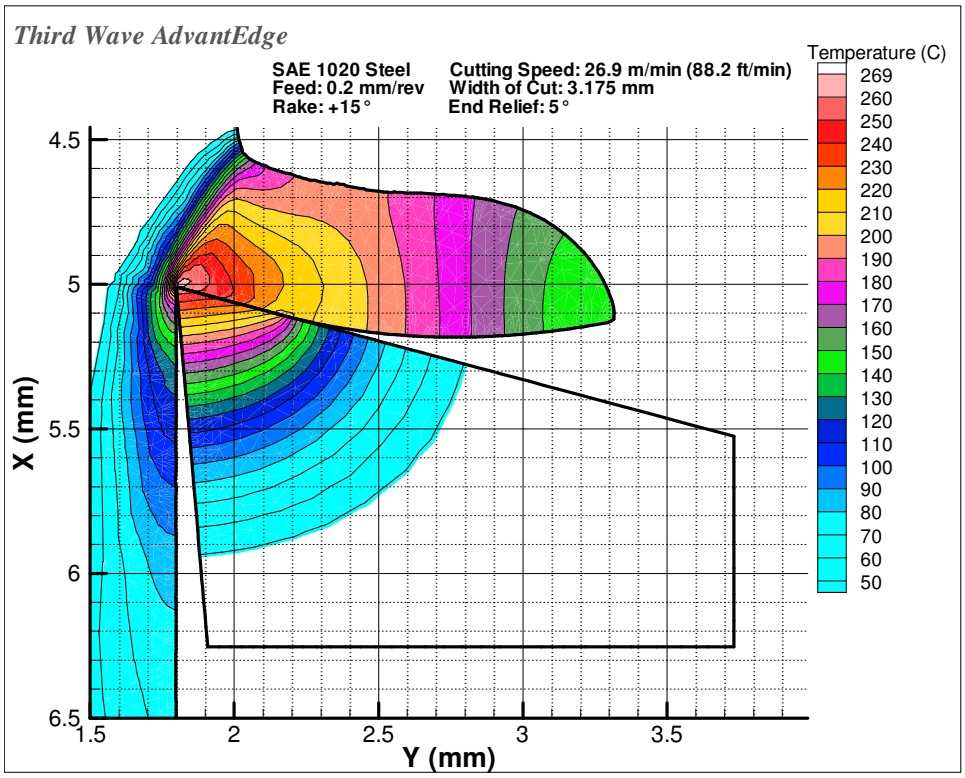

Fig.6.4 (b) Chip-tool contact length (0.5 mm) at cutting speed of 26.9 m/min computed by FEM.

From Figures 6.5 through 6.9, it can be seen that the images obtained using the infrared camera do not offer a clear distinction of chip and tool boundaries. This is because the camera records signals of all the infrared radiations in the field of vision which also include "halo" of infrared radiations typically radiated by hot objects. This creates a practical difficulty in locating the tool side edge and the chip side edge. This is overcome by locating the tool tip with utmost care and precision, and using the measured values of chip thickness. The machined surface edge, un-machined surface edge and tool edge are located with respect to the tool tip location. The chip edge is located with reference to the tool side edge. Thus a set of four straight line segments is superimposed on the temperature fields. The spatial resolution of the camera is 40 μm which is equivalent to possible errors in the location of tool tip and hence all the dependent entities.

In Figure 6.5(a), we can see that the maximum temperature ranges from 200°C to 224°C. This is because the infrared sensors, in the corresponding region, have reached values very close to the saturation temperature (231°C), indicating that the actual temperatures are higher than the upper limit of the NUC2. But, if the same temperatures are viewed through the next non-uniformity correction table (NUC3) then no signal is generated because the temperatures are very close to the lower limit (221°C). This is the reason that the tool appears at a relatively constant temperature and no temperature gradient is indicated in the tool.

It can be noted in Figure 6.6(a) that the workpiece temperatures are not visible. In this case, when the workpiece temperatures are measured using lower non uniformity correction table (NUC2), the sensors corresponding to tool tip region get saturated. This

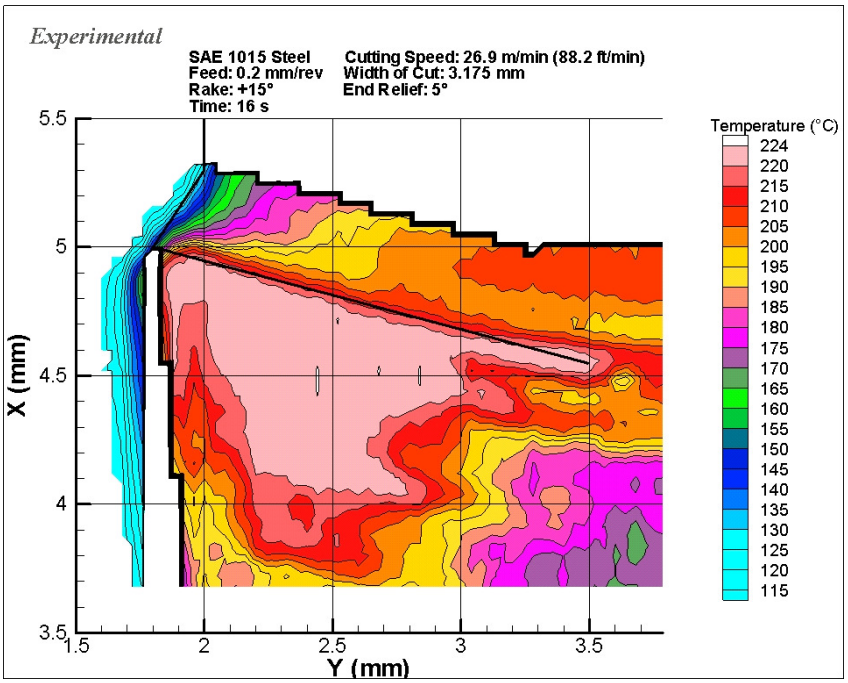

Fig.6.5 (a) Experimental temperature field for cutting speed of 26.9 m/min for SAE 1015 Steel after 16 s

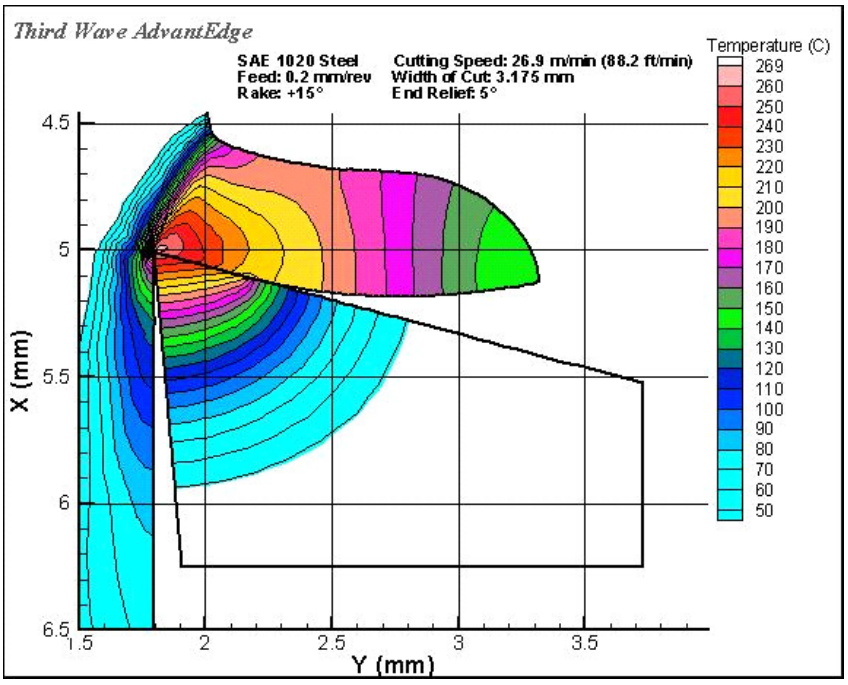

Fig.6.5 (b) Temperature fields calculated using FEM for cutting speed of 26.9 m/min for SAE 1020 Steel

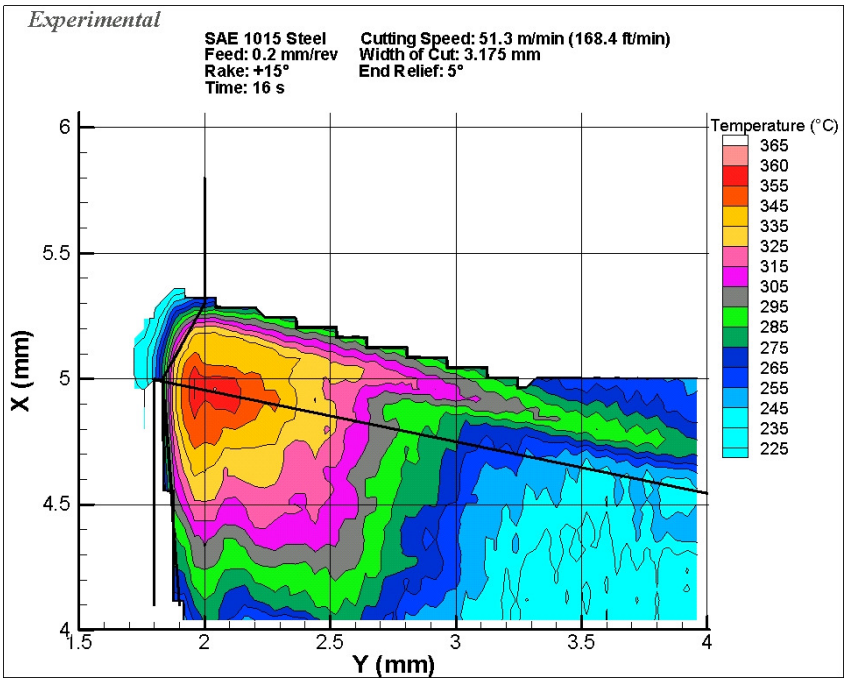

Fig.6.6 (a) Experimental temperature field for cutting speed of 51.3 m/min for SAE 1015 Steel after 16 s

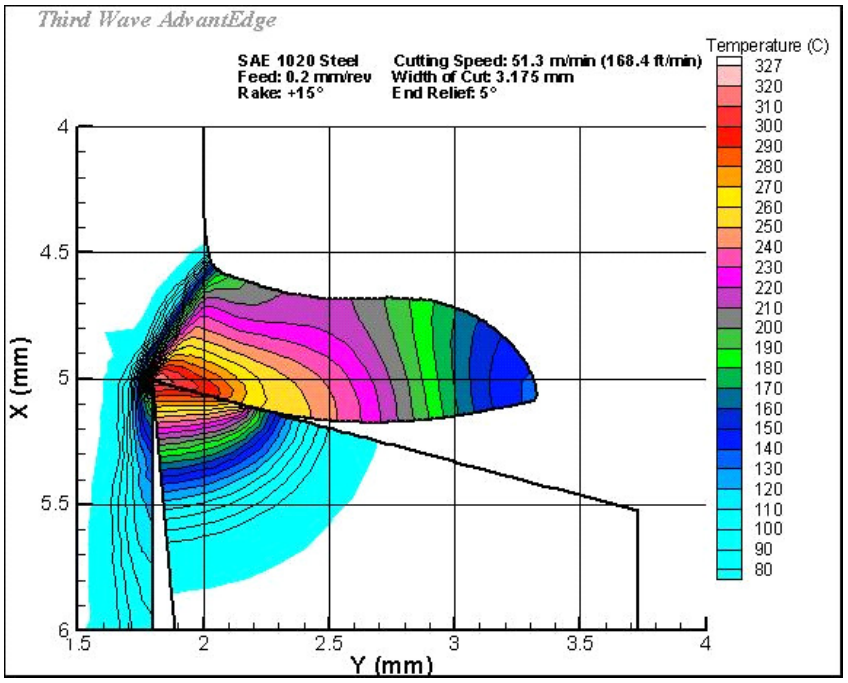

Fig.6.6 (b) Temperature fields calculated using FEM for cutting speed of 51.3 m/min for SAE 1020 Steel

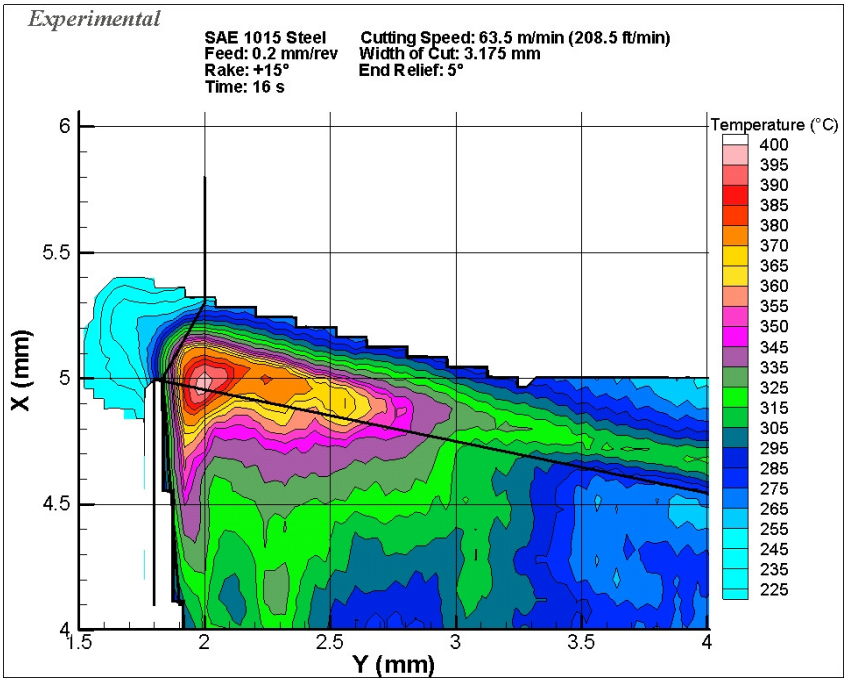

Fig.6.7 (a) Experimental temperature field for cutting speed of 63.5 m/min for SAE 1015 Steel after 16 s

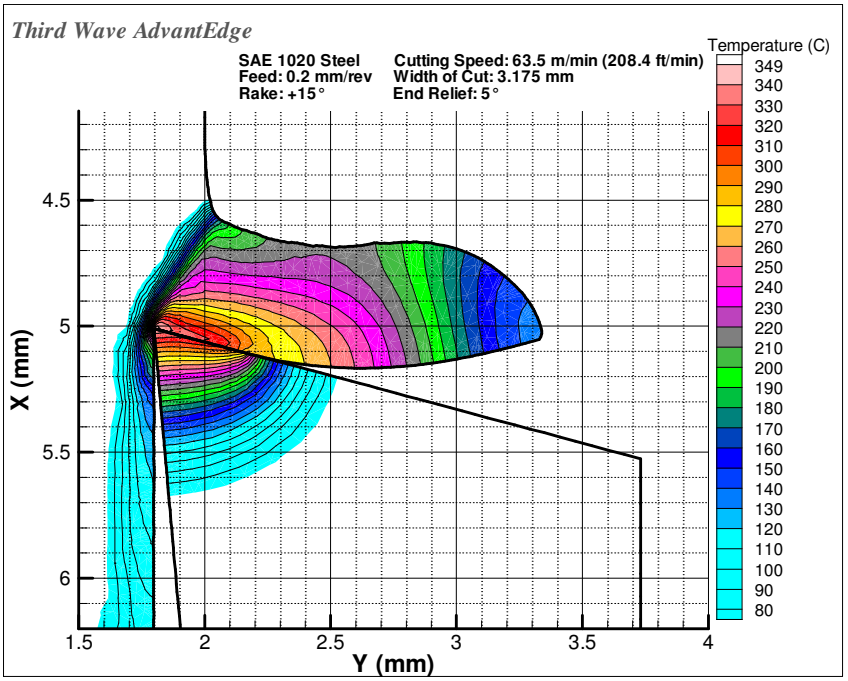

Fig.6.7 (b) Temperature fields calculated using FEM for cutting speed of 63.5 m/min for SAE 1020 Steel

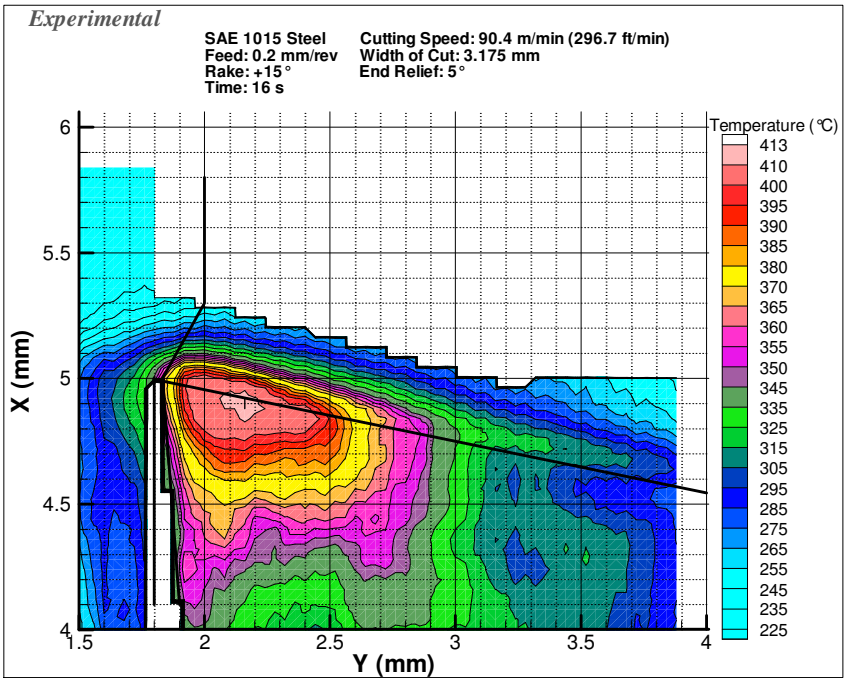

Fig.6.8 (a) Experimental temperature field for cutting speed of 90.4 m/min for SAE 1015 Steel after 16 s

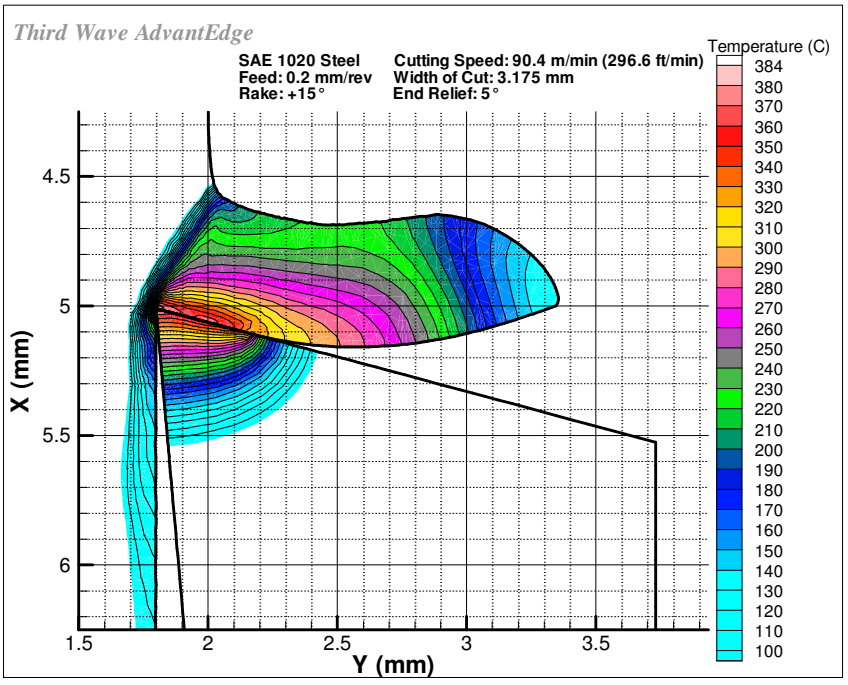

Fig.6.8 (b) Temperature fields calculated using FEM for cutting speed of 90.4 m/min for SAE 1020 Steel

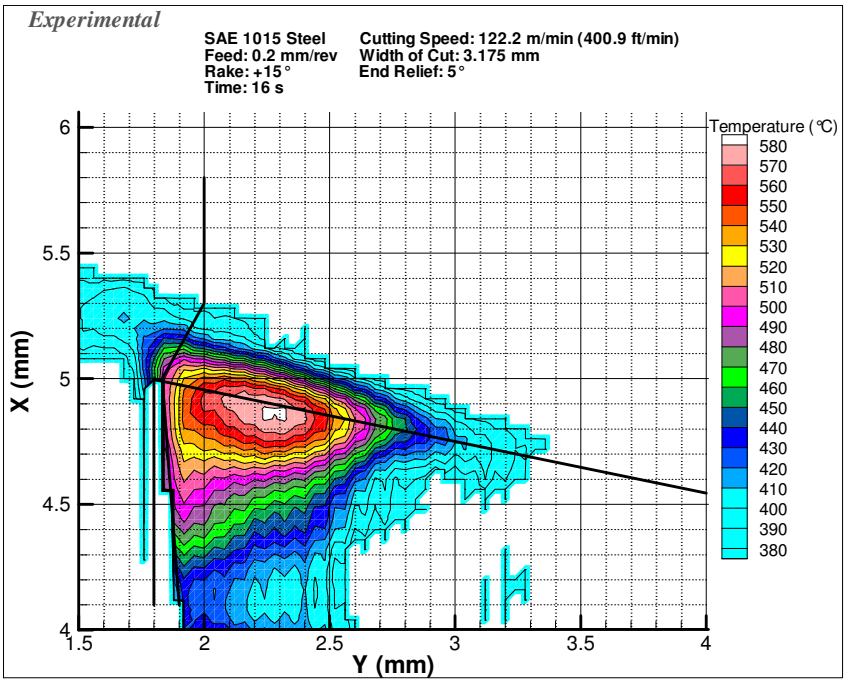

Fig.6.9 (a) Experimental temperature field for cutting speed of 122.2 m/min for SAE 1015 Steel after 16 s

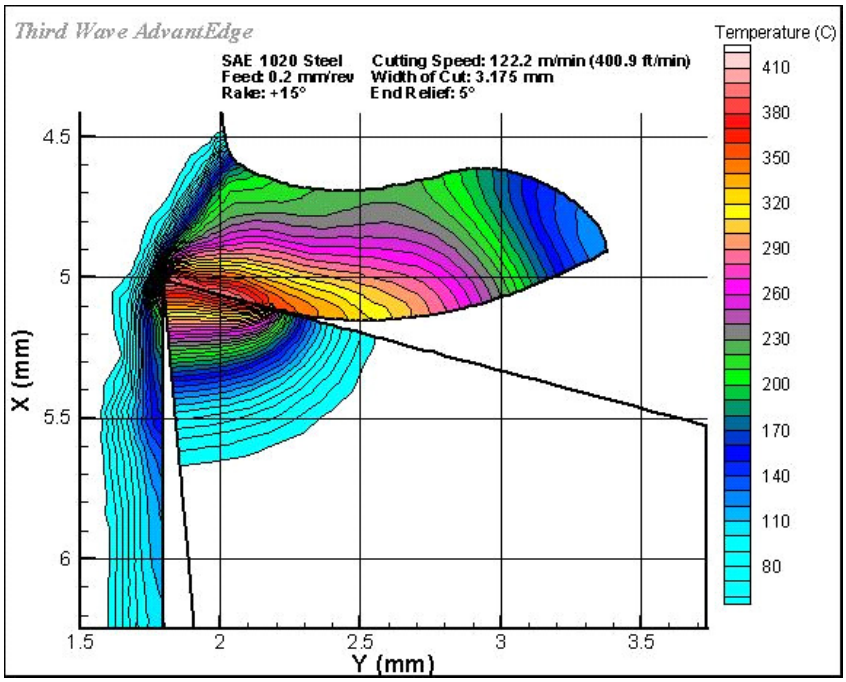

Fig.6.9 (b) Temperature fields calculated using FEM for cutting speed of 122.2 m/min for SAE 1020 Steel

is evident because the tool tip temperature is about 360°C whereas the upper limit of NUC2 is 231°C (Table 4.1). Thus, again the tool tip can not be located and hence measured temperature values can not be associated with a pair of co-ordinates.

It is noted that at about 1 mm distance below the tool side edge, sudden steps in isothermal lines are observed. These steps correspond to the grinding of the tungsten carbide insert. These steps are seen more prominently in Figures 6.5(a) and 6.6(a).

As can be seen from the infrared temperature fields, there exists a steep temperature gradient at the edges or the object boundaries. Reduced distances between two consecutive isothermal lines characterize this phenomenon. Furthermore, sudden steps in temperature contours are observed as the chip separates from the rake face.

From this series of figures, it can also be seen that finite element method exhibits steeper temperature gradients in tool than as observed using infrared camera. This could be due to the difference in the actual thermal properties of the tool material and properties considered in the FEM. The thermal conductivity value of the tool, considered by the FEM, can be considerably lower than the actual insert used in the experiments. In FEM the width of the tool is considered to be the same as that of the uncut chip width. On the other hand in the experimental setup the width of the tool is about 2.5 times the chip. Another possible reason is the relative volume of the tool and the chip. In the experimental setup the volume of the tool is about 120 times that of the chip that is in contact with the tool. Thus the tool may act as a heat sink and exhibit a lower temperature gradient than FEM.

Another important observation is regarding temperatures along the tool-chip contact length. It is observed that chip and rake face temperatures are the same along the

length of contact. This is observed in experimental as well as FEM temperature plots. This can be attributed to a higher pressure in the contact area, which causes rubbing of the rake face and underside of the chip and, as the chip moves away, there is a pressure drop due to contact friction. The chip separates exhibiting different temperature gradient than the tool. The contact length is observed to be about 0.5 mm long in the FEM plots, for all cutting speeds from 26.9 to122.2 m/min whereas in experimental work it is observed to increase with increase in speed. The minimum experimental chip-tool contact length (1.2 mm) is observed at cutting speed of 26.9 m/min and maximum (1.6 mm) at 122.2 m/min.

A careful study of the maximum temperature zone in the experimental temperature plots in Figures 6.5 through 6.9 shows a variation in the location of this temperature zone. It is observed that as the cutting speed increases, the distance of the maximum temperature spot from the cutting edge increases. This distance is observed to be ~0.15 mm at cutting speed of 26.9 m/min and ~0.5 mm at a cutting speed of 122.2 m/min. In Figures 6.5(a), 6.6(a) and 6.7(a), 6.8(a), and 6.9(a), it can be seen that the maximum temperature zone is shared by the tool and the chip.

Figure 6.10 shows the comparison of the present investigation with the work of Boothroyd [6]. Boothroyd [6] performed orthogonal machining tests on SAE 1014 and reocrded temperatures using infrared photographic plates. Because the photographic plates he used were insenstive to temperatures below 350°C he preheated the workpiece to that temperature. As can be seen from his observations the temperature at the chip-tool interface was ~350°C more than that of ambient temperature of the workpiece. A temperature rise of ~330°C is observed in case of the present investigation. This

difference in temperature rise can be due to two reasons: 1) Since Boothroyd [6] preheated the workpiece, lesser energy (than that for material at room temperature) was required to cut the material; 2) The depth of cut used by Boothroyd was greater (0.3 mm) than the present investigation (0.2 mm).

The main difference in the two images is the duration of exposure. The image by Boothroyd [6] was obtained after continuous exposure of the infrared photgraphic film for 15 s after steady state was achieved. The image in the present work is average of ten clutterfree images. These clutterfree images are collected after 16 s of starting the cut or after ~10 s of reaching steady state.

It is also observed that in both images the maximum temperature spot is at a certain distance from the cutting edge. In Boothroyd's work this spot is seen about 0.3 mm from the cutting edge and in the present investigation it is seen at 0.2 mm. The temperature distribution in the tool is observed to be somewhat similar in both the images. The countours are observed in the form of arcs of elongated concentric circles having center at the maximum temperature spot. The maximum temperature spot is distributed between the chip and the tool.

The temperature distribution in the chip is observed to be somewhat different in the two images. The majority of the contours, in the chip, obtained by Boothroyd [6] are parallel to the chip flow direction. Whereas the countours obtained in the present work, in the chip, are clearly divided into three types. One set of countours crosses the chip-tool interface in almost normal direction and is spread along the length of chip-tool contact. Another set of countours runs closely parallel to the chip-back and shows some amount

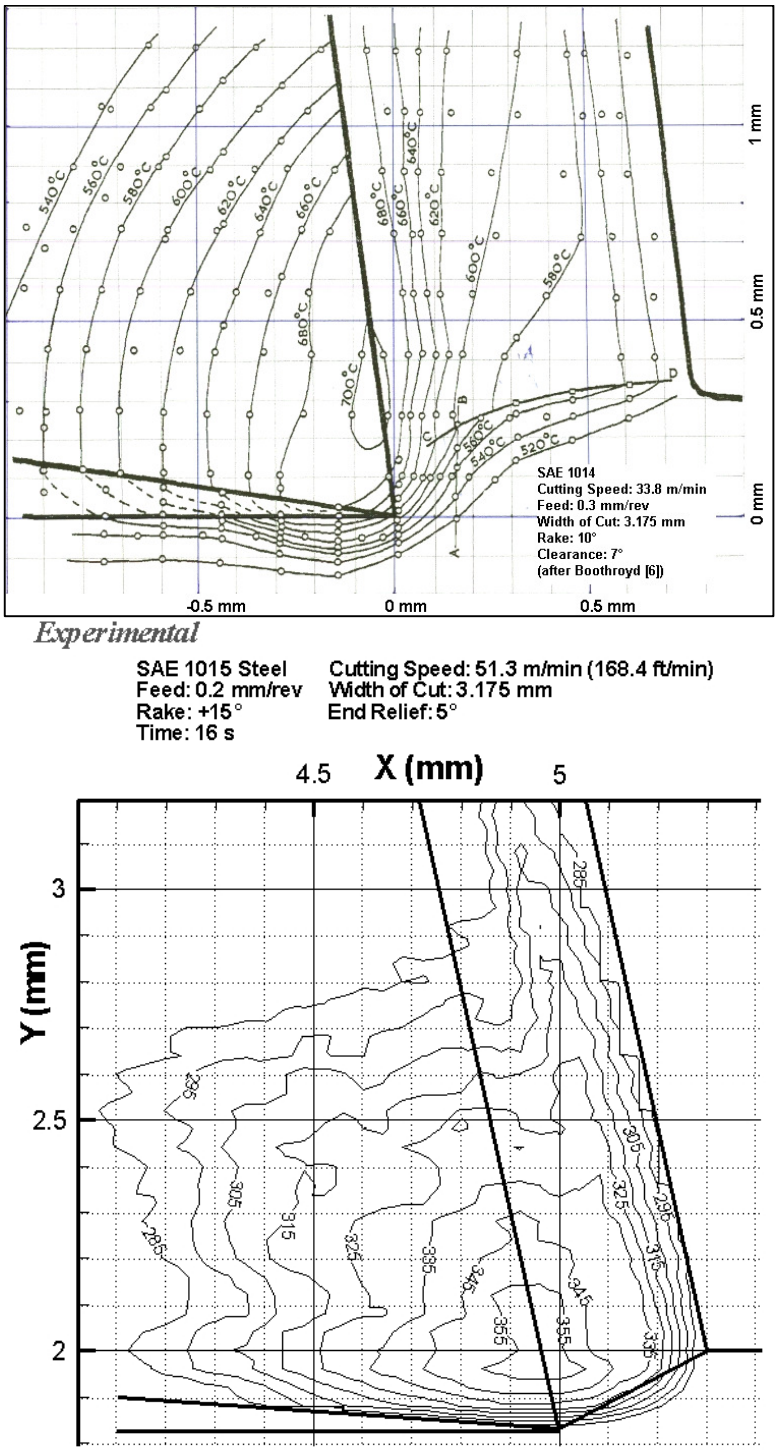

Fig.6.10 Comparison of the present investigation with experimental work of Boothroyd [6]

of crowding. These two sets of contour are connected by cap or delta or "/\" shaped contours. These cap shaped contours point towards the chip flow direction.

Another notable difference is about the contours in the shear zone. The infrared camera setup used in the present investigation has coarse (40 μm) resolution and does not render useful data as observed by Boothroyd [6].

A similar comparison of the present work with the analytical model developed by Komanduri and Hou [41] is shown in Figure 6.11. This analytical model of Komanduri and Hou [41] estimates temperatures in the chip, tool and workpiece region by considering a heat source in the shear zone and a frictional heat source at chip-tool interface. This model has an eleborate approach to calculate and apply the heat parition.

The temperature distribution in the tool is observed to be somewhat similar in both the images. The countours from analytical model are observed in the form of arcs of concentric ellipses having center at the maximum temperature spot. The maximum temperature spot is observed at certain distance from the cutting edge.

In these two images also we can see the similarity about the contours in the chip region. In the model of Komanduri and Hou [41] the contours in the chip are broadly divided into three sets as in the previous comparion.

It is a known fact that the temperature contours are always observed normal to the direction of flow of heat. From the images in the present work it can be concluded that the heat flow direction in the tool is radially outward in the tool with center at the maximum temperature spot. The heat flow direction in the chip is twofold:1) along the chip-tool contact and mid-thickness it flows in direction parallel to the chip flow, 2) near the chip back surface the heat flows normal to this surface. The cap like contours observed in experimental plot of the chip support the presence of a heat source in the

shear zone as assumed by analytical model of Komanduri and Hou [41]. Whereas, the contours in the viscinity of the chip-tool interface support the assumption of frictional

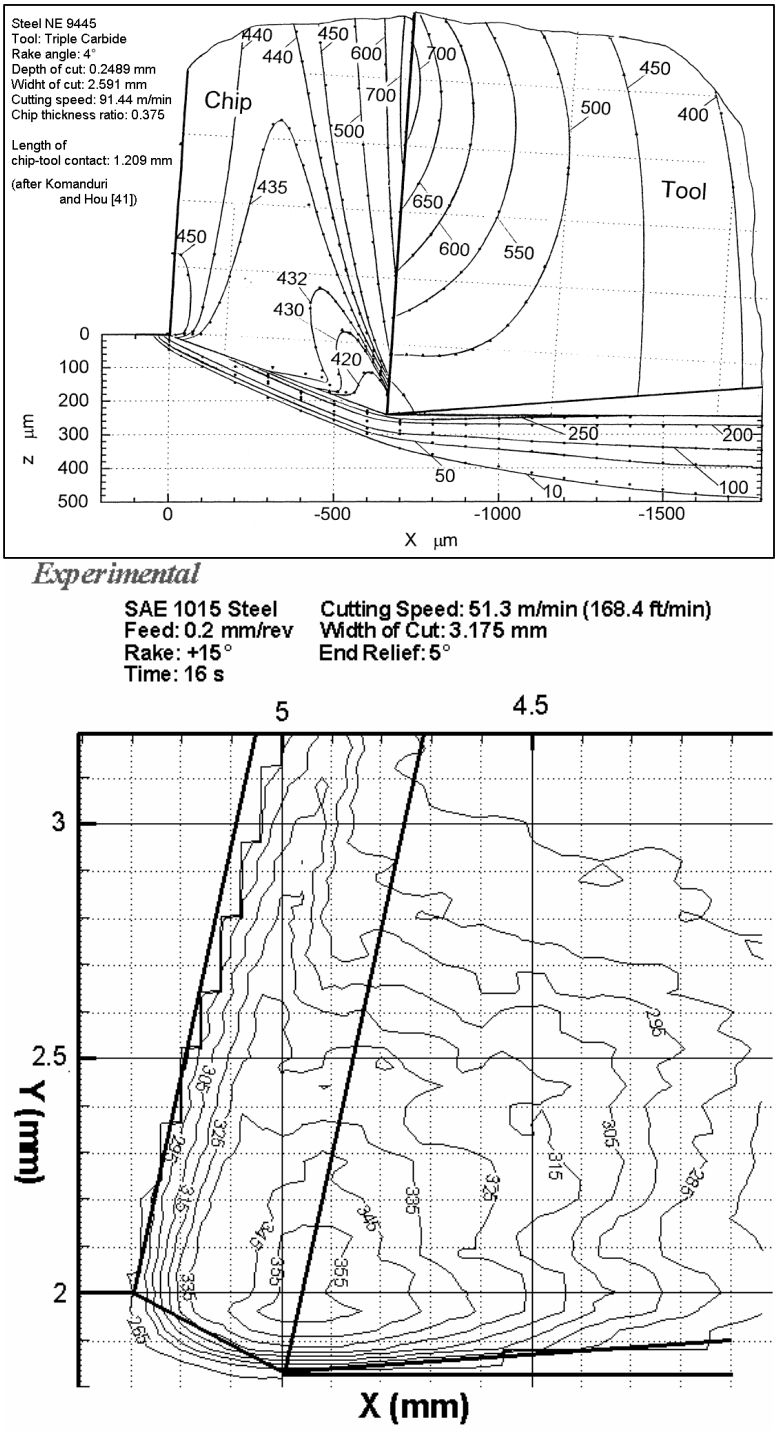

Fig.6.11 Comparison of the present investigation with analytical model of Komanduri and Hou [41]

heat source.

On comparison of temperature contours in the chip as shown in Figures 6.6(a) and 6.8(a) another observation can be made. In Figure 6.8(a) practically there is lack of any cap like contours. This can possibly be attributed to increase in heat generated at the chip-tool interface. There by increasing the heat flow in the direction normal to the chip flow. This is further highlighted by presence of contours that are predominantly parallel to the chip flow direction. This increased effect of frictional heat source is further highlighted in Figure 6.9(a) and can serve as explanation of drastic rise in tool-face temperatures as seen in Figure 6.3.

6.2.2 Tool Face Temperatures

Table 6.4 lists the average tool-face temperatures obtained experimentally, analytically (Shaw [37], Appendix-II), and those estimated using FEM. These are plotted in Figure 6.10. It is observed that the average tool-face temperatures show a continuously increasing trend.

Table 6.4 Average tool-face temperatures (°C)

Cutting Speed (m/min)	Experimental	FEM (AdvantEdge)	Analytical Model (Shaw[37])
26.9	215	238	371
51.3	319	298	462
63.5	356	317	508
90.4	380	355	563
122.2	487	389	536

It can be seen that the trends of experimental and analytical tool-face temperatures are somewhat similar. It can also be noted from Figure 6.12 that experimental and

analytical temperatures exhibit a similar trend. The difference in analytical and experimental values can be attributed to the simplified nature of the analytical model and assumptions made thereof. The analytical model assumes that all of the energy expended is converted into thermal energy and that none of the thermal energy goes to the environment [37]. Thus the analytical model underestimates the losses and assumes perfect conditions for orthogonal machining. Furthermore, the heat partition (proportions in which the heat energy is distributed between the chip and the tool) considered by the analytical model can be different than the actual heat partition.

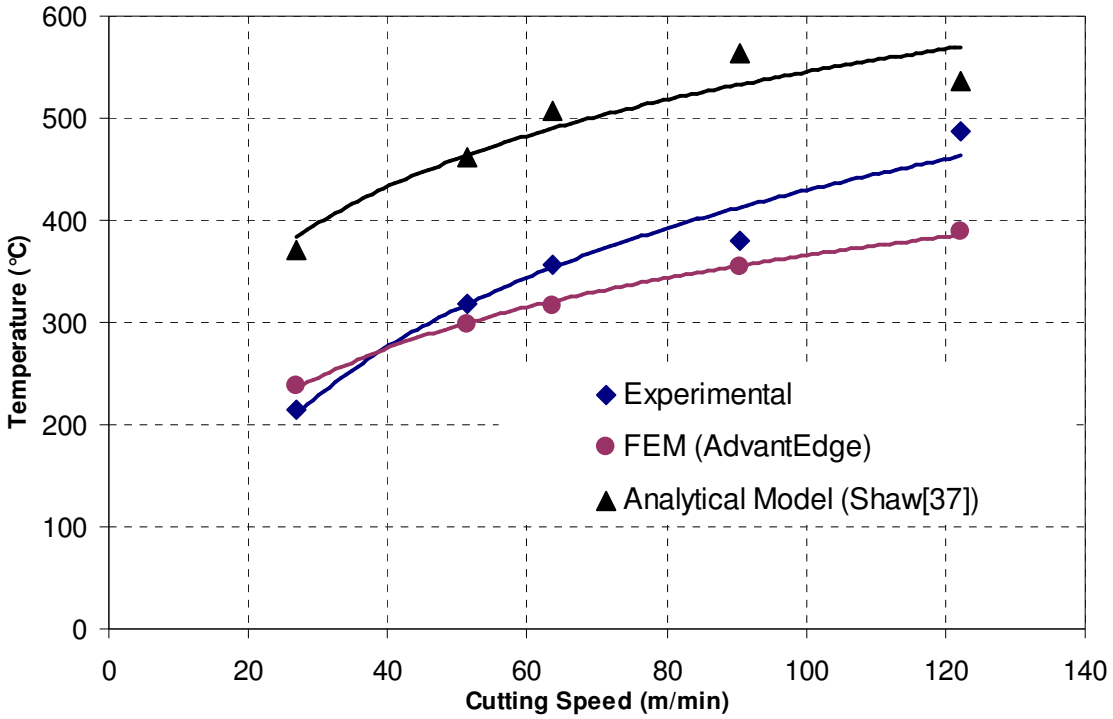

Fig.6.12 Experimental tool-face average temperatures compared with tool-face average temperatures obtained using FEM (AdvantEdge) and analytical model (Shaw [37])

It can also be noted from Figure 6.12 that experimental and FEM temperature plots have almost similar trend and show a reasonable agreement for cutting speeds from

26.9 to 90.4 m/min. The experimental temperature values are found to be considerably higher than the FEM temperatures at a cutting speed of 122.2 m/min.

This difference in FEM and experimental results can possibly be attributed to various parameters that are incorporated in the FEM model internally, for example coefficient of friction, heat partition, conductivity and diffusivity of tool and chip. The FEM model being proprietary, specific comments are difficult to make.

CHAPTER 7

CONCLUSIONS

1. An infrared camera technique has been developed for the non-contact in-situ measurement of the temperature distributions in chip and tool in orthogonal machining of steel. This technique is broadly divided into three steps of setup, infrared data acquisition and post processing of infrared data.
2. In the data acquisition step it is important to obtain a clutter free view so as to get reliable values of temperature distribution. If a clutter free view is possible to obtain, then machining tests at any practically possible cutting speed can be done.
3. In the post processing it is necessary to average multiple images so as to minimize the effect of instantaneous variations in temperatures.
4. Because of its non-contact nature this technique allows flexibility of machining parameters, such as cutting speed, rake angle and work material. Temperature measurement can be done on any metal that can be obtained in tubular form.
5. The maximum temperature in orthogonal cutting increases with increase in cutting speed.
6. The distance of the maximum temperature spot on the tool face from the cutting edge increases as the cutting speed increases. This distance is same for a given cutting speed and remains unchanged in the transient or steady state condition.

7. The shape of contour surrounding the maximum temperature spot is the same in the transient or the steady state condition.
8. The time required to reach steady state condition increases with increase in cutting speed.
9. The chip-tool contact length increases with increase in cutting speed. The difference in experimental contact length and that estimated by FEM is due to differences in the conditions considered in FEM.
10. The camera has "blind spots" between two NUC tables and hence temperatures at some cutting speed can not be resolved.
11. Sudden steps in temperature contours are observed at edges present in objects.
12. The temperature gradients estimated by FEM are steeper than measured. This is because the thermal conductivity of the tool, considered in FEM, is lower than actual. Also, the width of the tool considered in FEM is smaller than actual tool width and the tool may act as a heat sink because of volume difference.
13. The average tool-face temperature increases with increase in cutting speed.
14. The average tool-face temperature estimated using the analytical model is about 28% higher than the measured temperature. This difference can be attributed to the assumptions and simplifications made to enable analysis.
15. The average tool-face temperature estimated using FEM is about 8% lower than the measured temperature. This difference can be attributed to the various parameters that are incorporated internally in the standard setup of AdvantEdge.

CHAPTER 8

FUTURE WORK

1. The infrared setup needs to be modified using a bigger diameter lens to give higher spatial resolution, for example 5 μm. This modified setup can be used to measure shear zone temperatures. Such a resolution will possibly reduce the saturation of sensors in the shear zone. A greater spatial resolution can be used to investigate ultra precision machining process.

2. A VBA code needs to be developed that will help superimpose temperature data from two or more NUC tables. This code will replace saturated signal values with those from the higher NUC table. At the same time, this code will replace lower limit signal values with those from lower NUC table.

3. The present infrared setup has "blind spots" when temperatures are on a "cusp" of two NUC tables. For example, with the present setup a temperature field with temperatures in the range of 50-250 °C can not be measured with a single NUC table, thereby causing loss of data. With the help of the manufacturer, a new NUC table, with a temperature range of 50-700 °C or 50-1000 °C, needs to be developed. Such a NUC table will facilitate measurement of temperatures for all the possible ranges in one setting.

4. The co-ordinate system used for plotting the temperature contours has the origin at the tool tip. Hence in the present setup it is necessary to use a NUC table that clearly shows the tool tip. On tool, locating or indentation marks as used by Miller *et al.* [22] can be made. These marks along with the "PosiTrack" tool of ThermaGram can be an effective means of locating tool tip. This will make the task of tool tip location less dependant on the choice of the NUC table.

REFERENCES

1. Cohen, P.H., "Forces, power, and stresses in machining," ASM Handbook, 9th Edition, Vol.16 (2002).
2. Komanduri, R., "Machining and grinding: a historical review of the classical papers," Applied Mechanics Review Vol. 46 No. 3 (1993) 80-129.
3. Ivester, R., Kennedy, M., Davies, M., Stevenson, R., Thiele, J., Furness, R., and Athavale, S., "Assessment of machining models: progress report," Journal of Machining Science and Technology, Society of Manufacturing Engineers Vol. 4(3) (2000) 511-538.
4. Komanduri, R., and Hou, Z. B., "A review of the experimental techniques for the measurement of heat and temperatures generated in some manufacturing processes and tribology," Tribology International, Vol.34, Iss.10 (2001) 653-682.
5. Thompson B. (Count Rumford), "An enquiry concerning the source of heat which is excited by friction," Philosophical Transactions of Royal Society (London) Vol.18 (1798) 278-87.
6. Boothroyd, G., "Photographic techniques for the determination of metal cutting temperatures," British Journal of Applied Physics, Vol.12 (1961) 238–42.
7. Boothroyd, G., "Temperatures in orthogonal metal cutting," Proceedings of Institute of Mechanical Engineers (London) Vol.177 (1963) 789–810.

8. Reichenbach, G.S., “Experimental measurement of metal cutting temperature distribution,” Transactions of ASME Vol.80 (1958) 525.
9. Ueda, T., Sato, M., and Nakayama, K., “The temperature of a single crystal diamond tool in turning,” Annals of CIRP Vol.47 Iss.1 (1998) 41–4.
10. Ng, E. -G., Aspinwall, D.K, Brazil, D., and Monaghanc, J., “Modeling of temperature and forces when orthogonally machining hardened steel,” International Journal of Machine Tools & Manufacture Vol.39 (1999) 885–903.
11. M’Saoubi, R., Le Calvez1, C., Changeux, B., and Lebrun J. L., “Thermal and microstructural analysis of orthogonal cutting of a low alloyed carbon steel using an infrared-charge-coupled device camera technique,” Proceedings Institute of Mechanical Engineers Vol. 216 Part B: J Engineering Manufacture (2002) 153-165.
12. Young, H.T., and Chou, T.L., “Investigation of edge effect from the chip-back temperature using IR thermographic techniques,” Journal of Materials Processing Technology Vol.52 (1995) 213-224.
13. Wang, L., Saito, K., and Jawahir, I.S., “Infrared temperature measurement of curled chip formation in metal machining,” Transactions of NAMRI/SME Vol.24 (1996) 87-92.
14. Dewes, R.C., Ng, E., Chua, K.S., Newton, P.G., and Aspinwall, D.K., “Temperature measurement when high speed machining hardened mould-die steel,” Journal of Materials Processing Technology Vol.92-93 (1999) 293-301.

15. Chandrasekar, S., Ackroyd, B., Akcan N. S., and Chhabra P., Krishnamurthy, K, Madhavan, V., Compton, W.D., and Farris, T. N.,"Exploration of contact conditions in machining," Proc Instn Mech Engrs Vol.215 Part B (2001) 493-506.
16. Kwon, P., Schiemann , T., and Kountanya, R., "An inverse estimation scheme to measure steady-state tool–chip interface temperatures using an infrared camera," International Journal of Machine Tools & Manufacture, Vol. 41 (2001) 1015–1030.
17. O'Sullivan, D. and Cotterell, M., "Temperature measurement in single point turning," Journal of Materials Processing Technology Vol.118 (2001) 301-308.
18. Jaspers, S.P.F.C., and Dautzenberg, J.H., "Material behaviour in metal cutting-strains, strain rates and temperatures in chip formation," Journal of Materials Processing Technology Vol.121 (2002) 123-135.
19. Jaspers, S.P.F.C., Dautzenberg, J.H., and Taminiau, D.A., "Temperature measurement in orthogonal metal cutting," The International Journal of Advanced Manufacturing Technology Vol.14 (1998) 7-12.
20. Davies, M. A., Yoon, H., Schmitz, T. L., Burns, T. J., and Kennedy, M. D., "Calibrated thermal microscopy of the tool–chip interface in machining," Machining Science And Technology Vol.7, No.2 (2003) 167–190.
21. Davies, M.A., Cao, Q., Cooke, A.L., and Ivester, R., "On the measurement and prediction of temperature fields in machining 1045 steel", CIRP Annals – Manufacturing Technology, Vol.52(2003), n1, p.77-80.

22. Miller, M.R., Mulholland, G., and Anderson, C., "Experimental cutting tool temperature distributions," Journal of Manufacturing Science and Engineering, Vol.125 (2003) 667-673.

23. Ivester, R.W., and Whitenton E.P., "Simultaneous visual and infrared imaging for improved machining models," Proceedings of NSF workshop on Research Needs in Thermal Aspects of Material Removal Processes, Oklahoma State University, Stillwater, June 2003, 70-76.

24. Vernaza-Pena, K.M., Mason, J.J., Ovaert, T.C., and Li, M., "Experimental investigation of the temperature fields generated during orthogonal machining," Proceedings of NSF workshop on Research Needs in Thermal Aspects of Material Removal Processes, Oklahoma State University, Stillwater, June 2003, 77-84.

25. Chandrasekar, S., Narayanan V., Krishnamurthy, K., Hwang, J., Madhavan, V., and Farris, T. N., "Measurement of temperature field at the tool-chip interface in machining," Proceedings of NSF workshop on Research Needs in Thermal Aspects of Material Removal Processes, Oklahoma State University, Stillwater, June 2003, 63-69.

26. Sutter, G., Faure, L., Molinari, A., Ranc, N., and Pina, V., "An experimental technique for the measurement of temperature fields for the orthogonal cutting in high speed machining" International Journal of Machine Tools & Manufacture Vol.43 (2003) 671–678.

27. Rech, J., Kusiak, A., Battaglia, J.L., and Moisan, A., "Influence of cutting tool coatings on the tribological phenomena at the tool-chip interface in orthogonal

dry turning," Third International Conference on Advances in Production Engineering, June 2004.

28. M'Saoubi, R., and Chandrasekaran, H., "Investigation of the effects of tool micro-geometry and coating on tool temperature during orthogonal turning of quenched and tempered steel," International Journal of Machine Tools & Manufacture Vol. 44 (2004) 213–224.
29. Kececioglu, D., "Force components, chip geometry, and specific cutting energy in orthogonal and oblique machining of SAE 1015 steel," Transactions of the ASME, January 1958, 149-157.
30. Merlin™ Mid InSb MWIR Camera User's guide Version 1.1, 414-0001-10, Indigo Systems, 2003.
31. Burnay, S.G., Williams T.L., and Jones C.H., Applications of Thermal Imaging, Adam Hilger, Philadelphia, 1988.
32. Vanzetti, R., Practical Applications of Infrared Techniques, John Wiley and Sons, New York, 1972.
33. Santhanam, A.T., and Tierney, P., "Cemented Carbides," ASM Handbook, 9th Edition, Vol.16 (2002).
34. Instruction Manual 3-Component Measuring Platform Type 9257A, Edition 5/87, Kistler Instrumente AG, 1987.
35. Instruction Manual Dual Mode Amplifier Type 5010B-5010BM2, Edition 11/01, Kistler Instrumente AG, 2001.

36. Goldsmith, A., Waterman, T.E., and Hirschhorn, H.J., Handbook of Thermophysical Properties of Solid Materials, Vol.2, Pergamon Press, New York, 1962.
37. Shaw, M.C., Metal Cutting Principles, Oxford University Press, New York, 1984.
38. DeWitt, D.P., and Nutter G.D., Theory and Practice of Radiation Thermometry, John Wiley and Sons, New York, 1989.
39. Shaw, M.C., Piggot, J.D., and Richardson, L.P., "The effect of the cutting fluid upon chip-tool interface temperature", Trans of ASME, Vol. 73(1) (1951) 45-56.
40. Metals Handbook Desk Edition, Second Edition, 1998.
41. Komanduri, R., and Hou, Z. B., “Thermal modeling of the metal cutting process - Part III: temperature rise distribution due to the combined effects of shear plane heat source and the tool–chip interface frictional heat source,” International Journal of Mechanical Sciences, Vol. 43(1) January 2001, 89-107.

Appendix-I

Microsof Excel® with VBA code developed to convert infrared pixel data obtained from camera. This data is in matrix array format and is converted into tabular format using this code.

```
Sub clear_confirm()
    response = MsgBox("Are you sure that you want to clear all the data
?", vbYesNo, "Clear: Confirmation")
    If (response = vbYes) Then Call Clear
End Sub
Sub Clear()
    ActiveSheet.Range("A1:F65536").ClearContents
    ActiveSheet.Range("N7:N10").ClearContents
    ActiveSheet.Range("K9:K10").ClearContents
End Sub
Sub Shift_Origin_x()
    Dim x_pixels As Integer
    ActiveSheet.Cells(11, 10) = "Shifting X"
    camera_scale_x = 10160 / 239 ' converts to µm

    imax = ActiveSheet.Cells(9, 11) + 1
    x_shift = ActiveSheet.Cells(13, 11)
    x_pixels = x_shift / camera_scale_x
    x_pixels = ActiveSheet.Cells(3, 13) + x_pixels
    ActiveSheet.Cells(3, 13) = x_pixels

    Call Fetch

    ActiveSheet.Cells(13, 13) = x_shift
    ActiveSheet.Cells(13, 11) = 0
    ActiveSheet.Cells(11, 11) = ""
    ActiveSheet.Cells(11, 10) = ""
End Sub
Sub Shift_Origin_xy()
    Dim x_pixels As Integer, y_pixels As Integer
    ActiveSheet.Cells(11, 10) = "Shifting XY"
    imax = ActiveSheet.Cells(9, 11) + 1

    camera_scale_x = 10160 / 239 ' converts to µm
    camera_scale_y = 10160 / 238 ' converts to µm

    x_shift = ActiveSheet.Cells(13, 11)
    y_shift = ActiveSheet.Cells(14, 11)

    x_pixels = x_shift / camera_scale_x
    x_pixels = ActiveSheet.Cells(3, 13) + x_pixels

    y_pixels = y_shift / camera_scale_y
    y_pixels = ActiveSheet.Cells(2, 13) - y_pixels

    ActiveSheet.Cells(3, 13) = x_pixels
    ActiveSheet.Cells(2, 13) = y_pixels

    Call Fetch
```

```
    ActiveSheet.Cells(13, 13) = x_shift
    ActiveSheet.Cells(14, 13) = y_shift
    ActiveSheet.Cells(13, 11) = 0
    ActiveSheet.Cells(14, 11) = 0
    ActiveSheet.Cells(11, 11) = ""
    ActiveSheet.Cells(11, 10) = ""
End Sub
Sub Shift_Origin_y()
    Dim y_pixels As Integer
    ActiveSheet.Cells(11, 10) = "Shifting Y"
    imax = ActiveSheet.Cells(9, 11) + 1
    y_shift = ActiveSheet.Cells(14, 11)

    camera_scale_y = 10160 / 238 ' converts to µm

    y_pixels = y_shift / camera_scale_y
    y_pixels = ActiveSheet.Cells(2, 13) - y_pixels
    ActiveSheet.Cells(2, 13) = y_pixels

    Call Fetch

    ActiveSheet.Cells(14, 11) = 0
    ActiveSheet.Cells(14, 13) = y_shift
    ActiveSheet.Cells(11, 11) = ""
    ActiveSheet.Cells(11, 10) = ""
End Sub
Sub fetch_confirm()
    response = MsgBox("Are you sure you want to fetch all the data?",
vbYesNo, "Fetch: Confirmation")
    If (response = vbYes) Then Call Fetch
End Sub
Sub Fetch()
    Call Clear

    ActiveSheet.Cells(11, 10) = "Fetching Data"

    Pi = 3.14159265358979 / 180

    camera_scale_x = 10160 / 254 ' converts to µm
    camera_scale_y = 10160 / 254 ' converts to µm

    imax = ActiveSheet.Cells(2, 11)
    jmax = ActiveSheet.Cells(3, 11)

    HT_flag = ActiveSheet.Cells(5, 11)
    NUC = ActiveSheet.Cells(7, 11)

    tipy = ActiveSheet.Cells(2, 13)
    tipx = ActiveSheet.Cells(3, 13)

    e_chip = ActiveSheet.Cells(18, 11)
    e_tool = ActiveSheet.Cells(19, 11)
    e_work = ActiveSheet.Cells(20, 11)
    room_temp = ActiveSheet.Cells(24, 11)

    feed = e_work = ActiveSheet.Cells(22, 11) * 1000 'µm/rev
```

```
    rake = ActiveSheet.Cells(18, 14) * Pi
    relief = (ActiveSheet.Cells(19, 14) - ActiveSheet.Cells(18, 14)) *
Pi

    rake_tan = 0 - Math.Tan(rake)
    relief_tan = 0 - Math.Tan(relief)
    rake_cos = Math.Cos(rake)

    chip_thk = ActiveSheet.Cells(22, 14) * 1000

    ActiveSheet.Cells(7, 14) = (1 - tipx) * camera_scale_x 'µm
    ActiveSheet.Cells(8, 14) = (jmax - tipx) * camera_scale_x 'µm
    ActiveSheet.Cells(9, 14) = (tipy - imax) * camera_scale_y  'µm
    ActiveSheet.Cells(10, 14) = (tipy - 1) * camera_scale_y  'µm

    ActiveSheet.Cells(10, 11) = imax * jmax
    ctr = 0
    i_ctr = 1

    For i = 1 To imax 'row
        For j = 1 To jmax 'column
            x = (j - tipx) * camera_scale_x 'µm
            y = (tipy - i) * camera_scale_y  'µm

            If (x > -5001 And x < 5001 And y > -5001 And y < 5001) Then
                Select Case NUC
                    Case 0, 1, 4, 5
                        temp = Sheet1.Cells(i, j)
                    Case 2
                        temp = Sheet1.Cells(i, j)
                        If (temp < 112) Then temp = room_temp
                    Case 3
                        temp = Sheet1.Cells(i, j)
                        If (temp < 222) Then temp = room_temp
                    Case 9
                        Select Case HT_flag
                            Case 0
                            temp = 0.0851 * Sheet1.Cells(i, j) + 188.68

                            Case 1
                            cell_cube = Sheet1.Cells(i, j) *
Sheet1.Cells(i, j) * Sheet1.Cells(i, j)
                            temp = -0.0000000008 * cell_cube *
Sheet1.Cells(i, j) '^ 4) '
                            temp = temp + 0.000002 * cell_cube '*
(Sheet1.Cells(i, j) ^ 3) '
                            temp = temp + 1.6855 * Sheet1.Cells(i, j) +
189.55
                        End Select 'ht_flag
                End Select ' nuc

                If (x < 0) Then  'work
                    If (temp > room_temp) Then
                        temp = (temp - (1 - e_work) * room_temp) /
e_work
                    End If
                    ActiveSheet.Cells(i_ctr, 6) = "W"
```

```
                End If

                If (x >= 0 And y > x * rake_tan) Then
                    If (x <= feed) Then 'work: uncut chip thickness
                        If (temp > room_temp) Then
                            temp = (temp - (1 - e_work) * room_temp) /
e_work
                        End If
                        ActiveSheet.Cells(i_ctr, 6) = "W"
                    Else 'chip
                        If (x < 1500 And y > x * rake_tan + (chip_thk /
rake_cos)) Then
                            temp = room_temp
                        ElseIf (x >= 1500 And y > 0) Then
                            temp = room_temp
                        Else
                            If (temp > room_temp) Then
                                temp = (temp - (1 - e_chip) *
room_temp) / e_chip
                            End If
                        End If
                        ActiveSheet.Cells(i_ctr, 6) = "C"
                    End If
                End If

                If (x >= 0 And y <= x * rake_tan) Then 'tool
                    If (x < y * relief_tan) Then
                        temp = room_temp
                    Else
                        If (temp > room_temp) Then
                            temp = (temp - (1 - e_tool) * room_temp) /
e_tool
                        End If
                    End If
                    ActiveSheet.Cells(i_ctr, 6) = "T"
                End If

                ActiveSheet.Cells(i_ctr, 1) = x
                ActiveSheet.Cells(i_ctr, 2) = y
                ActiveSheet.Cells(i_ctr, 3) = temp

                ActiveSheet.Cells(i_ctr, 5) = Sheet1.Cells(i, j)

                ActiveSheet.Cells(9, 11) = ctr
                ActiveSheet.Cells(11, 11) = ctr

                ctr = ctr + 1
                i_ctr = i_ctr + 1
            End If
        Next j
    Next i

    ActiveSheet.Range("J11:K11").ClearContents
End Sub
```

Appendix-II

Calculation of average tool-face temperature using analytical model of Shaw [37].

Nomenclature

α	Rake angle
ß	Friction angle
ε	Emissivity
ϕ	Shear angle
ρ	Density
γ	Average shear strain in chip
$\bar{\theta}_0$	Ambient temperature of work
θ_0'	Ambient temperature of tool
$\bar{\theta}_S$	Average shear plane temperature
$\bar{\theta}_T$	Average temperature rise in cutting
$\Delta\bar{\theta}_F$	Average temperature rise on tool face
a	Chip-tool contact length
A	Area factor
b	Width of cut
c	Velocity of light in vacuum
C	Volume specific heat
F_C	Cutting force component parallel to the tool face
F_P	Cutting force
F_Q	Thrust force or feed force

F_S Shear force

J Mechanical equivalent of heat

k_1 Thermal conductivity of work material at estimated shear temperature

k_2 Thermal conductivity of work material at estimated tool-face temperature

k_3 Thermal conductivity of tool material at estimated tool-face temperature

K_1 Thermal diffusivity of work material at estimated shear temperature

K_2 Thermal diffusivity of work material at estimated tool-face temperature

F_S Shear force

r Chip thickness ratio

R_1 Heat partition coefficient

t Uncut chip thickness

u_F Friction energy per unit volume

u_S Shear energy per unit volume

V Cutting speed

V_C Chip velocity

V_S Shear velocity

Experimentally measured quantities:

Work material: SAE 1015 steel.

Tool material: Cemented tungsten carbide

Rake angle: $\alpha = 15°$

Clearance angle: 5°

Type of cut: Orthogonal.

Cutting speed: V = 51.3 m/min

Undeformed chip thickness: t = 0.2 mm

Width of cut: b = 3.175 mm

Chip contact length: a = 1.3 mm

Cutting force: F_P = 1389 N

Feed force: F_Q = 700 N

Chip-thickness ratio: r = 0.5249

Calculated values:

Shear angle: $\phi = \tan^{-1}\left(\frac{r.\cos\alpha}{1-r.\sin\alpha}\right) = 30.4°$

Shear strain: $\gamma = \tan(\phi - \alpha) + \cot\phi = 1.98$

Shear force: $F_S = F_P \cos\phi - F_Q \sin\phi = 843.7N$

Shear velocity: $V_S = \gamma V \sin\phi = 51.4\ m/\min$

Shear energy per unit volume: $u_S = \frac{F_S V_S}{Vbt} = 1332.6\ N/mm^2$

Cutting force component parallel to the tool face:

$$F_C = F_P \sin\phi + F_Q \cos\phi = 1389N$$

Chip velocity: $V_C = rV = 26.9\,m/\min$

Friction energy per unit volume: $u_F = \frac{F_C V_C}{Vbt} = 856.9\ N/mm^2$

Outline of solution:

(a) Estimate the value of shear zone temperature: $\bar{\theta}_S = 239°C$ and determine corresponding values of $K_1 = 12.9\,mm^2/s$ and $\rho_1 C_1 = 2.25\,J/cm^3.°C$ from Figure 12.25 of Shaw [37]

(b) Calculate: $\frac{Vt}{K_1\gamma} = 6.62$

(c) Obtain R1 from Figure 12.23 given by Shaw [37]: $R_1 = 0.66$

(d) Calculate: $\left(\bar{\theta}_S - \theta_0\right) = \frac{R_1 u_S}{JC_1\rho_1}$

(e) Repeat steps (a) to (d) until estimated and calculated values of $\left(\bar{\theta}_S\right)$ match.

(f) Estimate values of $\bar{\theta}_T = 462°C$ and determine corresponding values of $K_2 = 8.4\,mm^2/s$ and $\rho_2 C_2 = 2.96\,J/cm^3.°C$ from Figure 12.25 given in Shaw [37]

(g) Calculate aspect ratio: $\frac{b}{2a} = 1.22$

(h) Calculate: $\frac{u_F VtA}{Jk_3} = C' = 2548°C$, where k_3 is conductivity of carbide tool taken as $k_3 = 0.57\,J/s.°C$

(i) Calculate $\frac{0.754 u_F VtA}{J\rho_2 C_2}\left(\frac{Vt}{ark_2/t}\right)^{1/2} = B' = 252°C$

(j) Determine $R_2 = \frac{C' - \theta_S + \theta_0'}{C' + B'} = 0.83$

(k) Temperature rise due to friction: $\Delta\theta_F = R_2 B' = 209°C$

(l) Average tool-face temperature: $\bar{\theta}_T = \bar{\theta}_S + \Delta\bar{\theta}_F = 448°C$

(m) Compare this value with value assumed in (f) and repeat steps (f) to (l) until agreement is observed.

VITA

Amol A. Bhome

Candidate for the Degree of

Master of Science

Thesis: TEMPERATURE MEASUREMENT IN ORTHOGONAL MACHINING OF SAE 1015 STEEL USING AN INFRARED CAMERA

Major Field: Mechanical Engineering

Biographical:

Personal Data: Born in Baramati, Maharashtra, India on September 30, 1977, the son of Avinash and Ujjwal Bhome.

Education: Received Bachelor of Engineering degree in Mechanical Engineering from the University of Pune, Maharashtra, India, in May 1999. Completed the requirements for the Master of Science degree with a Major in Mechanical Engineering at Oklahoma State University, Stillwater, Oklahoma in December, 2004.

Experience: Worked with Thermax LTD, Process Heat Division, Pune from June 1997 to December 1997 and January 1999 to June 1999. Worked with L&T-John Deere LTD, Vehicle Assembly Factory, as Quality Assurance Engineer from August 1999 to July 2001. Teaching Assistant from January 2002 to December 2003 and Research Assistant from August 2001 to December 2003 in Mechanical and Aerospace Engineering at Oklahoma State University, Stillwater, Oklahoma.

Professional Membership: American Society of Mechanical Engineers

Name: Amol Bhome Date of Degree: December, 2004

Institution: Oklahoma State University Location: Stillwater, Oklahoma State

Title of Study: TEMPERATURE MEASUREMENT IN ORTHOGONAL MACHINING OF SAE 1015 STEEL USING AN INFRARED CAMERA

Pages in Study: 119 Candidate for Degree of Master of Science

Major Field: Mechanical Engineering

Scope and Methodology of Study: In the present investigation, a MerlinTM Mid InSb MWIR Camera is used to observe chip, tool and workpiece temperature fields in orthogonal machining of SAE 1015 steel tube. A cemented tungsten carbide tool insert (Valenite SECW-2.51.51) is used at 15° rake angle and width of cut 3.175mm, at a feed rate of 0.2 mm/rev and at different cutting speeds (26.9, 51.3, 63.5, 90.4, and 122.2 m/min) on a Vectrax 1660 lathe. The cutting forces were measured using a Kistler 3-Component piezoelectric dynamometer (Type 9257A). The temperature fields are recorded using Version 2.4.11 of ThermaGram Pro with Dynamite software. The temperature field data is then plotted using Version 9.2 of TecPlot software. The experimental results are compared with the analytical model and a commercially available Finite Element Method software (AdvanatEdge Version 4.4.)

Findings and Conclusions: The experimental tool-face temperatures are observed to be considerably lower (~30%) than analytical model. The experimental tool-face temperature values show reasonable agreement (~8%) with the FEM results. The study concludes that present infrared camera setup can be effectively used to measure tool-face temperatures in orthogonal machining of steel.

Advisor's Approval: Dr. Ranga Komanduri